Design of Flying Robots for Collision Absorption and Self-Recovery

PAR

Adam KLAPTOCZ

EPFL

ÉCOLE POLYTECHNIQUE
FÉDÉRALE DE LAUSANNE

Suisse
2012

Acknowledgements

Though presented as a personal contribution to science, this thesis would not have been possible without the help and contributions of a great number of people around me.

First and foremost I want to thank my two supervisors Dario Floreano and Jean-Christophe Zufferey for guiding me in my transition from an engineer to a scientist. Dario provided me with a dynamic and enriching workplace in which to do my research and taught me the importance of communicating my research beyond my little corner of the lab. His easygoing attitude and dedication to science showed me where my work fits into the much bigger picture of scientific advancement. I owe a particular debt of gratitude to my co-supervisor Jean-Christophe, whom I consider my personal mentor on all things flying and robotic. I am constantly amazed and inspired at his particular ability to ask the right questions that help me fill the holes in my work and am grateful for his time in correcting my manuscript.

Two of my colleagues, Adrien Briod and Ludovic Daler, were instrumental in the development of the platforms presented in this thesis. I fondly remember the long nights we spent in the workshop and experimentation rooms building, coding, flying, breaking and fixing robots together. Adrien's rigorous math and physics skills and Ludovic's knowledge of mechanics were the perfect complement to my electronics background and allowed us to build better platforms together than I could ever make on my own. The weekends and late nights they both spent in the last months to help me finalize my experiments will not be forgotten.

My other colleagues at the Laboratory of Intelligent Systems also deserve my gratitude, especially those who took the time to help with the redaction of this thesis in its last weeks, including Steffen Wischmann, Bryan Schubert, Ramon Pericet, Felix Schill and Przemek Kornatowski. To all the others, thank you for the cooking battles and evenings at Sat that kept me sane.

Acknowledgements

Abstract

Flying robots have the unique advantage of being able to move through the air unaffected by the obstacles or precipices below them. This ability quickly becomes a disadvantage, however, as the amount of free space is reduced and the risk of collisions increases. Their sensitivity to any contact with the environment have kept them from venturing beyond large open spaces and obstacle-free skies. Recent efforts have concentrated on improving obstacle detection and avoidance strategies, modeling the environment and intelligent planning to navigate ever tighter spaces while remaining airborne. Though this strategy is yielding impressive and improving results, it is limited by the quality of the information that can be provided by on-board sensors.

As evidenced by insects that collide with windows, there will always be situations in which sensors fail and a flying platform will collide with the obstacles around it. It is this fact that inspired the topic of this thesis: enabling flying platforms to *survive and recover from* contact with their environment through intelligent mechanical design. There are three main challenges tackled in this thesis: robustness to contact, self-recovery and integration into flight systems.

Robustness to contact involves the protection of fast-spinning propellers, the stiff inner frame of a flying robot and its embedded sensors from damage through the elastic absorption of collision energy. A method is presented for designing protective structures that transfer the lowest possible amount of force to the platform's frame while simultaneously minimizing weight and thus their effect on flight performance. The method is first used to design a teardrop-shaped spring configuration for absorbing head-on collisions typically experienced by winged platforms. The design is implemented on a flying platform that can survive drops from a height of 2 m. A second design is then presented, this time using springs in a tetrahedral configuration that absorb energy through buckling. When embedded into a hovering platform the tetrahedral protective mechanisms are able to absorb dozens of high-speed collisions while significantly reducing the forces on the platforms frame compared to foam-based protection typically used on other platforms.

Surviving a collision is only half of the equation and is only useful if a flying platform can subsequently return to flight without requiring human intervention, a process called *self-recovery*. The theory behind self-recovery as it applies to many types of flying platforms is first

Abstract

presented, followed by a method for designing and optimizing different types of self-recovery mechanisms. A gravity-based mechanism is implemented on an ultra-light (20.5 g) wing-based platform whose morphology and centre of gravity are optimized to always land on its side after a collision, ready to take off again. Such a mechanism, however, is limited to surfaces that are flat and obstacle-free and requires clear space in front of the platform to return to the air. A second, leg-based self-recovery mechanism is thus designed and integrated into a second hovering platform, allowing it to upright into a vertical takeoff position. The mechanism is successful in returning the platform to the air in a variety of complex environments, including sloped surfaces, corners and surface textures ranging from smooth hardwood to gravel and rocks.

In a final chapter collision energy absorption and self-recovery mechanisms are integrated into a single hovering platform, the first example of a flying robot capable of crashing into obstacles, falling to the ground, uprighting and returning to the air, all without human intervention. These abilities are first demonstrated through a contact-based random search bahaviour in which the platform explores a small enclosed room in complete darkness. After each collision with a wall the platform falls to the ground, recovers and then continues exploring. In a second experiment the platform is programmed with a basic phototaxis behaviour. Using only four photodiodes that provide a rough idea of the bearing to a source of light the platform is able to consistently cross a 13x2.2 m corridor and traverse a doorway without using any obstacle avoidance, modeling or planning.

Keywords: *Flying robots, contact energy absorption, robustness, self-recovery, uprighting, indoor exploration, minimal sensing*

Résumé

Les robots volants ont l'avantage unique de pouvoir se déplacer dans l'air sans être affectés par les obstacles ou précipices se situant au-dessous. Néanmoins, cet avantage se réduit vite lorsque l'espace de vol devient limité, et que le risque de collision augmente. Leur sensibilité aux contacts avec leur entourage les a empêchés de s'aventurer ailleurs que dans de grands espaces libres de tout obstacle. Récemment, les efforts se sont concentrés sur des stratégies de détection et d'évitement d'obstacles, impliquant la modélisation de l'environnement et le suivi de trajectoires permettant de les contourner afin de rester en l'air. Même si ces stratégies permettent d'obtenir des résultats impressionnants, elles sont limitées par la qualité des informations qui sont fournies par les capteurs embarqués.

Comme on peut l'observer chez les insectes qui entrent en collision avec les fenêtres, il existe toujours des situations où les capteurs ne fonctionnent pas, et où la plateforme peut entrer en collision avec les obstacles environnants. C'est en s'inspirant de cela que le sujet de cette thèse est né : permettre aux plateformes volantes de survivre et de se rétablir suite aux contacts avec leur environnement, grâce à l'intelligence de la conception mécanique. Cette thèse adresse trois défis principaux : la robustesse aux contacts, le rétablissement après une collision et l'intégration du tout sur une plateforme volante.

La robustesse aux contacts implique la protection des hélices tournant à haute vitesse, du corps rigide du robot ainsi que des capteurs embarqués, grâce à l'absorption élastique de l'énergie des collisions. Une méthode pour la conception de structures protectives permettant de minimiser la force transmise au corps de la plateforme tout en gardant le poids minimum est présentée. La méthode est d'abord appliquée à la conception d'une structure en forme de goutte d'eau permettant d'absorber l'énergie des collisions frontales typiquement subies par des plateformes à ailes fixes. C'est ainsi qu'une première plateforme volante utilisant cette structure et pouvant supporter des chutes de 2 mètres de hauteur est réalisée. Un deuxième design est ensuite présenté, cette fois utilisant des structures tétraédriques qui absorbent l'énergie par flambage. Lorsque cette protection est utilisée sur une plateforme volant en mode stationnaire, les structures de protection tétraédriques permettent d'absorber l'énergie de douzaines de collisions à haute vitesse, tout en réduisant de manière significative les forces transmises au corps du robot comparé à une protection en sagex typiquement utilisée sur d'autres plateformes.

Résumé

Survivre aux collisions n'est que la moitié du travail, car cela est utile uniquement si la plateforme peut se rétablir, c'est-à-dire retourner en vol sans intervention humaine. La théorie permettant le rétablissement de plusieurs types de plateformes volantes est d'abord présentée, suivie d'une méthode pour concevoir et optimiser différents types de mécanismes de rétablissement. Un premier mécanisme basé sur la gravitation est utilisé sur une plateforme à aile fixe ultralégère (20.5 g), dont la morphologie et le centre de masse sont optimisés pour toujours atterrir sur le côté après une collision, en position de décollage. Un tel mécanisme est néanmoins limité aux sols plats et sans obstacles sur une certaine distance en face de la plateforme afin de permettre le décollage. C'est pourquoi un deuxième mécanisme utilisant des pattes pour le rétablissement est donc conçu et intégré à une deuxième plateforme capable de voler en mode stationnaire, les pattes permettant de la redresser en position verticale appropriée au décollage. Ce mécanisme permet de redresser avec succès la plateforme dans des environnements variés, y compris des surfaces inclinées, des coins et des sols allant du plancher lisse aux graviers et cailloux.

Dans le chapitre final, l'absorption de l'énergie et les mécanismes de rétablissement sont intégrés dans une plateforme unique, démontrant pour la première fois pour un robot volant la capacité de rentrer en collision avec les obstacles, de tomber par terre, de se redresser et retourner en l'air, le tout sans aucune intervention humaine. Ces capacités sont dans un premier temps démontrées par un comportement d'exploration aléatoire basé sur les contacts, et par lequel la plateforme explore une petite salle dans une obscurité totale. Après chaque collision avec un mur, la plateforme tombe par terre, se rétablit puis continue l'exploration. Lors d'une deuxième expérience, le robot est programmé avec un comportement de suivi de lumière basique. En utilisant uniquement quatre photodiodes indiquant grossièrement la direction de la source lumineuse, la plateforme est capable de traverser un corridor de 13x2.2 m et de traverser un pas de porte sans aucun mécanisme d'évitement d'obstacle, de modélisation ou de planification de trajectoire.

Mots-clés : *Robot volant, absorption d'énergie de collision, robustesse, rétablissement, redressement, exploration d'intérieurs, capteurs simples*

Contents

Contents

1 Introduction

Flying robots have great potential in the exploration of confined and cluttered spaces inaccessible to humans, but at the moment are ill-adapted to the specific constraints of flight in close proximity to obstacles. This introductory chapter begins with a review of current navigation and obstacle avoidance methods, their failure in highly cluttered environments and presents the challenges inherent to flight in cluttered environments, specifically in the mechanical design of flying robots. A state of the art subsequently describes the most recent work in the field of platform protection and self-recovery after collisions with obstacles. Finally the main contributions of this thesis are stated and followed by an outline of the work to come.
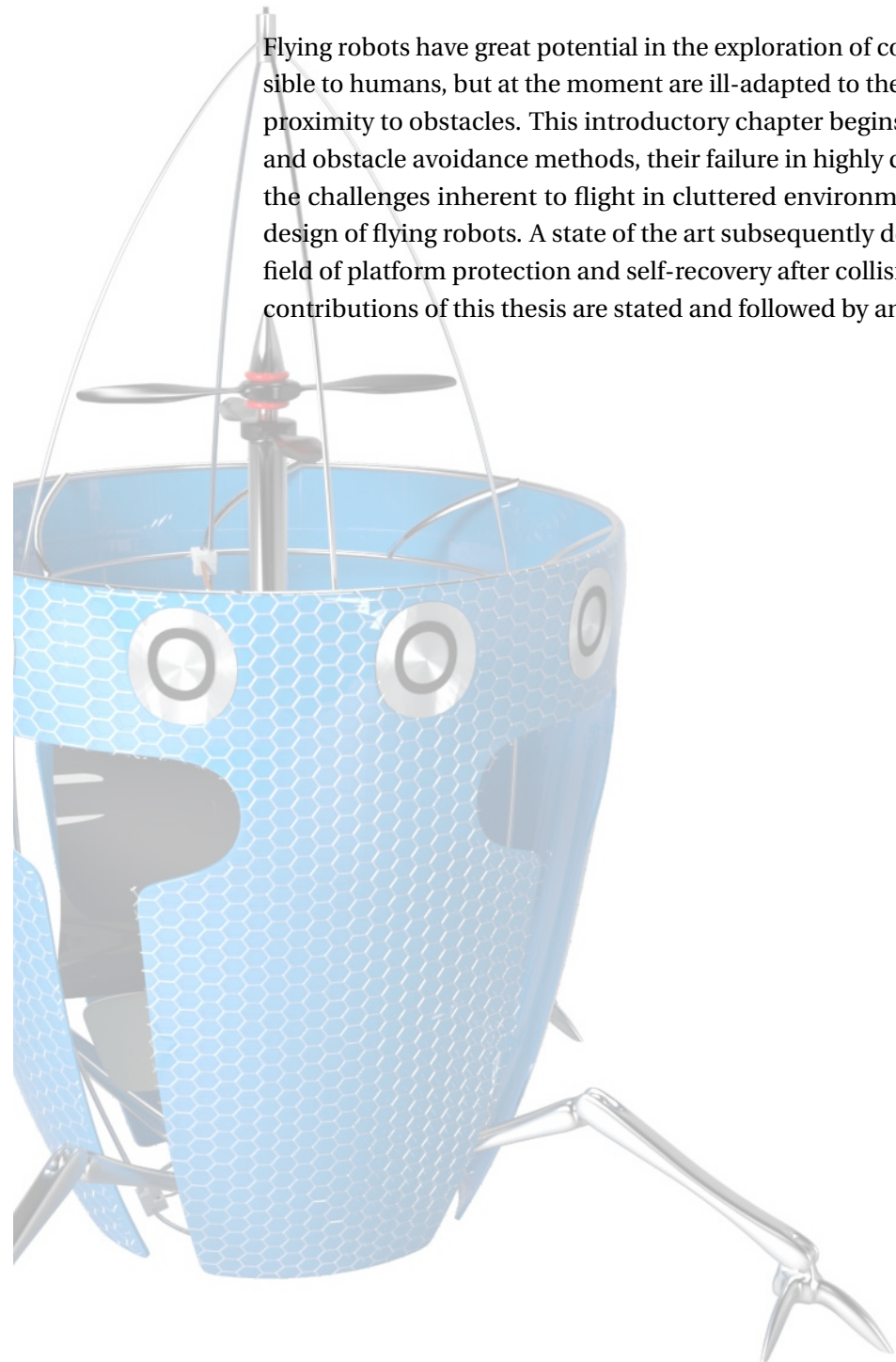
Figure 1.1: An artist's impression of the inside of a damaged building. The ability of flying robots to access elevated areas and pass over rubble on the ground make them uniquely suited for exploring such environments.

1.1 Motivation and Challenges

In the last decade flying robots have evolved from being the dreams of science fiction to mature aerial sensor platforms deployed in an increasing variety of applications [1, 2]. Recent advances in the miniaturization of electronics and sensors driven by the mobile computing industry, along with the constant evolution of energy storage and composite materials, have enabled ever smaller hovering platforms. Though infamous for their use by the military, Unmanned Aerial Vehicles (UAVs) are increasingly being used in civilian applications as diverse as aerial photography and photogrammetry [3], automatic detection of forest fires [4] and even the transportation of medical samples in rural Africa [5]. In all these applications flying robots navigate in open, obstacle free environments and have access to precise localization data through the Global Positioning System (GPS).

Flight as locomotion is particularly interesting in the exploration of cluttered environments such as the damaged building depicted in Fig. 1.1 as it can provide human operators with an elevated viewpoint of places otherwise inaccessible to people. Flying robots are not constrained by the morphology of the ground and can be used to navigate across rubble, through staircases or up elevator shafts much quicker than ground-based robots.

Practical applications for the aerial exploration of cluttered environments are common. On March 11, 2011 a tsunami destroyed large portions of the Japanese coast and rendered a nuclear power plant unstable. High levels of radiation kept human rescuers from entering the plants, and ground robots had trouble surmounting the large amounts of rubble on the ground[1]. A single Honeywell T-Hawk UAV[2] was used for aerial imagery outside the plant, but was unable to penetrate inside the plant due to its large size[3]. In February of the same year an earthquake in Christchurch, New Zealand, caused extensive damage to the city. In what was one of the first uses of a flying robot inside a building in a disaster situation, rescuers used a commercially-available Parrot AR.Drone [6] to fly into a collapsed church to assess the damage inside, though were unable to venture beyond the large open church hall. UAVs have also been proposed for use in mine rescue and recovery [7], though their current limitations are best described by the paper's author:

> In theory, UAVs could be used for the Side Entry scenario, though in practice, ... how they could operate in total darkness and avoid protrusions from the roof are unanswered questions. [7]

Indeed, as opposed to flight outdoors and in large open spaces, indoor flight poses several additional challenges to navigation. Precise positioning is difficult due to the absence of GPS along with low visibility due to smoke or the lack of light. The presence of a large number of irregular obstacles and the fragility of current flying systems to any impact, make the survival in such an environment for most flying systems next to impossible. Developing innovative designs and methodologies to enable UAVs for flight in such cluttered, difficult indoor environments is the goal of this thesis.

Though having some success, current obstacle avoidance methods are far from robust even in ideal conditions. As the size of the environment shrinks, obstacles multiply and visual conditions deteriorate, collisions with obstacles become inevitable. In fact even nature's most successful flyers such as insects, though capable of impressive flight indoors, still frequently crash into obstacles such as windows and low-contrast walls. As opposed to flying robots however, insects can withstand repeated collisions and can use their legs and wings to return to the air [8, 9].

It is this fact that brings about the main focus of this thesis: if contact with obstacles is unavoidable, then the platform must be designed to survive and recover from this contact. There are three main challenges resulting from this conclusion:

---

[1] A great summary of a blog written by a ground robot operator at Fukushima can be found at http://goo.gl/EMfWm, accessed 21.05.2012.

[2] http://www.thawkmav.com/, accessed 24.04.2012

[3] Some videos taken by the T-Hawk can be seen at http://goo.gl/Pk7Mj, accessed 21.05.2012. Another interesting online article discusses the lack of flying robots at Fukushima: http://goo.gl/Ks2X6, accessed 21.05.2012.

- **Robustness to Contact:** The mechanical structure of the platform must be robust to repeated physical contact with the environment, whether from the slightest brush against a wall to a high-energy impact resulting from a free-fall from an elevated position.

- **Self-Recovery**: Surviving a collision is only useful if the platform can keep flying. It must be able to return to the air from any possible landing position without human intervention.

- **Integration with Flight Systems**: Perhaps the most difficult challenge is to integrate robustness and self-recovery into a platform that is still capable of flying. This requires minimizing the weight and power requirements of the additional mechanisms and placing them intelligently within the structure of the platform to limit their effect on the platform's centre of gravity (COG) and aerodynamics.

Only after a flying platform can consistently absorb multiple bumps with walls and objects and take off again after falling will it be able to fulfill complex missions in real human environments truly autonomously.

1.2 State of the Art

Flying robot is a broad term that can be applied to autonomous platforms that travel through the air using a variety of locomotion modes and span several orders of magnitude in size and weight. The challenges presented above, however, limit the types of platforms that can be used in cluttered environments.

The final goal of this thesis is to design a flying system that can autonomously navigate within an environment originally intended for use by humans and as such features hallways, doorways, windows and stairwells. We thus limit the size of the platform to <100 cm in its largest dimension. Though there is no minimum size, current limitations in energy storage, miniaturized control electronics and sensing required for autonomous flight [10] keep fully autonomous platforms smaller than 10 cm out of reach. There is no limit to the weight of the platform, but as will be explained in Ch. 2 higher weight translates to higher-energy impacts, and thus this thesis focuses on low-weight platforms.

To fly in cluttered environments a platform must be able to hover in place or travel at low speeds and be highly maneuverable to avoid obstacles when necessary. There are many types of flying vehicles, such as airships, wing-based airplanes, flapping-wing platforms, and various configurations of rotorcraft, all of which present their particular advantages and drawbacks. There are also other types of robots that travel through the air, such as jumping [11, 12] or gliding [13, 14] robots. Although they encounter similar challenges and can provide design inspiration, they represent a different field of research and are beyond the scope of this thesis.

Airships have been used extensively in robotics research [15, 16] because of their ability to naturally float in the air, requiring little power to move around. They have a very poor

volume-to-lift ratio and a large inertia, however, making them difficult to maneuver and impractical in cluttered environments. Flapping-wing platforms [17, 18] have had success on small scales due to their ability to fly in both forward flight and in hover, and are particularly inspiring to researchers due to their similarity to biological systems. On the downside, at the scales considered in this thesis they are less efficient than rotary platforms [19, 20], and more importantly are mechanically complex and their wings are difficult to protect in case of collisions with the environment.

There remain two classical types of platforms: wing-based [21, 22, 23] and rotor-based [24, 25, 26]. Compared to rotorcraft, wing-based platforms are more efficient in forward flight [27] but require a minimum forward speed to remain aloft [28]. Rotorcraft can hover and are highly maneuverable but require more energy since they must create all their lift using their rotor. As they share the same basic source of actuation (a motor with a propeller) there are also many possibilities to combine the two modes in a single platform [29]. Both types of platforms have been used extensively in indoor flight and constitute the core body of work presented in this state of the art as well as the prototype designs presented in this thesis.

This section begins with a review of the latest work in localization and obstacle avoidance, as it's the main strategy currently used by researchers to access confined spaces with flying robots. Current methods of protecting platforms from collisions are then presented, followed by some examples of self-recovery in flying and jumping robots.

1.2.1 Localization and Obstacle Avoidance

As opposed to withstanding collisions, most approaches taken so far in indoor flying robotics have looked at actively avoiding them. Several sensor modalities have been proposed for detecting obstacles of varying sizes. In the simplest cases, one or several discrete distance sensors pointed in specific directions can be used to detect the global presence of an obstacle. Infrared (IR) triangulation [30] or ultrasonic (US) [31] sensors have been used for obstacle avoidance, but are relatively heavy and have high power requirements, and are thus ill-suited for flying platforms in large numbers. Discrete optic flow[4] sensors such as those found in optical computer mice are much smaller and low-power, and have demonstrated obstacle avoidance on platforms as light as 10 g, notably on the ultra-light microflyer presented in [32]. Optic flow, however, is very dependent on surface texture and fails to detect transparent and low-contrast objects. The main drawback of using discrete sensors is that they can only detect obstacles in a limited number of directions defined by the number of sensors used.

A greater number of obstacles can be detected either by placing a discrete sensor on a mechanical scanner or by using wide-angle sensors such as visual or IR cameras. Recent advances in lightweight laser scanners, cameras and embedded computation have enabled great strides in Simultaneous Localization and Mapping (SLAM). Rather than avoiding obstacles reactively as they're detected, platforms running SLAM algorithms can map all the obstacles in their sur-

---

[4]Optic flow is a vision-based technique for extractive distance information from vision field motion.

roundings before planning a path to avoid them. Impressive results have been demonstrated outdoors where large platforms are capable of carrying heavy payloads. The modified Yamaha RMax presented in [33] has a payload of 29 kg, enough to mount a custom 3D laser scanner and a full Pentium-based linux computer for on-board processing. For indoor platforms where payload is more limited, the Hokoyu miniature laser range finder is the most popular sensor for high-density obstacle detection, used predominantly on quadrotor hovering platforms [25, 34, 24]. The sensor's weight (160 g) and power requirements (2.5 W), along with the significant computational requirements of SLAM algorithms, reserve this technique to larger platforms with weights above 500 g. SLAM has also been demonstrated using cameras [35], a much lighter alternative to laser scanners. Extracting distance information from visual data is much noisier than from a laser scanner, however, and is dependent on light and contrast in the environment.

The ability of an algorithm to detect obstacles is also dependent on the quality of the information provided by the sensors. Low light limits the use of visual and even IR cameras, whereas smoke and suspended dust can corrupt the readings of active range-finders such as lasers, radars and IR triangulation sensors. Multi-modal sensing that merges information from multiple redundant sensors can mitigate some environmental effects, as shown on the Shrimp [36] or Argo [37] ground robots, or more recently on a quadrotor [24]. Multiple sensors translate to increased weight and computation, and thus larger and more dangerous systems.

Alternately, in the absence of light a platform can create its own light. For example, in [38] a quadrotor is mounted with a laser circle projector and a fisheye camera to estimate altitude in dark environments. Though removing the need for light, such a system still suffers from susceptibility to smoke and cannot be used to detect obstacles all around the robot.

1.2.2 Collision Protection

As opposed to the fragility of most current flying robots, nature has evolved flying animals robust to collisions and provides some inspiration for protective structure design. Flying insects have a very low mass to air drag ratio, thus never achieving high impact forces during free-fall [42]. Their rigid exoskeletons are compliant enough to absorb these minimal forces. Small microrobots such as the RoACH [43] walking robot or the RoboBee [44] miniature flying robot have similar properties. As animals grow in size however air drag can no longer limit impact energy, as their mass increases cubically whereas their surface area only increases quadratically [45]. The hard exoskeletons of insects give way to the endoskeletons of vertebrates surrounded by soft tissue better adapted for impact energy absorption [46], though not without damage in the form of bruising and broken bones.

Similarly to nature and its endo- and exoskeletons, in the domain of flying robots existing solutions to collision protection can be categorized into two broad types of structures: stiff bump protection and flexible protection. Stiff protection is the most common strategy and is sufficient for protecting spinning propellers from low-energy contact. Many commercial

Stiff protection

A   B   C

D   E
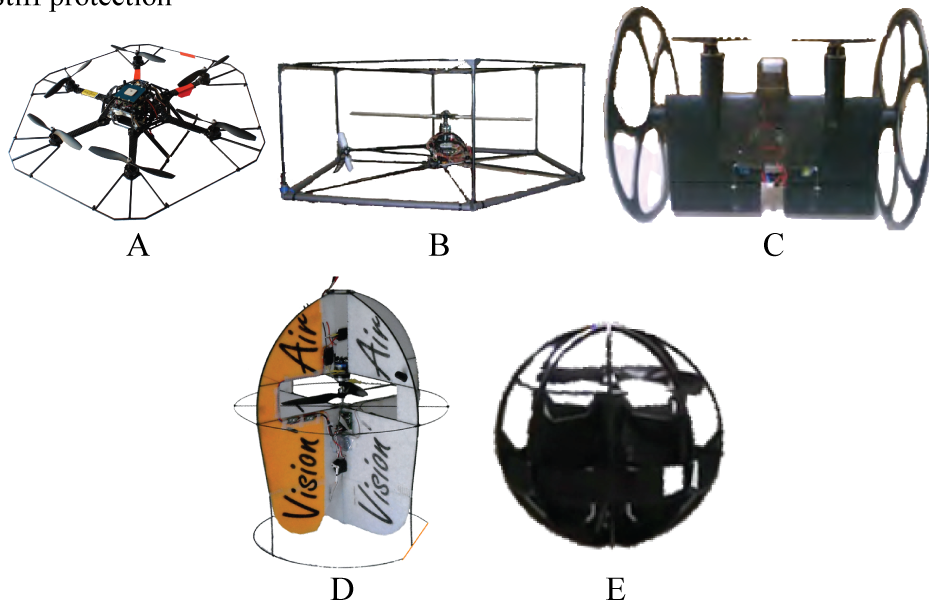
Flexible protection

F   G   H

I   J
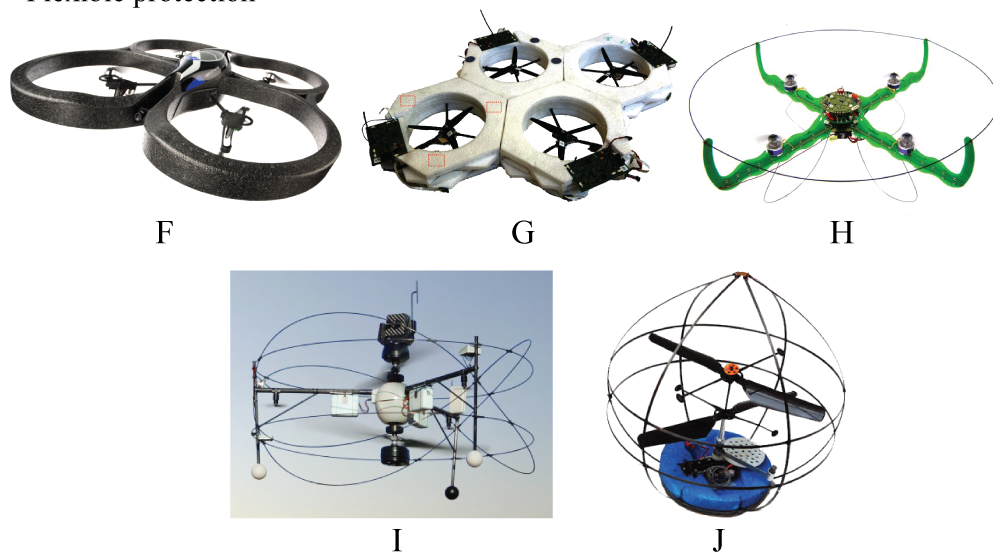
Figure 1.2: Some examples of the different types of protection mechanisms used on flying robots. Top, robots that use a rigid frame and stiff protection mechanisms to survive low-intensity contact. (A) Ascending Technologies Firefly with fiberglass protection of its six propellers. (B) A single-rotor helicopter [39] with a stiff carbon frame. (C) MAVion offshoot RollFly [29] with wheels used simultaneously as propeller protection. (D) Vision'Air and (E) the JSDF spherical robot, two coaxial robots that protect their propellers within their hard outer frame. Bottom, robots that use flexible protection mechanisms to absorb collision energy. (F) AR.Drone [6] and (G) Distributed Flight Array [40], two examples of foam propeller protection. (H) A quadrotor [30], (I) the FanCopter and (J) the Hopping Rotochute [41], three examples of using carbon fibre rods in circular shapes to make a protective cage around a flying robot.

platforms, such as the Ascending Technologies Firefly[5] (Fig 1.2A), come with *indoor flight conversion kits*, essentially stiff protection that can be mounted around propellers for protection from side impacts. Other platforms extend the idea to three dimensions, such as the single-rotor helicopter presented in [39] (Fig. 1.2B) which is surrounded by a cage made of carbon tubes, protecting from impacts in all directions. In a more original design, a modified version of the dual-rotor MAVion called RollFly [29] (Fig. 1.2C) features two wheels that both protect the rotors from contact and can be used to roll on the ground or even along the wall or ceiling when in flight. Finally, the Vision'Air built at the ISAE[6] (Fig. 1.2D) and a spherical robot built at the JSDF[7] (Fig. 1.2E) are two examples of platforms designed specifically with collision robustness in mind. Both of these coaxial design house their propellers within the robots stiff outer structure and thus protected from collisions. The major drawback of stiff protection is the high forces that are produced at the impact point and transferred directly to the platform's frame.

Soft protection typically takes the form of either compressible materials such as foam or deformable cages made up of thin components such as carbon fibre rods. A typical example is the mobile-phone-controlled AR.Drone [6] (Fig. 1.2F) which has a 2 cm-thick foam hull to protect its propellers. A styrofoam frame is also used by the Distributed Flight Array [40] (Fig. 1.2G), a unique flying robot made of individual single-propeller modules that cannot fly by themselves but can connect to other modules and thus create different multi-rotor systems. Foam is an improvement to stiff protection, as it increases absorption distance and distributes the force over a larger area. Its low stiffness, however, make it inefficient for absorbing large amounts of energy. The protection around the AR.Drone, for example, increases the 370 g platform's weight by 60 g, but a force of only 6 N[8] results in a deformation of the structure sufficient to contact the propeller. A further disadvantage to foam is its fragility, as its main energy absorption mechanism is the crushing of the foam [47]; though it may survive several collisions, repeated impacts progressively reduce the energy it can absorb.

Another popular protective structure solution is using one or several flexible carbon rods to absorb collision energy. Compared to foam, carbon is stiffer for a similar weight and is thus more efficient in absorbing energy (see Sec. 2.2.2 for a more detailed description of material properties). The quadrotor presented in [30] (Fig. 1.2H) uses a single rod for propeller protection, though it is only dimensioned for minor bumps and would not survive a high-speed collision. The commercial multi-rotor FanCopter[9] (Fig. 1.2I) extends this idea to several rods around the platform for better protection. Finally, the Hopping Rotochute [41] (Fig. 1.2J), a hybrid flying-jumping platform, completely surrounds its two coaxial rotors with a carbon fibre cage, protecting it from contact in all directions. This solution has been used on several jumping robots as well, such as the Jollbot [48] or the EPFL jumper [49], as they

---

[5]http://www.asctec.de/home-en/, accessed 24.04.2012

[6]Institut Supérieur de l'Aéronautique et de l'Espace, http://recherche.isae.fr/fr/cas/les-activites-aeronautiques, accessed 07.05.2012

[7]Japan Ministry of Defense, http://www.mod.go.jp/e/index.html, accessed 07.05.2012

[8]The force is applied on the edge of one of the protection rings towards the centre of the platform.

[9]EMT Penzberg, http://www.emt-penzberg.de/index.php?10, accessed 07.05.2012

must be capable of absorbing impact energy if they are to jump again and thus provide some inspiration.

The use of bent circular springs around a platform has the advantage of absorbing collision energy through several interconnected springs instead of a single one. A major disadvantage of such a system, however, is that the rods used to produce the cage are sourced as straight rods and must be bent into a circular shape, storing energy that cannot be recovered until the cage is disassembled. As every material has a maximum strain it can absorb, this initial strain reduces the additional collision energy that the rods can absorb before failure and is thus not an efficient use of the material. A second problem arises from their manner of deflection; when a circular spring contacts a flat surface it creates inflection points which a much higher radius of curvature, and thus failure-inducing stress, than the rest of the spring.

1.2.3 Self-Recovery

When flying in a cluttered environment, detecting and surviving a collision is not sufficient to navigate from one point to another; sooner or later a collision will result in a fall to the ground, and thus the platform must be able to recover from the crash and return to the air. This process of autonomously returning to flight after a collision that causes a fall to the ground is referred to as *Self-Recovery*.

Several flying platforms exhibit the capability of perching (that is controlled landing on a predefined surface) and subsequently taking off again. Most hovering platforms for example have landing gear and can land on and take off from flat surfaces, in some cases even autonomously [56, 57]. The helicopter presented in [58] takes this idea further by landing on angled surfaces, though always in a controlled manner and on its landing gear. The MMALV [50] (Fig. 1.3A), a small fixed-wing platform with wheel-legs, can land on a flat surface but can only take off again from an elevated position and with a sufficient runway. A glider capable of attaching to a vertical wall and subsequently detach has also been demonstrated [51] (Fig. 1.3B), as was a powered airplane that can actively return to flight after attachment [52] (Fig. 1.3C). All of these systems, however, can only take off if they land in a predefined position and generally cannot return to flight from any arbitrary position. No provisions are made for landing upside-down, or for collisions with obstacles that cause loss of flight control.

Jumping robots that locomote through consecutive jumps have considered the problem of righting themselves after falling to the ground to prepare for subsequent jumps and thus provide some inspiration. The EPFL jumper [11] (Fig. 1.3D) and the Jollbot [53] (Fig. 1.3E) are two examples of gravity-based self-recovery, using spherical cages and specific placement of COG to roll into takeoff position. All gravity-based mechanisms suffer from the same drawbacks, however, requiring flat and obstacle-free ground to properly upright. Some jumping robots use active mechanisms to upright themselves, such as a series of robots designed by NASA [54] (Fig. 1.3F) that use direct actuation of flaps to stand up. The mechanism only works in some landing positions, however, and is not optimized for weight, which is an important

Flying robots that can land and takeoff again
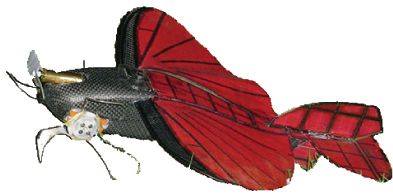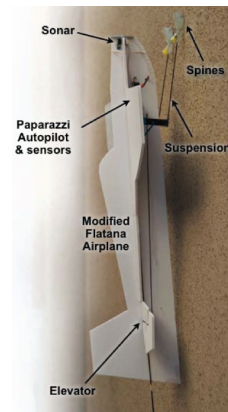
A   B   C

Jumping robots that can upright
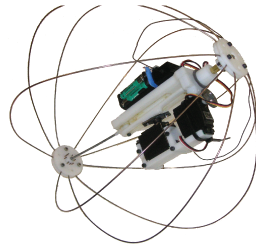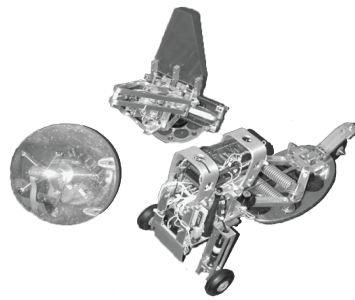
D   E   F

Flying robots that can land, upright and takeoff again

G

Figure 1.3: Top, robots that can land and take off again in specific orientations and from specific surfaces: (A) The MMALV [50], capable of taking off from elevated surfaces with a runway. (B) Glider [51] capable of attaching to vertical surfaces. (C) Scansorial flying platform [52] capable of landing on and taking off from vertical surfaces. Middle, jumping robots that can self-recover: (D) EPFL Jumper [11], (E) Jollbot [53] and (F) three generations of jumping robots with active uprighting [54]. Bottom, (G) flying Scout robot [55] capable of uprighting and limited flight.

consideration for flying systems. Though providing some inspiration, jumping robots do not have to worry about aerodynamic constraints on their COG inherent to flying systems.

To the best of our knowledge, the only flying robot to explicitly consider the problem of self-recovery is a flying version of the Scout wheeled robot [59] (Fig. 1.3G) that features an extendable leg meant to upright the platform before flight. This platform, however, is primarily designed as a ground platform, and thus has very limited flight capabilities; a first version [59] was not able to successfully fly with its uprighting mechanism, and an improved second version [55] has not advanced beyond the design stage.

1.3 Main Contributions and Thesis Organization

This thesis brings together elements from such varied fields as mechanical engineering, aerodynamics, electronics, robotics and control theory to design small flying platforms capable of navigating cluttered environments currently inaccessible to robots. This thesis is organized around the three main challenges that it addresses, and the subsequent contributions that are presented.

Chapter 2 discusses the problem of absorbing collision energy. A method is presented for designing and optimizing *elastic* energy-absorbing protective structures and integrating them into the mechanical structure of a flying robot. It begins by describing the different types of springs that can be used to mechanically absorb energy as well as the materials best suited for the task. The method is successfully applied to a winged platform that is optimized to absorb head-on collisions when in forward flight. The platform is tested using high-speed video, demonstrating its ability to survive collisions in a single direction. A second platform is then designed for absorbing collisions of equal energy in all directions using Euler springs[10] in a tetrahedral configuration. The platform is tested extensively in dozens of drop tests and through autonomous flight in a small room, where it consistently survives contact with obstacles and the ground.

Chapter 3 formalizes the theory of self-recovery as it applies to flying robots and presents a method for designing different self-recovery mechanisms that prepare a platform for takeoff. The method is first applied to a winged platform whose morphology and COG placement is optimized for forward flight and gravity-based self-recovery. Though successfully demonstrated on flat ground, the gravity-based mechanism is sensitive to the presence of obstacles in the environment. A second platform is thus presented that complements the gravity-based self-recovery with an active leg-based mechanism. This platform represents the first example of a flying robot able to consistently upright from any position on the the ground and take off in a variety of environmental conditions, including sloped and textured surfaces ranging from hardwood to rocky ground.

---

[10]Euler springs are long columns that absorb energy through buckling when they are loaded axially. They are explained in detail in Chapter 2.

Chapter 4 unites the previous two chapters in the design of a single flying robot that can both absorb collisions and self-recover. The resulting robot is the first example of a platform capable of surviving high-energy collisions with obstacles, uprighting itself in complex environments and returning to flight without human intervention. The platform is demonstrated through two novel navigation strategies adapted to its unique abilities. In a first experiment the platform explores a room using contact-based random search in complete darkness where vision-based navigation is not possible. The fully-autonomous behaviour is then extended to the traversing of a long corridor using the light detected by four photodiodes as the only source of directional information. Though the platform often comes into contact with the walls of the corridor, its ability to survive and recover from collisions allow it to successfully reach the end of the corridor without the use of any obstacle detection, localization or mapping.

Chapter 5 concludes the thesis and reiterates the main conclusions that were drawn in the work. As no thesis is truly ever finished, some ideas of future avenues of research enabled by this work are presented.

Beyond the main topic of the thesis, Appendix A presents the 11 prototypes in chronological order that were designed, built and tested throughout the work. Each prototype's contribution to the work is described to give the reader a sense of the iterative design process that yielded the final platform. It should be noted that although all the platforms presented in this thesis can fly, optimizing the performance of their drivetrain or their specific aerodynamic characteristics is not the focus of this thesis. The selection of motor, gearbox and propeller combinations for maximum efficiency and flight time is a problem already tackled by many other researchers [60, 61, 62, 63] and is thus not developed further. Similarly, the flight performance of the presented platforms could surely be improved through aerodynamic modeling and wind tunnel testing [29, 64], though this would not improve the collision energy absorption and self-recovery mechanisms developed in this work.

2 Absorbing Collision Energy

This chapter addresses the challenge of protecting a flying robot from the high impact energy of collisions with obstacles or the ground due to a free fall. The chapter begins by describing the need for protective structures, proposing a method for their design and describing common spring types and materials that can be used. The method is then applied to a wing-based platform that can survive head-on collisions with the ground when dropped from a height of 2 m. The chapter concludes with the design of protective structures using springs in a tetrahedral configuration applied to a small hovering platform, allowing it to survive dozens of high-energy collisions with its environment.

This chapter is partly based on the publication *Elastic Collision Protection for Flying Robots Using Euler Springs* [65].
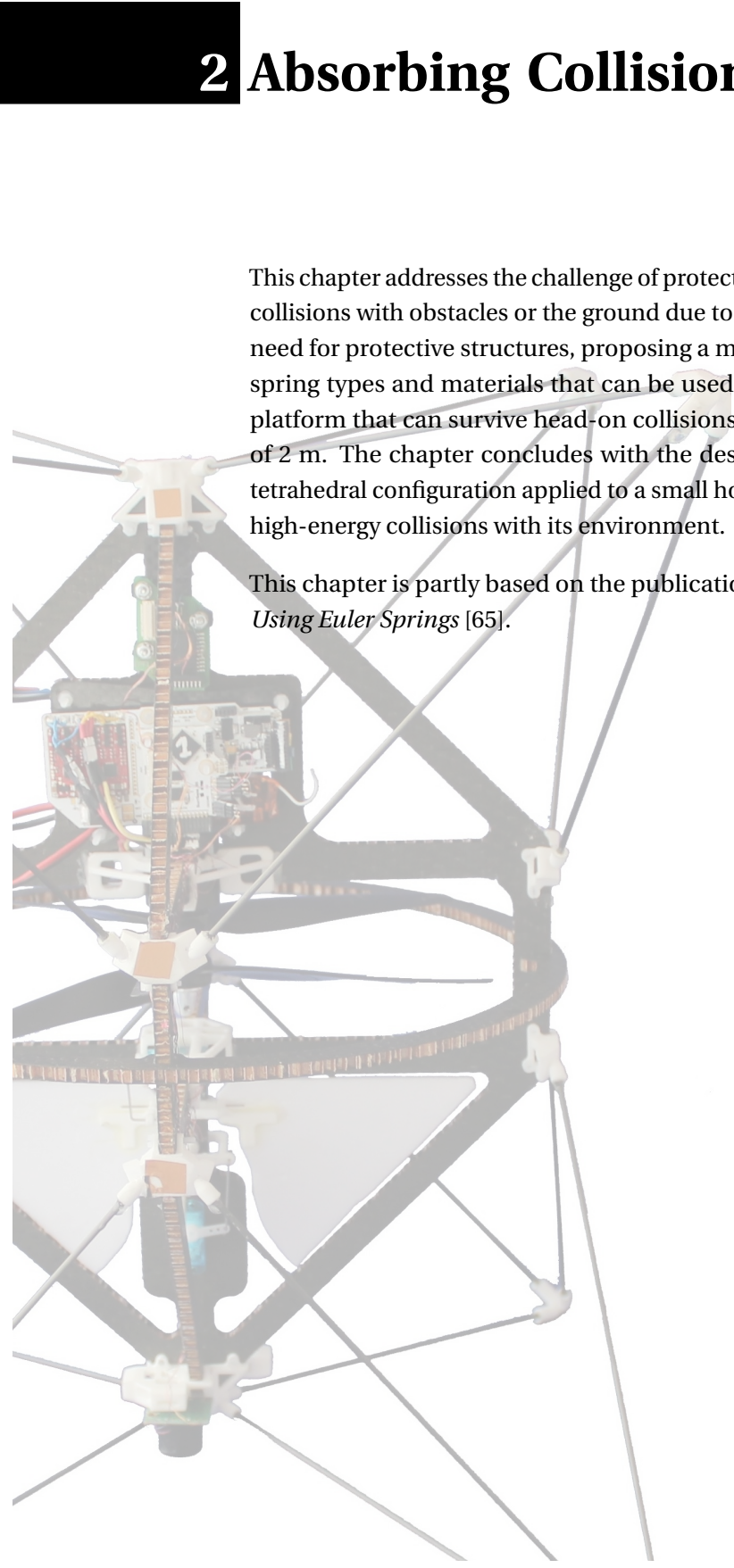
2.1   The Need for Elastic Protection Mechanisms

Propeller-based flying platforms require a stiff inner frame, as their aerodynamics depend on the geometric positions and angles between rotors, the COG and/or control surfaces. Perhaps more importantly, flight motors cannot be allowed to flex out of plane in relation to the robot's frame to prevent fast-spinning propellers from contacting other parts of the platform. The main requirement of protective structures on a flying robot is thus to shield this frame, the sensitive components mounted on it and the spinning propellers from damage resulting from a collision.

Many current platforms use stiff protection mechanisms attached to an equally stiff frame to absorb collision energy through compression of the material [39, 29]. Though resistant to low-energy collisions and simple to design, stiff protection transfers all the impact energy of a collision to the platform's frame. As the absorption distance is minimal, the force on the structure quickly reaches high values and anything beyond a low-speed bump can cause inelastic damage to the frame.

This is particularly a problem during the repeated collisions a flying robot is likely to encounter in a cluttered environment. In the case of carbon fibre, the most common material used for the frame of current platforms, impact damage is directly related to the impact force on a structure [66] and can cause extensive de-lamination and matrix shear cracking [67]. A single impact is enough to reduce the residual strength of the material [68], making it more vulnerable to subsequent collisions. In addition to compression forces on the structure, impact force on a stiff protection mechanism can cause high torques on its connection point to the robot's frame, often failing at these points. Some platform minimize this damage by using "mechanical fuses" such as nylon screws or rubber bands around propellers which can be easily and quickly replaced. Though preventing expensive damage, a single impact still renders a platform unusable without human intervention.

As opposed to the stiff protective structures currently used in most flying platforms, nature has evolved flying organisms with bodies resilient to multiple impacts. The stiff inner skeleton of birds and other vertebrates is surrounded by soft tissue which absorbs energy during impact. As an example, simply adding a thin layer of skin and hair on the bones of a rabbit increases its strength by 35% [46]. The greater stiffness of insect exoskeletons is countered by increased air drag relative to mass, which in turn limits the impact speed and thus energy of collisions incurred by insects during normal flight.

Even animals, however, have their limits, as is apparent to anyone that has seen a bird crash into a window or had to clean the bugs off their windshield. This brings about the question: until which point can we reasonably expect to elastically absorb the energy of a collision without injury or damage? In the case of animals this limit seems to be an impact speed of around 5 m/s [70], which corresponds to a free fall from a height of about 1.3 m (without considering drag or other aerodynamic effects). This limit holds for both insects and birds, as it can be shown through dimensional arguments that the landing stresses on bodies and

limbs are roughly the same for all sizes at the same landing speed [69].

To be considered adequately protected from collisions we thus make the assumption that a flying platform should survive an impact with a surface at a speed of 5 m/s. In order to survive the dozens or even hundreds of collisions a flying platform can encounter over its lifetime a protective structure must absorb all the energy of an impact while minimizing the force placed on the frame. Assuming that impact occurs with a stiff, inelastic surface (such as a concrete floor), the protective structure must mechanically absorb all the kinetic energy of the entire platform.

2.2 Protection Mechanism Design

We propose the following steps to design and dimension elastic protective structures adapted to flying platforms:

1. **Spring Type Selection and Configuration:** The type of spring and its configuration on the platform should be selected to increase absorption distance, minimize force on the platform's structure and protect from impacts in the most likely directions.

2. **Material Selection:** A material should be chosen that has the required stiffness, yield strength and density to absorb the required energy.

3. **Dimensioning:** Individual elements should be optimized to minimize weight.

2.2.1 Spring Type Selection and Configuration

A spring working in its elastic range absorbs energy U over a distance x_{max} according to the formula:

$$U(x_{\mathrm{max}}) = \int_0^{x_{\mathrm{max}}} F(x)\,\mathrm{d}x. \tag{2.1}$$

where $F(x)$ is the force provided by the spring at displacement x. The total energy a spring can absorb is the area under the curve of $F(x)$ at the spring's maximum deflection, or the integration of Eq. 2.1. An ideal protective structure should thus limit the maximum force by increasing the absorption distance x_{max} and optimizing the the force profile $F(x)$.

There are three common types of springs: traditional linear or 'hookean' springs, non-linear springs (generally made of two or more different linear springs in series) and Euler-mode buckling springs (Euler springs) (Fig. 2.1A). The force and energy profiles of these springs are shown in Fig. 2.1B and C. Besides these main spring types, specific configurations of several

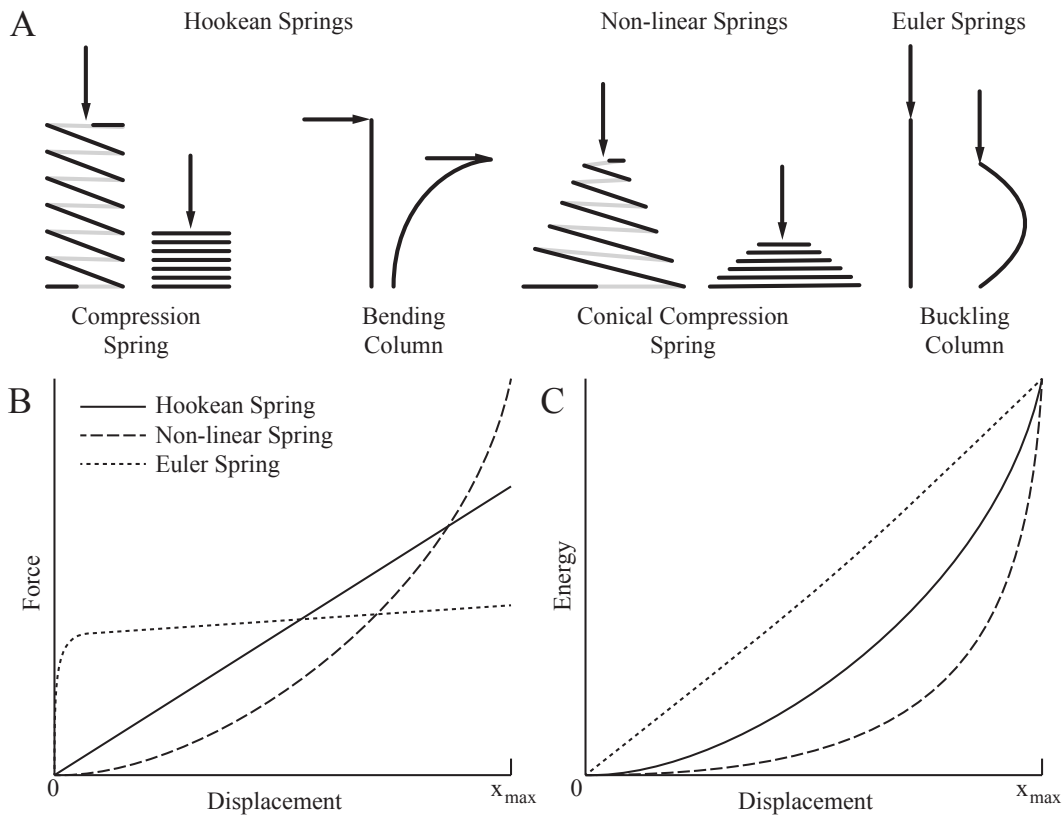Figure 2.1: (A) Some examples of the three common types of springs. Note that a column must be loaded *axially* to act in its buckling mode, otherwise in bending mode it acts as a Hookean spring for small displacements. (B) A representative schematic of relative force and (C) energy profiles for the three types of springs, scaled for an equivalent amount of energy absorbed at maximum displacement x_{max}.

springs can yield different force profiles that do not fit into the main spring categories. A spring type and configuration should be selected to minimize the force transferred to the platform's frame. Profiles that resemble that of an Euler spring are ideal, as they have the lowest maximum force for an equivalent deflection and total energy. Non-linear springs such as the conical springs shown in Fig. 2.1A should be avoided, as most of their energy is absorbed at a large displacement and with a much higher force than an Euler spring.

A common spring configuration often used in flying [41] and jumping [49, 48] robots is that of a spherical cage made of rods surrounding the frame of a platform. As presented in Sec. 1.2.2, however, circular springs sourced as straight rods store energy statically that cannot be subsequently absorbed during a collision and can fail prematurely at inflection points when impacting a flat surface, and should thus be used with caution.

2.2.2 Material Selection

The material used for the spring should absorb the largest amount of energy without breaking (or plastic deformation) at the lowest weight. The three factors that must be considered are thus the material's stiffness (higher stiffness absorbs more energy) defined by its Young's modulus E, tensile yield strength μ (higher strength resists plastic deformation), and density ρ (lower density yields lower weight). Materials can be optimized for weight by dividing the first two factors by their density, yielding Specific Stiffness and Specific Yield Strength, respectively. Some important material properties can be seen in Table 2.1.

The material most adapted for use in flying robots is carbon-fibre reinforced plastic (or simply carbon fibre), as it has a specific stiffness more than 3x higher than the stiffest metals. The only competing material, aramid fibre, has a higher specific yield strength[1] and will fail at a higher deflexion than carbon fibre, but as it has a much lower stiffness it would absorb less energy before failure. The values available in literature are approximate values, as they vary greatly depending on samples and testing methods. It is even more variable with composite materials as it depends on thread size, weaving pattern, percentage of fibre to plastic, type of plastic and weave direction.

Pulltruded Carbon Fibre

Pulltruded columns are often used in protective mechanisms for flying [30, 41] (Fig. 1.2H-J) and jumping [49] robots due to their high compression strength and stiffness [71] and low cost. Pulltruded columns are made of unidirectional fibres pulled though a resin and subsequently polymerized.

---

[1]The comparison is made between strength values for aramid and CFRP available in literature. The strength of pulltruded carbon fibre columns, as measured in the following section, is significantly higher due to the unidirectional nature of the fibres used for pulltrusion. No comparison was made to pulltruded aramid columns though it is assumed they will also be stronger than aramid plates.

Material	Young's Modulus [GPa]	Tensile Yield Strength [MPa]	Density [g/cm^3]	Specific Stiffness [MNm/kg]	Specific Yield Strength [kNm/kg]
Rubber (small strain)	0.055 +/- 0.045	8 *	1.055 +/- 0.145	0.0521	7.5
Nylon	3.0 +/- 1	78	1.13	1.15	69
Brass	112.5 +/- 12.5	247	8.560 +/- 0.165	13.14	29
Aluminum	69	275 +/- 35	2.700	25.56	102
Stainless Steel	200	600	7.900 +/- 0.150	25.32	76
Titanium alloy	112.5 +/- 7.5	977	4.510	24.94	217
Glass-Fibre-Reinforced Plastic (GFRP)	31.65 +/- 14.45	1500 *	1.800	17.58	833
Aramid (e.g. Kevlar)	70.5	2757 *	1.440	48.96	1915
Carbon-Fibre-Reinforced Plastic (CFRP)	135 +/- 15	2000 *	1.570	85.99	1273
Diamond	1220	2800	3.530	345.61	793
Pulltruded Carbon Fibre Columns	**113 +/- 15**	**2992 +/- 700**	**1.47**	**76**	**2035**

Table 2.1: Material Properties for Selected Materials. Materials marked with a (*) have the same yield (limit of elastic deformation) and ultimate (limit of failure) strengths. Values for Pulltruded Carbon Fibre Columns are measured in the lab, the source of other material data is http://www.matweb.com/. These are just indicative figures.
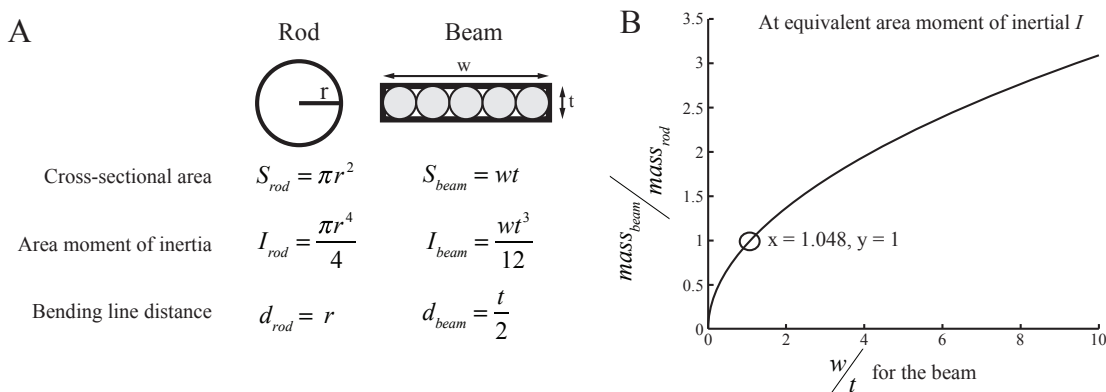

Figure 2.2: (A) Cross-sectional area and area moment of inertia for rods and beams. A beam can be compared to a row of rods attached side-by-side. (B) Comparison of the ratio of the weight of a rod and a beam for different dimensions of beams, at an equivalent second moment of inertia. For all width-to-thickness ratios greater than 1 a rod has a lower weight than a beam.

Pulltruded columns are often sourced as either rods (circular cross-section) or beams (rectangular cross-section), both of which have particular uses. Cross-sectional area S defines the weight of a column whereas its area moment of inertia I defines its resistance to bending (formulas are presented in Fig 2.2A). In general rods are lighter than beams for the same value of I (as shown in Fig 2.2B) of all cross-sections other than square[2] and should be used in most cases when weight is a limiting factor. However, beams have two advantages over rods: they resist bending in all directions except in the axis of their thickness, and can be made stiffer than a rod for a given bending angle[3]. A simple analogy is to think of a beam as a series of thin rods attached to each other in a row (Fig. 2.2A): when a force is applied to the beam each rod takes a part of the force and thus the resulting stress for each section is smaller than that for a single thick rod.

Pulltruded columns have slightly different characteristics than woven and stacked carbon fibre plates, and thus we tested some samples to extract their relevant properties. Deflection tests were performed using a linear stage and a load cell to measure the axial loading force required to bend carbon fibre columns of varying length and cross-sectional profiles in their buckling mode. As shown in Fig. 2.1B, columns loaded axially will absorb force in compression up to a critical force F_{crit} [72], at which point they will buckle:

$$F_{\text{crit}} = \frac{\pi^2 E I}{L^2} \tag{2.2}$$

where L is the column's length. Figure 2.3A shows the force profiles for 24 samples of various dimensions, whereas Fig. 2.3B shows the same profiles normalized for L and I. Figure 2.3D is a boxplot of the buckling point of the columns used to extract an average value of E of 113 GPa.

A similar test is performed to measure tensile yield strength μ, which in the case of carbon fibre is the same as its ultimate yield strength[4]. Pulltruded carbon fibre rods were once again loaded axially, but this time continued to be loaded until failure (when individual fibres started breaking). μ can be calculated using the formula:

$$\mu = \frac{F_{\text{max}} y}{I} \tag{2.3}$$

where F_{max} is the force at which the column fails and y is the displacement of the rod per-

---

[2]Beams with a width/thickness ratio of less than 1 are unlikely to bend in the axis of the width and are thus not considered.

[3]The stress is proportional to the distance of the bending line, and thus a beam can be made much wider than the diameter of a rod while keeping the same thickness as the rod's radius.

[4]Ultimate yield strength or UTS is the point at which a material fractures or fails catastrophically, as opposed to tensile yield strength which is the point at which a material starts deforming plastically instead of elastically. Carbon fibre behaves elastically up to its UTS.

pendicular to its axis at $F_{\max}$. We can estimate y with good accuracy using the following formula [72]:

$$y = 0.900L\left(\frac{F_{\max}}{F_{\mathrm{crit}}} - 1\right)^{\frac{1}{2}} \tag{2.4}$$

Figure 2.3C shows some of the 17 various columns that were loaded to failure and Fig. 2.3E is the resulting boxplot of calculated values of μ, the average value being 2.992 GPa with a standard deviation of 22%.

Density was measured by weighing a series of carbon fibre columns and was found to be 1.47 g/cm^3. The extracted material properties are added to Table 2.1.

2.2.3   Dimensioning

The goal of dimensioning is to select the lightest possible springs to absorb the desired energy without failing. There is generally a compromise to be made between the force transferred to the robot's frame, the weight of the spring and the amount of energy that it can absorb before failure, as well as secondary effects such as available materials, platform dimensions and integration. After selecting a spring type and configuration the first part of dimensioning is to determine the force profile of the protective structure independent of the second moment of inertia of the spring. The exact dimensions of the spring elements are then selected based on the required energy to be absorbed, material properties and weight.
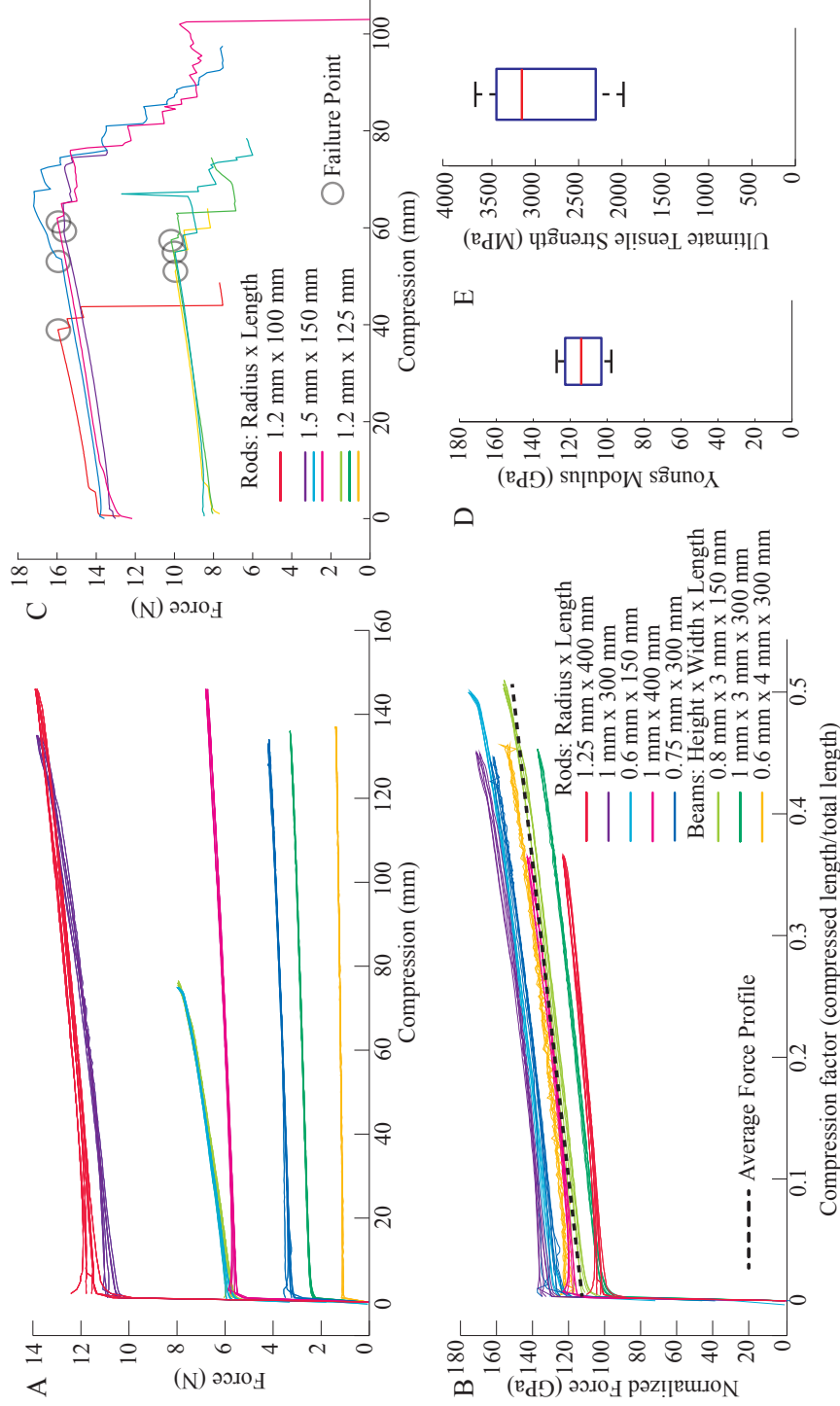
Figure 2.3: Results from a series of deflection tests performed by loading carbon fibre columns axially using a linear stage to induce bucking and recording the subsequent force using a load cell. (A) Deflection to force profiles performed on 24 pulltruded carbon fibre columns of various lengths and profiles when loaded axially (multiple samples of the same dimensions were tested). (B) The same profiles normalized for length and second moment of inertia used to determine Young's Modulus. (C) Profiles for some columns that failed, with their failure points highlighted. (D) Boxplot of Young's Modulus based on displacement profile of 24 columns, including those presented in (B). (E) Boxplot of Ultimate Tensile Strength based on the displacement at failure of 17 columns, including those presented in (C).

21

2.3   Protection of a Winged Platform from Head-on Collisions

This section is partially based on the semester project work of Florentin Marty.

The protective structure design method presented in Sec. 2.2 is first applied to the protection of a wing-based flying platform that travels primarily through forward flight. A winged platform can travel more efficiently than a hovering one over long distances [27] and can thus be useful for the exploration of large spaces such as deep caves or mines. As it must always travel forward to remain aloft it is most likely to collide with obstacles head-on. The need to protect the platform in only a single direction simplifies the protective mechanism design and is thus well-suited as a first case study of the design method.

In its simplest form (Fig 2.4), a typical winged platform consists of central frame with two attached wings for lift, a motor with a propeller at its front for thrust and control surfaces at its back for pitch, roll and/or yaw control. For this particular application we choose a frame length of 20 cm and a propeller diameter of 15.2 cm, a platform size small enough to fit through doorways and small windows but with a wing loading large enough to fly at the low speeds required for cluttered flight.

2.3.1   Protection Mechanism Design

Spring Type and Configuration

The priority for a winged platform is to protect the spinning propeller at the front of the platform and ensure it does not come into contact with obstacles or the rest of the platform. Collision energy must be dissipated over a distance (according to Eq. 2.1), and thus any protection mechanism should stick out a certain distance beyond the propellers and be dimensioned not to impact the propellers in case of high impact.

A design is proposed based on two identical teardrop-shaped springs surrounding the platform with the point of the teardrops facing forward (Fig. 2.5B). The teardrop shape ensures that all frontal collisions occur at the same point and are spread to all four springs, which bend outwards around the platform and thus away from the wings and control surfaces. The teardrops are attached to the platform at the back of the frame as well as through two attachment springs mounted directly behind the motor. These attachment springs also bend backwards and thus away from the spinning propeller, absorbing additional energy. The length of the teardrop and the diameter of the attachment spring are set to 40 cm and 23 cm, respectively, large enough to fit the platform frame and propeller with space for deflection of the springs.

Material Selection

As suggested in Sec. 2.2.2, pulltruded carbon fibre columns provide the highest stiffness for a given weight. For the teardrop-shaped outer structure there is no need to limit the deflexion

direction, and thus carbon fibre rods are selected. The attachment springs however must remain orthogonal to each other and must not be allowed to bend perpendicular to the robot's frame, and thus carbon fibre beams are selected.

Dimensioning

The first step in dimensioning the springs is to determine the force deflection profile of the protective structure. To simplify the analysis the structure is modelled as two teardrop and two attachment springs all mounted in parallel (Fig. 2.5A). The force profile for the entire protective structure F_{tot} takes the form:

$$F_{tot}(x) = 2F_t(x) + 2F_a(x) \tag{2.5}$$

where F_t and F_a are the force profiles of a single teardrop spring and a single attachment spring, respectively. A simple setup is designed in which carbon fibre rods of various cross-sections are held in the desired teardrop and attachment spring shapes (Fig. 2.5C). The springs are then deflected using a force meter and the resulting displacement is measured. The resulting force profiles, with the force normalized for second moment of inertia of the teardrop I_t and attachment spring I_a, are shown in Fig. 2.6.

The teardrop-shaped spring (Fig. 2.6A) has a linear force profile F_t which, based on the experimental data and normalized for I_t, takes the form:
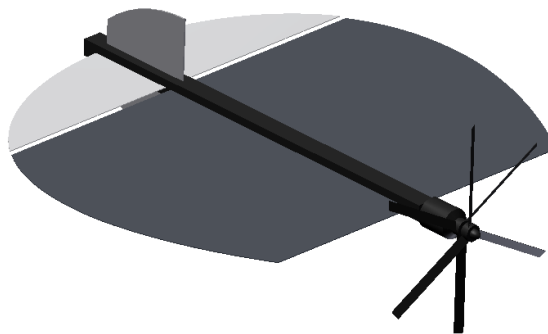
$$F_t(x) = 0.59 I_t x \tag{2.6}$$

Figure 2.4: A simple schematic of a winged flying platform. Wings used for lift generation, a motor and propeller generate thrust, elevators used for pitch control and a rudder is used for yaw control

A

$$F_{tot} = 2F_a + 2F_t$$

$2F_t$ $2F_t$

$2F_a$

$\frac{1}{2}F_a$
$\frac{1}{2}F_a$
$\frac{1}{2}F_a$
$\frac{1}{2}F_a$

B

23 cm
15.2 cm

20 cm   4 cm   7 cm   9 cm

40 cm

C

x

F_t

x

F_a
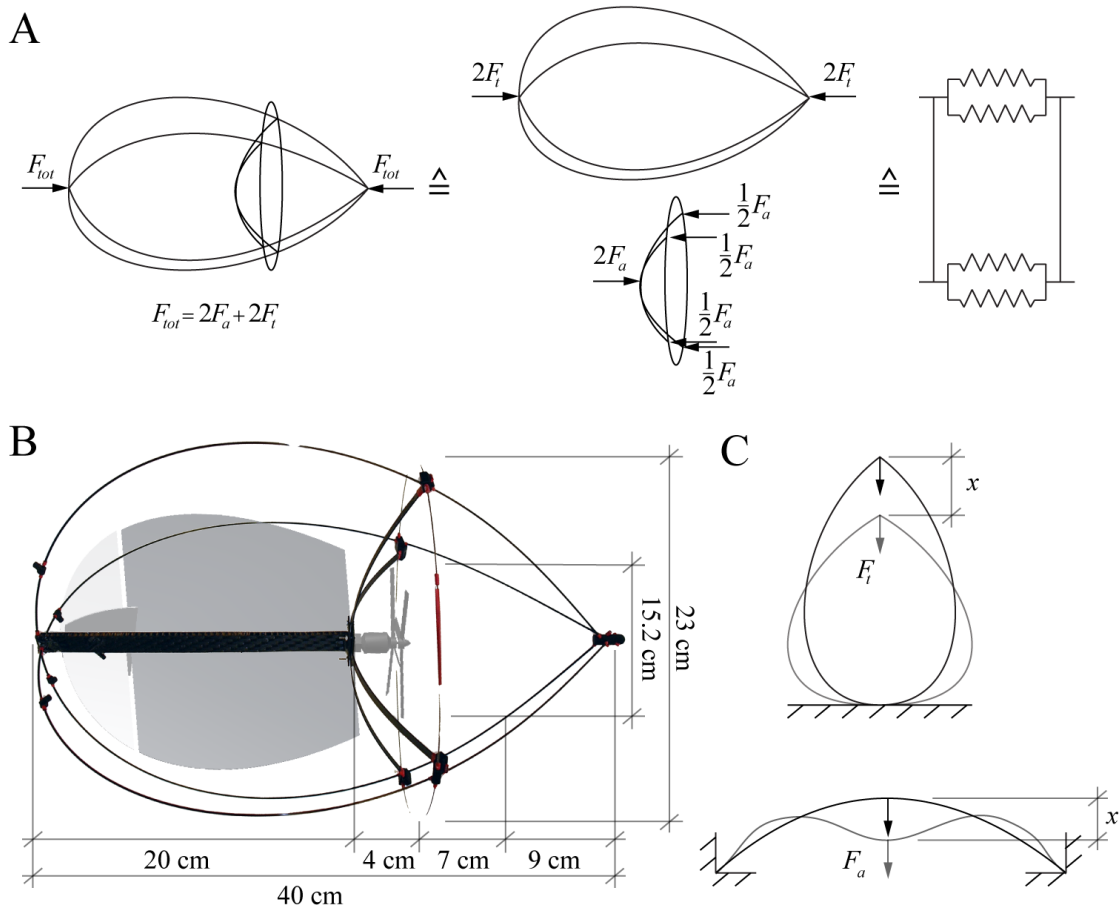
Figure 2.5: The proposed protective structure for absorbing head-on collisions. (A) The entire structure can be decomposed into two teardrop-shaped outer springs mounted to the frame in parallel with two attachment springs. (B) The structure and its dimensions overlaid on a basic wing-based flying platform. (C) Schematic of the loading used to measure displacement profiles for the teardrop and attachment springs.

The force profile F_a for the attachment spring (Fig. 2.6B), however, is non-linear, and can be approximated with a second order polynomial:

$$F_a(x) = I_a(8.13x - 0.353x^2) \tag{2.7}$$

Substituting Eq. 2.6 and 2.7 into Eq. 2.5 results in a total force profile of:

$$F_{tot}(x) = I_a(16.26x - 0.706x^2) + 1.18I_t x \tag{2.8}$$

Figure 2.6: Force profiles for (A) a single teardrop-shaped spring and (B) a single attachment spring. The force is normalized for the area moment of inertia of the tested columns.
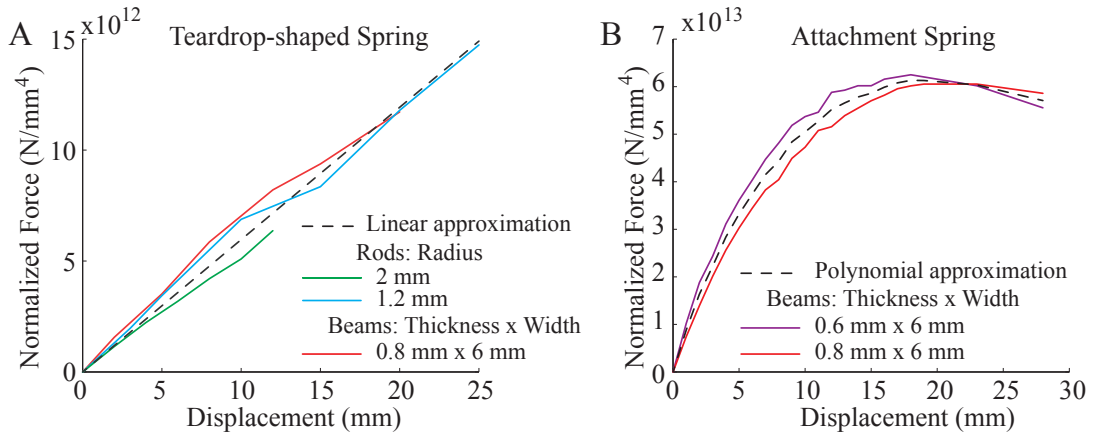
With some simplification a model has thus been created for the combined protective structure. Two interesting observations can be made based on this model:

1. For the same dimensions of spring, the linear term of the spring constant for the attachment spring is 14 x higher than that of the teardrop-shaped spring, and thus has a much higher impact on the collision force transferred to the platform's frame.

2. The attachment spring's force profile is nonlinear and has a similar shape to that of an Euler spring. This is advantageous, as it minimizes the maximum force exerted on the platform's frame.

The next step is to use this model to dimension the carbon fibre columns used as the springs to absorb the desired collision energy. We can calculate the energy absorbed by the protective structure by substituting Eq. 2.8 into Eq. 2.1:

$$
\begin{aligned}
U(x) &= I_a(8.13x^2 - 0.235x^3) + 0.59I_t x^2 \\
&= (8.13I_a + 0.59I_t)x^2 - 0.235I_a x^3
\end{aligned}
\tag{2.9}
$$

We dimension our protective structure to survive a drop of a height of 2 m, equivalent to a impact speed of 6.26 m/s, slightly above the 5 m/s limit seen in nature [70]. For an estimated final platform weight of 120 g this is equivalent to 2.35 J. Equation 2.9 is solved for various values of I_a and I_t at an energy of 2.35 J and the resulting displacement of the robot frame is plotted in Fig. 2.7.

The proposed protective structure has a space of about 7 cm between the propellers and the teardrop spring. Taking into account a safety factor, a displacement of between 5-6 cm is
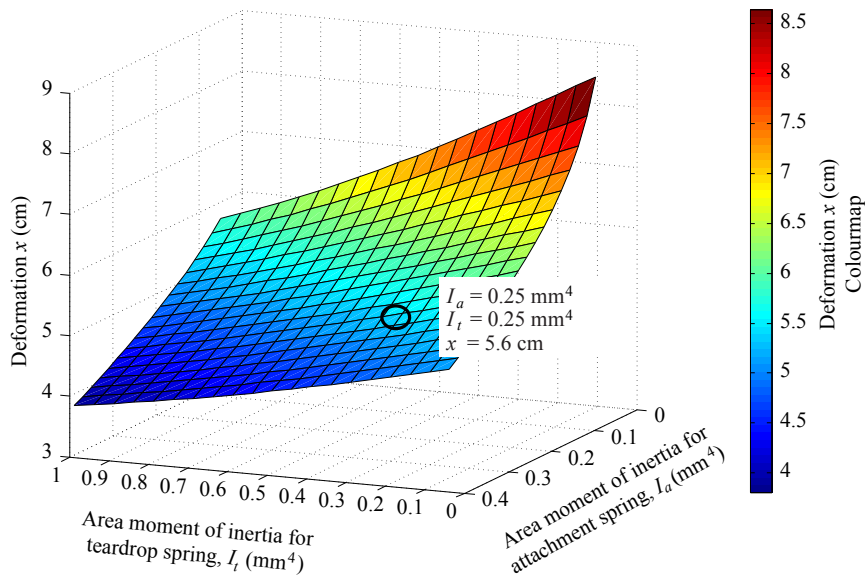
Figure 2.7: A graph of the deformation of the protective structure for a fall from a height of 2 m and a structure weight of 120 g.

allowable, equivalent to the turquoise band in Fig. 2.7. To distribute the energy onto both springs an identical area moment of inertial of $I_t = I_a = 0.25\,\text{mm}^4$ was chosen for both teardrop and attachment springs. As we are using beams for the attachment springs and rods for the teardrop springs, this is roughly equivalent to a beam with a cross-section of 6 mm x 0.8 mm and a rod of diameter 1.5 mm.

2.3.2 Prototype Realization

The protection mechanism designed and dimensioned in Sec. 2.3.1 was integrated into the frame of a small winged platform (Fig. 2.8E). Aramid honeycomb sandwiched between two carbon fibre plates makes up the frame of the platform. The attachment springs made of carbon fibre beams are held between the frame and the motor mount using two small carbon fibre plates (Fig. 2.8A). The teardrop-shaped springs are connected to the attachment springs using 3D-printed linkages (Fig. 2.8B) and mounted to the back of the platform's frame using cured carbon fibre (Fig. 2.8C). The weight of the frame and protection mechanism, including attachment and teardrop springs with linkages is 24 g.

2.3.3 Characterization and Validation

The platform was put through a series of tests to validate the energy absorption capabilities and resilience of the protective structure as well as its flight performance.
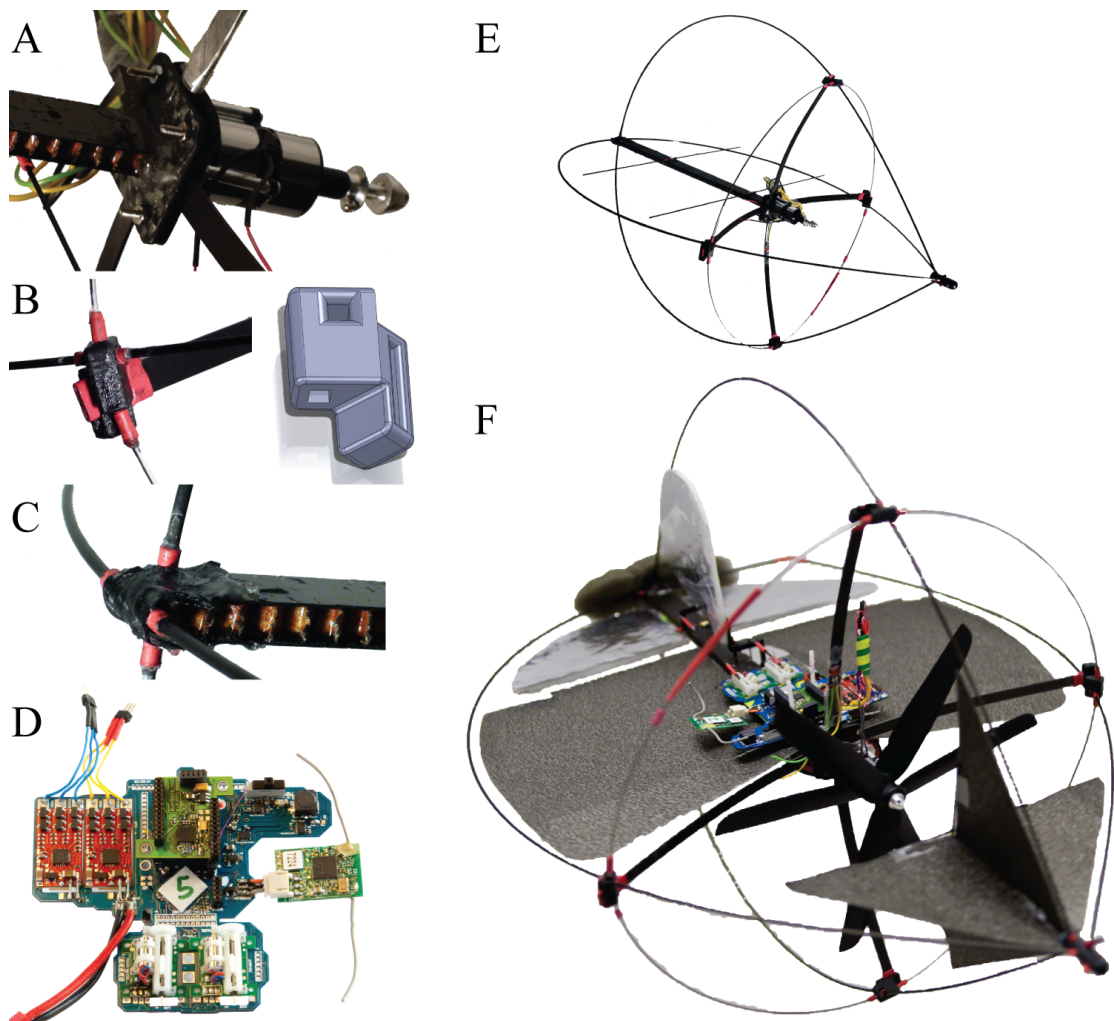
Figure 2.8: The completed prototype ready for flight and collision absorption testing. (A) Motor mount for dual coaxial brushless DC motor and placement of attachment springs. (B) Linkages between attachment springs and teardrop springs. (C) Attachment of teardrop springs to platform frame. (D) Embedded flight electronics, motor controllers and servo-motors. (E) The platform frame with embedded protection mechanisms. (F) The completed flying platform used in flight experiments.

Spring Compression Validation

The first experiment is designed to validate the spring compression mechanism and model that was developed in Sec. 2.3.1. The weight of the additional components required for flight (wings, motors, control surfaces and embedded electronics) is added in the form of a corresponding dead weight of 100 g attached to the platform frame at the COG position of the complete platform. A styrofoam model of the propellers is also added to see whether they come into contact with anything during a collision.

High-speed video is used to analyze the performance of the protective structures. Figure 2.9A shows the timeseries of a drop test from a height of 2 m, equivalent to 2.43 J. The structure was designed to deform by 5.1 cm, but in the experiment the structure deforms by only 4.5 cm, 12% less than predicted. This error is in an acceptable range of the largely simplified model. The compression motion follows well the desired movement of the springs, with both the attachment springs and the teardrop springs absorbing part of the collision energy.

Resilience

The next experiment is used to test the resilience of the protective structure to multiple head-on collisions. The platform is dropped onto its front several times from increasing heights up to a height of 2 m. The results of the drop tests is shown in Table 2.2.

Drop height [m]	Equivalent energy [J]	Number of drop tests	Failures
0.5	0.61	3	no damage
1	1.22	6	1x the propeller touched the attachment springs
1.5	1.82	6	1x the propeller touched the attachment springs 1x a teardrop spring failed
2	2.43	4	1x a teardrop spring failed

Table 2.2: Results from drop tests.

Of the 19 drop tests 15 are successful in absorbing collision energy and protecting the platform's frame. Two of the failures are the result of contact between the propellers and the attachment springs, which may not have caused any permanent damage. Only two of the higher-energy collisions resulted in failure of the protective mechanisms through a ruptured teardrop spring.

High-speed video is used to further analyze the failure modes of the protective mechanisms. Figure 2.9B shows the timeseries of a drop test from a height of 2 m that resulted in a broken teardrop spring. The platform touches the ground at an angle, and thus instead of bouncing back (as in Fig. 2.9B) it rotates onto its back, transferring collision energy to the back of the teardrop spring which is not designed to absorb force from this direction and subsequently breaks. In a similar test, Fig. 2.9C shows a timeseries of a drop test from a height of 1.5 m where the platform contacts the surface at an even greater angle and thus not on its tip but on
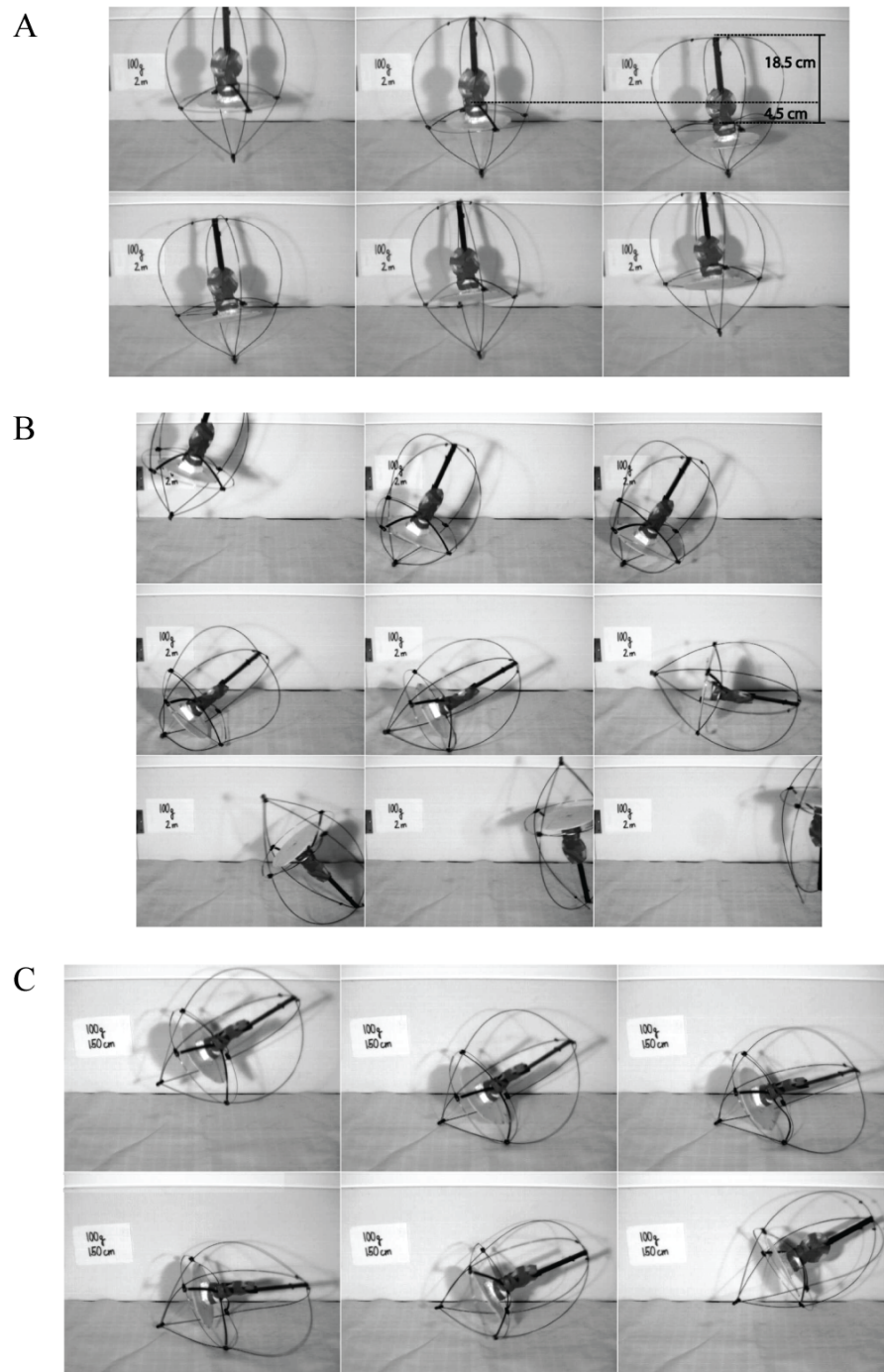
Figure 2.9: Timeseries of drop tests taken with a high-speed camera. (A) A successful head-on collision from a height of 2 m, corresponding to an impact energy of 2.43 J. The springs are deflected by a distance of 4.5 cm. (B) Head-on collision from a height of 2 m with subsequent induced rolling and rupture of a teardrop spring. (C) Side impact from a height of 1.5 m which causes deformation in the attachment springs that impacts the propellers.

the linkage of the attachment spring. The energy is absorbed without damage, but results in the springs bending in unplanned directions and thus impacting with the propeller.

This experiment shows that the protective structure is resilient to repeated head-on collisions from heights of up to 2 m. The few failures result from side impacts instead of the designed head-on impacts during which a single spring absorbing all the impact energy. Fortunately individual springs can be easily replaced due to the modular design and 3D-printed linkages.

Flight Tests

The goal of this experiment is to demonstrate that the protective structure can be integrated into a flying platform without greatly affecting its aerodynamics and weight, and thus its ability to fly. The platform frame (Fig. 2.8E) is equipped with two styrofoam wings, control surfaces for pitch and yaw control when in forward flight and a coaxial brushless DC motor with two propellers used for thrust and roll control. The addition of coaxial motors allow the robot to fly in hovering mode as well as in forward flight mode. The robot is equipped with the inertial sensor package BurrMove v4 and BurrSens v4[5] which also house the motor controllers, servo-motors for the control surfaces, radio transmitter and embedded microcontroller. The total weight of the platform is 124 g.

The robot is flown within an 6x7 m experimentation room and demonstrates good stability and maneuverability. The on-board Inertial Measurement Unit (IMU) is used to stabilize the robot in both hovering and forward flight mode. The small size of the wings compared to the weight of the platform results in high speed when in forward flight mode, and thus the robot must remain in hovering mode when in constrained environments. This experiment confirms that the protective structure is light enough and unobtrusive enough to be integrated into a flying platform.

2.3.4 Discussion

This section presented a novel protective structure design that uses a combination of carbon fibre rods and beams and a teardrop shape to distribute the energy of high-velocity head-on impacts. The structure is optimized to minimize weight and is then tested to absorb collision energies of over 2 J. The structure is lightweight and is integrated into a flying robot that can fly within a confined space using both forward and hovering flight modes.

Though capable of absorbing the head-on collisions most likely to occur during forward flight, the protective structures can fail due to secondary impacts resulting from subsequent rebound and loss of stability. Indeed, the main lesson that can be learned from these results is that irrespective of its flight mode, a platform's protective structures should be designed to absorb collision energy in all directions. This challenge is thus presented in the next section.

---

[5]See App. A for more details on embedded electronics.

2.4 Protection of Hovering Platforms in Three Dimensions

To truly navigate in a confined, cluttered environment a platform must be able to hover and move in all directions. Independent of the number of rotors a rotorcraft has, they all share the same basic method of lift generation: one or several propellers pushes air downward to create lift. For proper lift there must be clear space above and below the propellers. Efficiency and lift improves with propeller size [10] and thus it makes sense to maximize the size of the propellers within the platform's dimensions. Flying in cluttered environments necessitates the protection of the propeller(s), and thus a protective cage surrounding them is required. Thus most rotor-based flying platforms take roughly the shape of a cylinder, their diameter defined by the size of their propellers. Figure 2.10 shows the three most common robotic rotorcraft configurations (quadrotors, coaxial helicopters and tailsitters) and how they fit this general model.

As demonstrated in Sec. 2.3.1, simply protecting from head-on collisions is insufficient when the platform is surrounded by obstacles. The goal of this section is thus to design protective structures for a small hovering platform of similar dimensions but modified based on the experience of the previous section in the following manner:

1. For a platform to fly at slow enough speeds with such a wing size it would have to have a weight of around 10 g [21]. As the platform is an order of magnitude heavier, it is likely to spend most of its time in hovering mode. The wings are thus removed.

2. A major issue in the previous design was contact between the propeller and the rest of the platform's frame. In the new design the propellers will be housed within the platform's stiff inner frame instead of above it and thus prevented from impacting with exterior objects or the protective structures.

In its simplest form the hovering platform is thus modelled as a cylinder containing two coaxial motors with propellers for thrust and yaw control, and control surfaces for pitch and roll control right below the propellers (Fig. 2.10).

2.4.1 Protection Mechanism Design

Spring Type and Configuration

Once again the goal of a protective structure is to absorb collision energy while minimizing the force transferred to the platform's frame. Euler springs are long columns that are loaded along their axis to the point at which they buckle. As shown previously in Fig. 2.1, for a given amount of energy and displacement Euler springs have the lowest maximum force exerted on their attachment point to a frame and are thus a strong candidate for protective structure design. They are simple to produce (simple straight rods can be used) and do not store energy
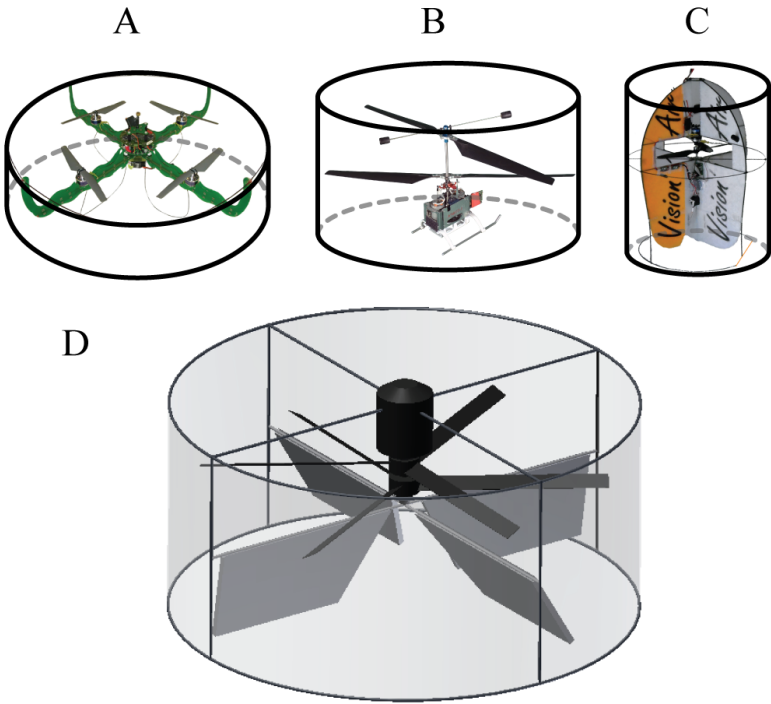
Figure 2.10: Above, three types of hovering platforms that, when adapted with protective cages for flight in cluttered environments, take the general shape of a cylinder: (A) a quadrotor, (B) a coaxial helicopter and (C) a tailsitter. Below, (D) a simplified schematic of the hovering platform for which protective structures will be designed. Two coaxial motors with counter-rotating propellers provide lift and yaw control, whereas control surfaces just below the propellers provide pitch and roll control.

statically. Euler springs have had very limited use in robotics (with the notable exception of the Bow leg hopper [73]) and thus represent a novel solution to impact energy absorption.

Attaching a single Euler spring to the fuselage without fixing the other end will result in the spring slipping on the contact surface and bending (thus acting as a hookean spring) instead of buckling (acting as an Euler spring) (Fig 2.1A). To fix the end of the spring in place in three dimensions we propose using three Euler springs in a tetrahedral configuration as shown in Fig. 2.11A. The springs are attached to the fuselage and to each other using rotating joints to ensure that they are only loaded axially. If we model a rotor-based platform as a cylinder (Fig.2.10) we can protect the platform from collisions in all directions by using eight tetrahedrals placed symmetrically around the platform.

The length of the individual spring elements is critical, as it defines the direction of the force loading during impact. If the elements are too short, an impact will bend them inwards, no longer in the direction of the force (Fig. 2.11B) and thus not absorbing energy through buckling. Conversely, if the elements are too long an impact bends the elements outwards (Fig. 2.11C). There is thus an optimized length of spring element that keeps the impact force close to the axial direction of the spring (Fig. 2.11D). In the case of eight tetrahedrals used symmetrically around a platform this formula can be derived through trigonometry (as shown in Fig. 2.11E and F):

$$y = \sqrt{\frac{8}{3}} x \tag{2.10}$$

where y is the length of the spring and x is the radius of the platform.

Material Selection

Once again pulltruded carbon fibre rods provide the highest specific stiffness for their weight and are thus used to build the Euler springs used in the tetrahedrals.
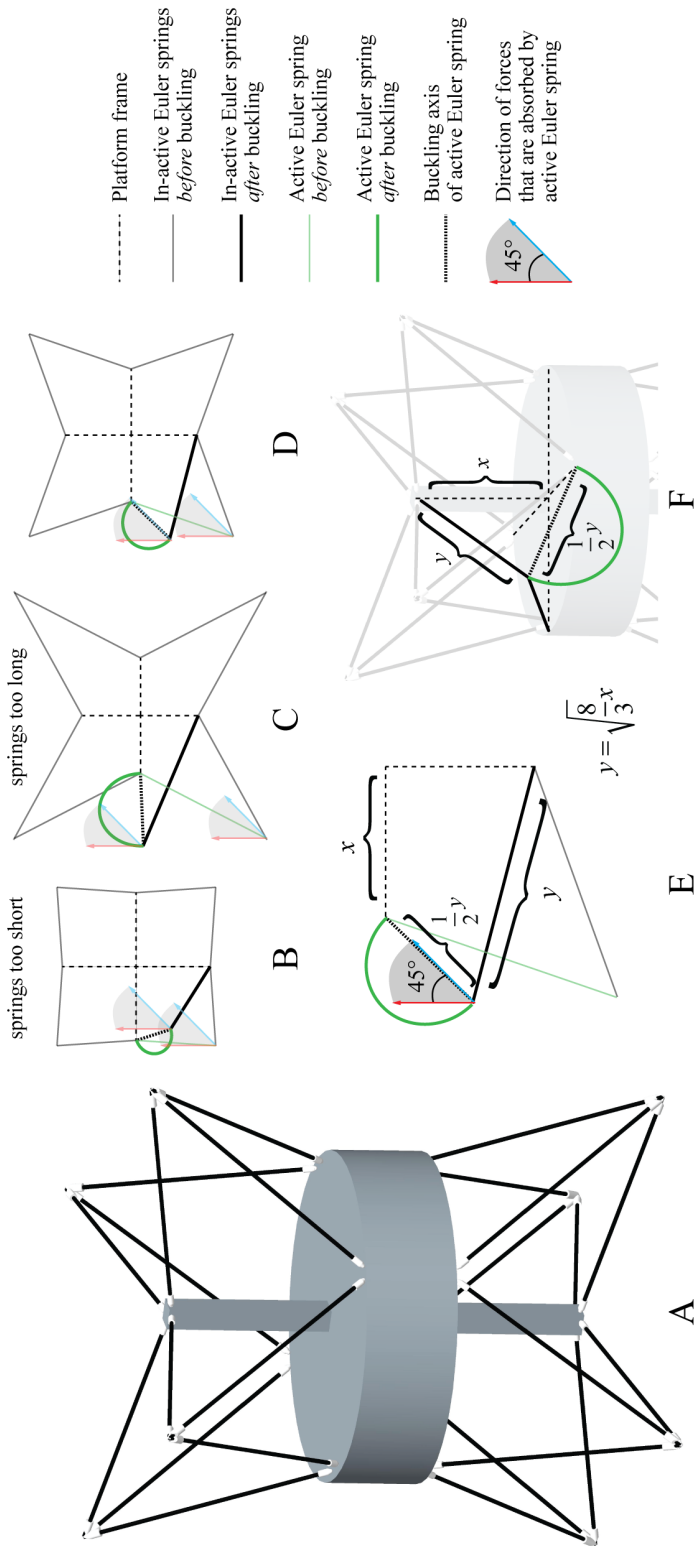
Figure 2.11: (A) A proposed configuration of 8 tetrahedral structures consisting of three Euler springs for protecting a hovering platform. The length of the Euler springs is important, as it determines the amount of force that is applied in the axis of the spring during compression. The effect of spring length is illustrated in two dimensions in (B)-(D). The area between the red and blue force arrows show the range of force directions that must be absorbed by the green bending spring. (B) A spring that is too short bends inward, whereas (C) a spring that is too long bends outward. (D) An optimal length results in the force being directed near the axis of the spring throughout its compression. (E) The optimal length y can be determined in the two-dimensional case based on the length of the base x using trigonometry. (F) The same trigonometric calculation can be extended to three dimensions.

Dimensioning

Having decided on the type and material of the spring and its configuration around the platform there remains the dimensioning of the spring itself. We want to choose the lightest possible spring while still being able to absorb the required energy. As we are using pulltruded carbon fibre rods whose length is determined by the platform's dimensions according to Eq. 2.10 the problem is reduced to dimensioning the radius r of rod to be used that absorbs the required energy without failure while minimizing weight.

We begin by deriving the force profile $F(x)$ of an Euler buckling spring which can be written as [74]:

$$\begin{aligned}
F(x) &= F_{\text{crit}} + \frac{EI}{L^2} k \frac{x}{L} \\
&= \frac{EI}{L^2} (\pi^2 + k \frac{x}{L})
\end{aligned} \tag{2.11}$$

where k is the spring factor and $0 < x < L$. Using deflection tests described in Sec. 2.2.2 and shown in Fig. 2.3A we determine the spring factor of a pulltruded rod to be $k = 8.09$. We can normalize Eq. 2.11 for a given compression factor c by substituting the following equation:

$$c = \frac{x}{L} \tag{2.12}$$

(where $0 < c < 1$) which results in:

$$F(c) = \frac{EI}{L^2} (\pi^2 + 8.09c) \tag{2.13}$$

We can calculate the energy absorbed by a column by substituting Eq. 2.13 into Eq. 2.1:

$$\begin{aligned}
U &= L \int F(c) \, dc \\
&= \frac{EIc}{L} (\pi^2 + 4.045c)
\end{aligned} \tag{2.14}$$

Solving for I we can compute the minimum second moment of inertia I_{min} required to absorb

this energy:

$$I_{\min} = \frac{UL}{Ec} \frac{1}{\pi^2 + 4.045c} \tag{2.15}$$

For a cylindrical rod with radius r,

$$I = \frac{\pi r^4}{4} \tag{2.16}$$

Therefore the minimum radius of rod required to absorb energy U is:

$$r_{\min} = \sqrt[4]{\frac{4 I_{\min}}{\pi}} \tag{2.17}$$

In terms of L, c and U we can write:

$$r_{\min} = \sqrt[4]{\frac{4UL}{\pi Ec} \frac{1}{\pi^2 + 4.045c}} \tag{2.18}$$

The upper limit of allowable rod radius $r_{\max}$ depends on the strain that the rod can take before breaking. For this we calculate the maximum force at the desired compression ratio:

$$r_{\max} = \frac{\mu I}{F_{\max} y} \tag{2.19}$$

where y is the displacement of the rod perpendicular to its axis, as presented previously in Eq. 2.4. Substituting Eq. 2.4 into Eq. 2.19 and writing once again in terms of L, c and U we have:

$$r_{\max} = \frac{\mu L}{0.9 E} \frac{\pi}{(\pi^2 + 8.09c)\sqrt{8.09c}} \tag{2.20}$$

In order to absorb the desired energy U without breaking there must exist values of L and c for

which $r_{\min} < r_{\max}$.

Finally, the weight of the rod can be computed using its volume and density:

$$W_{\text{rod}} = \rho \pi r^2 L \tag{2.21}$$

The minimum weight $W_{\min}$ at $r_{\min}$ in terms of L and c can be derived by substituting Eq. 2.18 into Eq. 2.21:

$$
\begin{aligned}
W_{\min} &= \rho \pi r_{\min}^2 L_{\min} \\
&= \rho \pi \sqrt{\frac{4 U L_{\min}}{\pi E c} \frac{1}{\pi^2 + 4.045c}} \\
&\quad \times \sqrt[3]{\frac{0.9^4 4 E^3 U (\pi^2 + 8.09c)^4 (8.09c)^2}{\mu^4 c \pi^5 (\pi^2 + 4.045c)}}
\end{aligned} \tag{2.22}
$$

The derived equations can now be used to dimension the optimal compression ratio and radius of rods that should be used to absorb impact energy. The equations are applied to a hovering platform with a core defined by a coaxial motor with 10 cm-diameter rotors. Allowing for protection around the rotors, the platform's stiff internal frame takes a cylindrical shape with a radius of 12 cm. Using Eq. 2.10 the optimal length of the Euler springs is approx. 20 cm. To dimension the radius of rod required we use Eqs. 2.13, 2.14, 2.18, 2.19, 2.22 to get a sense of the amount of energy we can expect to absorb.

Figure 2.12 plots the radius, weight and force of a 20 cm rod as a function of compression ratio. As a general trend, maximizing the compression ratio will lower both the force on the structure and the weight of the rod. There is a fixed maximum radius however which decreases with the compression ratio, since a thicker rod will fail at a lower bend angle than a thinner one. As this robot is designed to fly indoors (low altitude, slow speeds) it should not encounter high-energy impacts and thus we optimize for minimal weight and force rather than maximum energy. We select a rod radius of 1 mm (dashed line in Fig. 2.12), which will allow the platform to absorb 1.5 J at a compression ratio of 0.34. With an estimated platform weight of 300 g, this is the energy of a freefall from a height of 51 cm. It should be noted that this is the energy that can be absorbed by a *single* rod. As there are 24 rods surrounding the platform, in most cases there will be several rods that will absorb the energy at once.
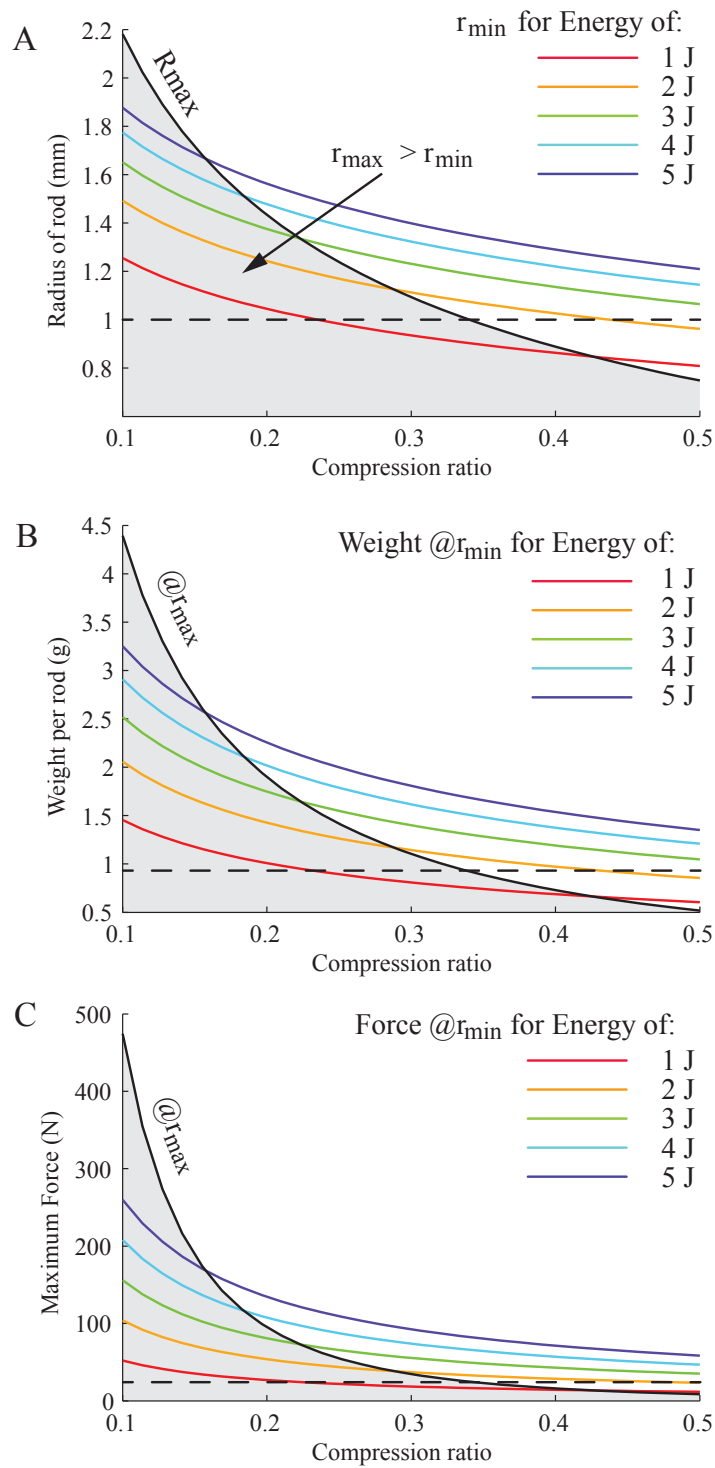
Figure 2.12: (A) Rod radius, (B) weight and (C) maximum force for a 20 cm carbon fibre rod as an Euler spring. Shaded areas represent possible combinations of compression ratio, radius and energy for which the rod will not fail.
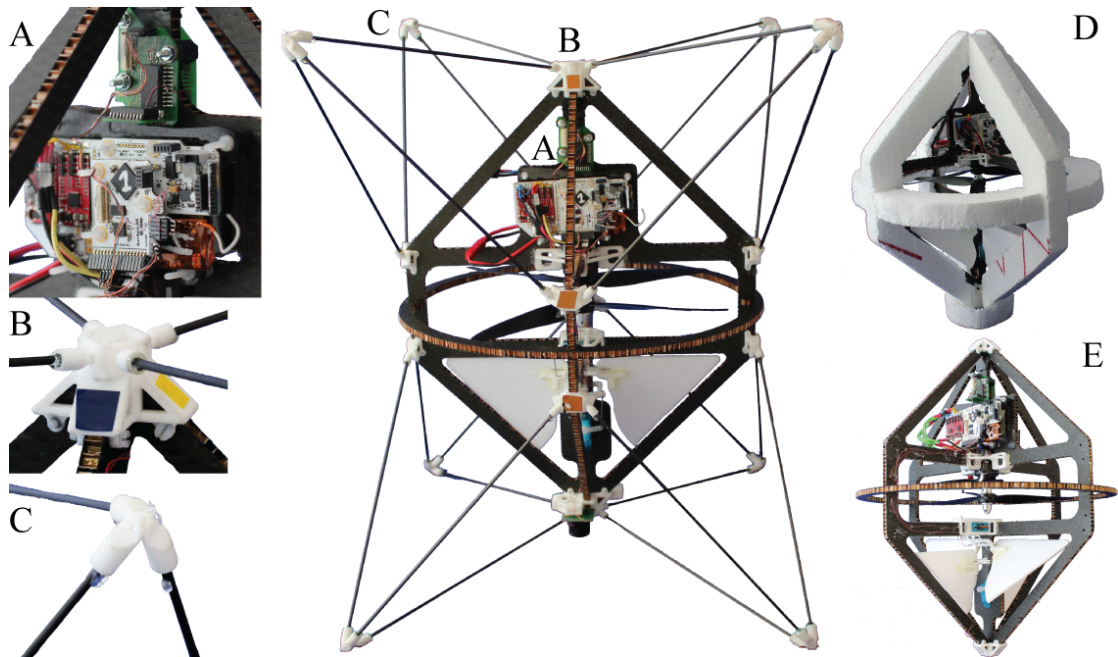
Figure 2.13: (D) The hovering flying robot equipped with Euler-spring protection structures. (A) shows the on-board electronics, including high-G accelerometers (top circuit board) mounted directly to the robot's frame whereas (B) and (C) show the two endpoints of the Euler springs. The same core frame is outfitted with (E) styrofoam and (F) stiff protection for force comparison experiments.

2.4.2 Prototype Realization

Figure 2.13D shows the completed flying platform including protective structures attached to a rigid internal frame. The frame houses flight motors, control surfaces and flight electronics composed of BurrMove v5 and BurrSens v5 boards (Fig. 2.13A). The carbon-fibre Euler springs are inserted into end pieces made of laser-sintered ABS plastic which are subsequently attached to the frame (Fig. 2.13B) and to each other (Fig. 2.13C) using nylon fishing line. The weight of the protective structures including end pieces is 40 g, and the total weight of the platform is 282 g.

2.4.3 Characterization and Validation

The platform with its protective structures is put through a series of tests to evaluate its robustness to contact. Impact force on the frame is measured using 3 orthogonally-positioned single-axis high-G accelerometers (Freescale MMA3204, range of +/- 100 G, Fig. 2.13A) coupled directly to the platform's frame. Depending on the direction of the impact vector, the total acceleration that can be measured ranges from 100 to 173 G or 980-1695 m/s^2. With a platform mass of 282 g this corresponds to a maximum measurable force of 276 to 478 N.
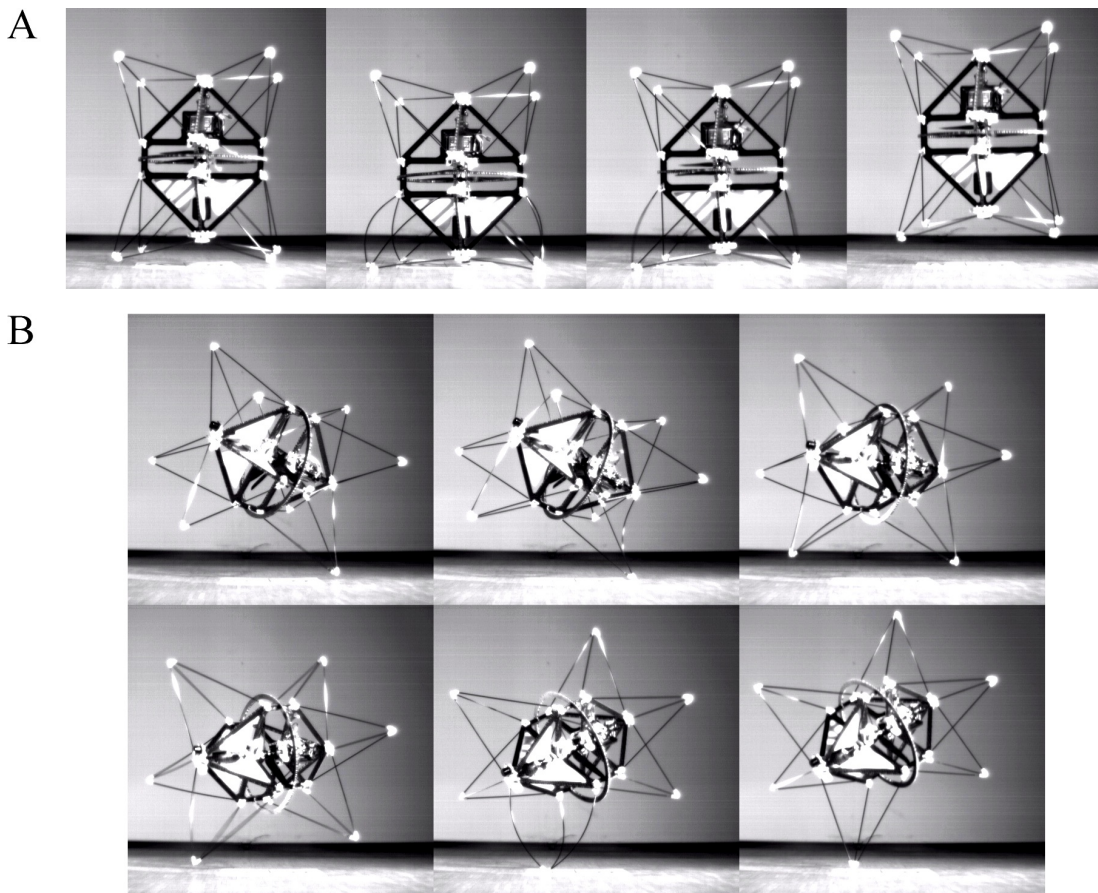
A

B

Figure 2.14: Timeseries of drop tests on (A) the platform's base and (B) on a single tetrahedral from a height of 75cm.

Buckling Motion Validation

The goal of the first experiment is to validate that the Euler springs are indeed buckling during a collision. The platform is dropped from a height of 1 m, 5 times on its base (the position most likely to occur during a hard landing) and 5 times on a single tetrahedral protective structure, and filmed at 1000 fps using a high-speed camera. All the videos are subsequently analyzed, confirming that in each case one or more Euler springs is buckling to absorb impact energy. Figure 2.14A shows a timeseries of an impact on the platform's base in which four Euler springs, one from each tetrahedral, are buckling concurrently. In Fig. 2.14B a single Euler spring absorbs impact energy and subsequently releases it, causing the platform to spin. The remaining energy is then absorbed by two Euler springs of a different tetrahedral.

Impact Force Minimization

The goal of this experiment is to compare the force minimization capability of the Euler-spring protective structures to foam-based protection, a common protective structure used in other
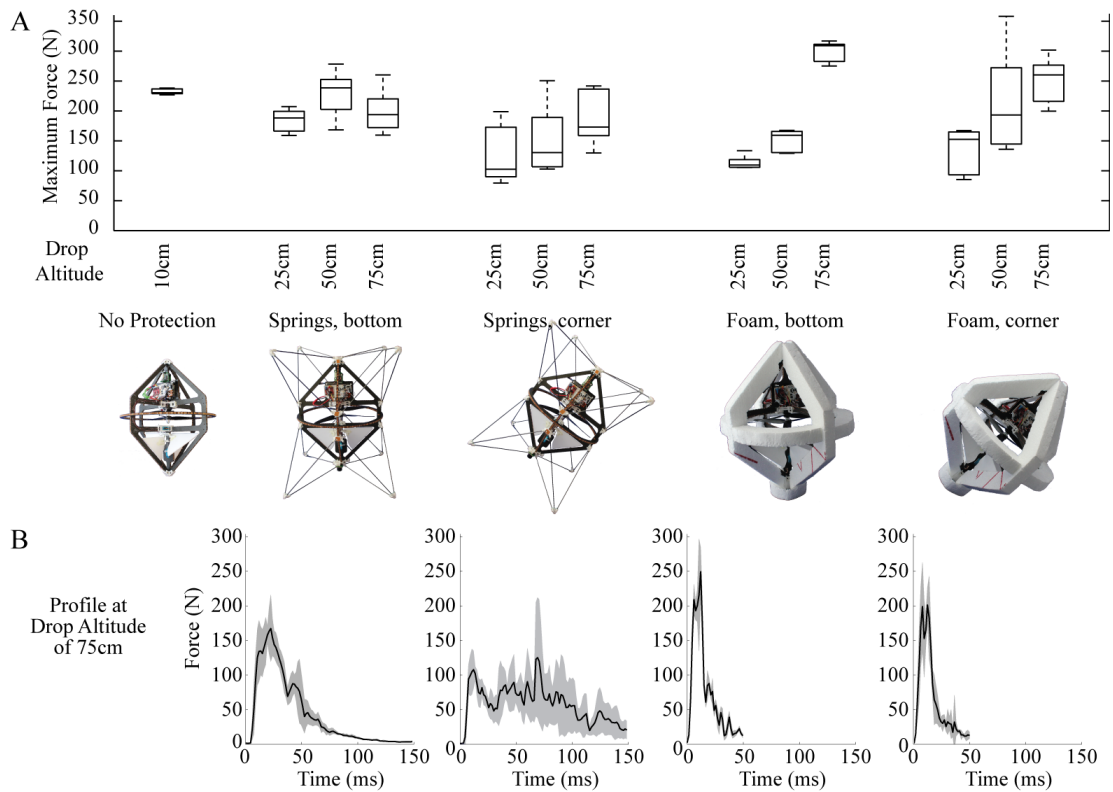
Figure 2.15: (A) boxplot of the maximum force measured on the platform's frame over 5 trials for drop tests from varying altitudes and using various protection mechanisms. (B) Force profile over time averaged over 5 trials for a free fall from 75 cm. Shaded regions represent standard deviation. As only a limited amount of data points can be sent to the ground station, and initial tests showed a flat force curve after 50 ms using foam protection, it was decided to only record data from the first 50 ms to increase temporal resolution.

flying robots. For this comparison a styrofoam structure with the same weight as the Euler spring structures is built for the platform and is shown in Fig. 2.13E. The platform is dropped 5 times from increasing heights with either the Euler spring structures or the styrofoam structures, first on its base and then on a corner (vertex of a tetrahedral for Euler spring structures, between the propeller-protecting ring and two sides for styrofoam structures). The height is increased until the high-G accelerometers saturate. A drop test using a stiff protection mechanism only (Fig. 2.13F) is also done for comparison.

Figure 2.15A shows a box plot of the force measured on the platform for each experiment whereas Fig. 2.15B shows the profile of the force through time for a drop height of 75 cm. The following conclusions can be derived from these plots:

- Using only stiff protection of rotors results in high impact forces from even the smallest heights.

- When falling on its base, the Euler spring mechanism has high initial forces even at low

heights. This is due to the initial buckling force F_{crit} from 4 contact points that is reached before any energy is absorbed. Once this force is reached however it does not increase significantly even at 75 cm in accordance with the near-flat force profile of Euler springs.

- Foam-based protection transfers significantly more force to the platform's frame at high drop heights.

- Force profiles show that Euler springs absorb energy over a longer time period, thus decreasing the force on the frame.

As a general conclusion Euler spring protection mechanisms perform similarly to foam-based mechanisms at low heights, but significantly decrease impact force on the robot's frame in high-energy impacts. These trends could be better observed with higher drop heights but were not done for two reasons: accelerometers with higher thresholds were not available, and more importantly subjecting the stiff internal frame to higher forces would risk breaking the frame, making subsequent tests impossible.

Resilience during Flight

In this test we evaluate the robustness of the protective structures to repeated collisions from all directions during a realistic scenario. The robot is placed in the centre of a 3.5x6 m experimentation room. A simple behaviour is programmed on the on-board micro-controller which makes the platform take off, stabilize at a hovering altitude of 1 m for 3 s, then move in a random direction until it collides with a wall. Once a collision is detected with the on-board accelerometers and gyroscopes the motors are cut and the platform allowed to fall to the ground. More specific details on the controller and algorithms used for collision detection can be found in Ch. 4.

The experiment is repeated 50 times to simulate collisions from many directions with varying amounts of impact energy. From the 50 trials, only 4 collisions resulted in damage to the platform: twice the soft propellers flexed and touched each other and twice the nylon strings connecting end pieces failed. Using stiffer propellers (as used in a subsequent platform presented in Sec. 4.3) and increasing the thickness of the nylon string should limit these failure modes. This experiment demonstrates the robustness of the protective structures to repeated high-energy collisions. A sample of the many collisions can be seen at http://lis.epfl.ch/airburr.

2.4.4 Discussion

This section presents a novel protection structure design using Euler springs optimized for flying robots that must survive repeated high-energy impacts with their environment. The structure is shown to greatly reduce the impact forces transferred to a robot's frame compared to existing solutions using stiff or foam-based protection. The design is adapted to a small

hovering platform and validated through static drop tests and collision tests during flight in an indoor environment. Though presented on a specific platform type, the protective mechanism design is based on a simple cylindrical model of a hovering platform and thus can be applied to other types of platforms such as quadrotors.

An interesting behaviour was noticed during flight as a secondary effect of the Euler spring protection mechanisms: if the platform is contacting a wall with four tetrahedrals when in flight it has a tendency of staying in contact with the wall. Using a control surface to fly towards the wall makes the platform rotate around its top tetrahedrals. When trying to fly away from a wall, however, the low position of the control surfaces creates much less torque around the bottom tetrahedrals, and the platform has difficultly moving away from the wall. This behaviour can be both advantageous and disadvantageous; staying against a wall instead of bouncing off can be used for contact-based navigation such as wall-following or for easier attachment to surfaces (explained further in Sec. 5.3), but slow down progression through an environment. There are two possible ways of preventing this behaviour, if desired: using different lengths of springs for the top and bottom protection (though taking care that they are still close to the optimal length of Eq. 2.10) or simply cutting the motors when stuck against a wall, falling to the ground and taking off again (this option is only possible if the platform is capable of self-recovery).

2.5   Conclusion

The ability to absorb impact energy elastically allows flying robots to access constrained and cluttered environments that were previously unattainable. This chapter presents a method for designing protective structures that are uniquely adapted to the constraints of flying robots. This method is then applied to the protection of two flying robots with different morphologies and flight modes. The novel design and use of Euler springs on a hovering platform results in the first demonstration of a robot that can withstand dozens of high-speed collisions in a confined environment and continue flying, ready for further exploration.

3 Self-Recovery

Surviving collisions with obstacles is only one half of the equation; if a flying platform cannot get back into the air after a collision than it can no longer fulfill its purpose as a flying robot. This chapter considers self-recovery mechanisms that can be used to upright a flying platform after a fall to the ground and proposes a method for integrating such mechanisms into a flying platform. The method is first applied to a winged platform that uses gravity and optimized morphology to upright into a takeoff position. Lessons learned from this first prototype are then applied to a hovering platform which complements the gravity-based mechanism with active spring-based self-recovery. This second platform demonstrates the ability to upright after a collision in less than 30 s in a variety of realistic environments.

This chapter is based on the publications *An Indoor Flying Platform with Collision Robustness and Self-Recovery* [75] and *An Active Uprighting Mechanism for Flying Robots* [76].
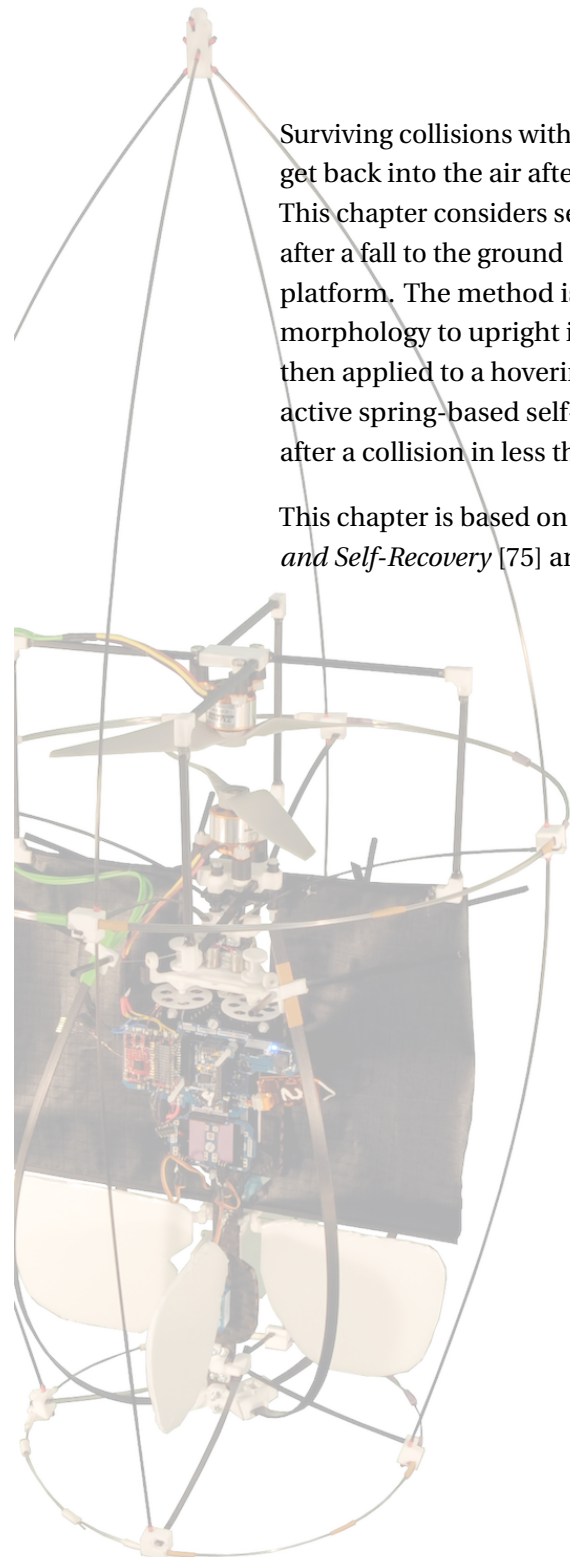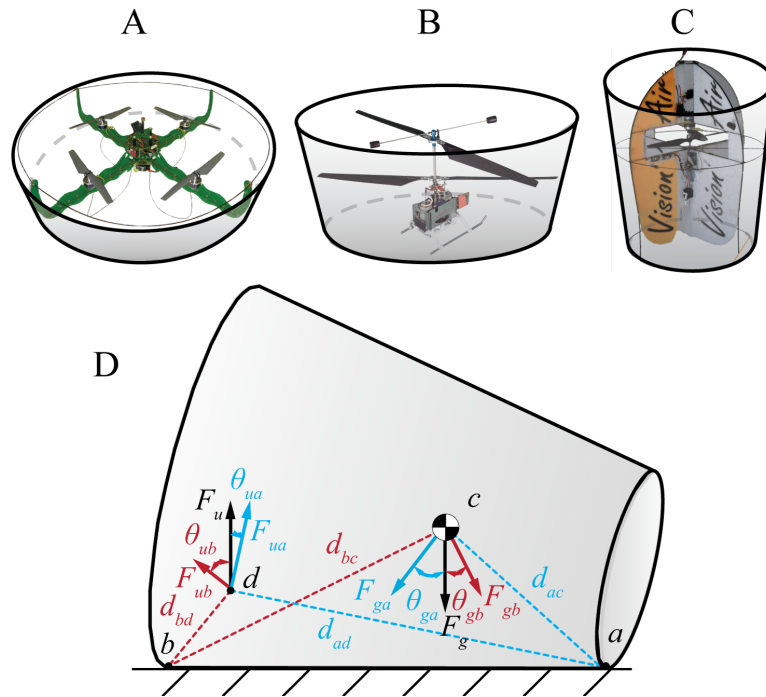
Figure 3.1: Three types of hovering platforms that, when adapted with protective cages for flight in cluttered environments, take the general shape of a truncated cone: (A) a quadrotor, (B) a coaxial helicopter and (C) a tailsitter. Below (D), a simplified diagram of the same truncated cone on its side before uprighting. A mass with a Center of Gravity at point c must rotate about point a using uprighting force F_u located at an arbitrary point d to return to the upright position depicted in (A-C).

3.1 Defining Self-Recovery

This chapter addresses the challenge of returning a flying platform to the air after an uncontrolled landing that may result from a collision without external intervention. More specifically, the topic of this chapter is *Self-Recovery*, which is defined as the process of returning a hovering flying platform to a position ready for subsequent takeoff, and *Self-Recovery Mechanisms*, the actuator(s) or and/or mechanisms used to generate the uprighting force required for self-recovery. To be successful a self-recovery mechanism must fulfill three major requirements:

- **Repeatability:** it must be able to consistently upright the platform from any possible position that it may fall in.

- **Adaptability to the environment:** it must work on different surface types, angles and with various amounts of obstacles such as walls or objects.

- **Integration:** it must not impede the flight capabilities of the robot and thus remain lightweight, low-power and unobtrusive.

In order to devise a method for designing self-recovery mechanisms, we must first define the global shape and Center of Gravity (COG) position of a hovering platform. As presented in the previous chapter (Sec. 2.4), most hovering platforms adapted for cluttered environments can be modelled as a cylinder. When a platform lays on its side the angle between its vertical axis and the ground plays an important part in self-recovery. As this angle can be changed relatively easily without affecting the performance of a flying platform, we extend the model to that of a truncated cone. Figure 3.1 shows the three most common robotic rotorcraft configurations (quadrotors, coaxial helicopters and tailsitters) and how they fit this general model.

Self-recovery can be reduced to the process of returning a truncated cone to its upright position, ready for vertical takeoff. Due to the symmetry of a cone in the vertical axis, the problem can be further reduced to a 2-dimensional rotation of a mass (as depicted in Fig. 3.1D) about point a through the application of an uprighting force F_u at an arbitrary point d. Two conditions must be met for this rotation to occur. Firstly, the uprighting moment created by the force F_u at the point d about point a must be greater than the moment created by gravity acting on the COG with a force F_g. The minimum magnitude of F_u for this condition, F_{uamin}, follows the equation:

$$F_{uamin} = \frac{F_g cos\theta_{ga} d_{ac}}{d_{ad} cos\theta_{ua}}$$

(3.1)

Secondly, the uprighting force F_u also creates a moment about point b. There is thus also a minimum force F_{ubmin} at which the mass will rotate around point b which follows a similar equation:

$$F_{uminB} = \frac{F_g cos\theta_{gB} d_{BC}}{d_{BD} cos\theta_{uB}}$$

(3.2)

As neither points a nor b are fixed to the surface, in order for the mass to rotate around point a and not point b, F_{uamin} must be less than F_{ubmin}:

$$F_{uamin} < F_{ubmin}$$

(3.3)

$$\frac{cos\theta_{ga} d_{ac}}{d_{ad} cos\theta_{ua}} < \frac{cos\theta_{gb} d_{bc}}{d_{bd} cos\theta_{ub}}$$

(3.4)

Equations (3.1) and (3.4) provide interesting insight into the position, direction and magnitude of the uprighting force F_u and the position of the COG required for rotation around point a. It can be summarized as follows:

- The COG position c should be as close to the rotation point a as possible, as minimizing d_{ac} decreases F_{gamin} (Eq. 3.1). In addition, moving the COG to the right towards point a moves it away from point b, increasing d_{bc} and thus increasing F_{ubmin}.

- If the COG can be moved to the right of point a the angle θ_{ga}, and subsequently F_{gamin} become negative (Eq. 3.1). This corresponds to the case of *gravity-based self-recovery* where no uprighting force is required.

- Point d should be as far as possible from point a and as close as possible to point b to avoid rotation around point b (Eq. 3.4).

Implementing the above guidelines in the design of an active uprighting mechanism is not always a straightforward process as aerodynamics, weight, morphology, position of control surfaces and the COG must all be balanced in order for the platform to be able to fly.

3.2   Self-Recovery Mechanism Design

We propose the following method for designing active uprighting systems:

1. **Uprighting Force Generation:** select a method of generating uprighting force best adapted to the current platform

2. **Modelling and Morphological Optimization:** model the self-recovery mechanism throughout uprighting action and optimize the morphology

Uprighting Force Generation

The selection of a self-recovery mechanism depends on many factors such as platform type, weight, complexity or morphology and must be adapted to the platform being used. Separate mechanisms may also be required to upright a platform when it is upside-down and when it is on its side. Some common force generation methods are presented in Table 3.1 along with their respective advantages and weaknesses.

Gravity-based self-recovery occurs when the morphology of the platform and its COG placement result in a negative θ_{ga} and thus gravity itself uprights the platform, removing the need for any additional uprighting force. If the COG is not placed favourably after a fall to the ground, an additional actuator can be used to displace the COG until θ_{ga} becomes negative. This strategy is used by many jumping robots [11, 53]. If the morphology of the platform does not allow the use of gravity for self-recovery another source of uprighting force is required.

Using existing rotors (in forward or reverse) has the great advantage of not adding any weight to the platform and should be used whenever possible. The force available from onboard rotors, however, is limited due to several reasons; the force is not always in the desired direction

throughout uprighting, rotors turning in reverse are less efficient and the individual rotors of a multi-rotor system provide limited force. To increase uprighting efficiency thrust can be vectored in the desired direction using smartly-placed control surfaces or by rotating the motors, though at the cost of additional mechanical components, servo-motors and increased complexity. A second option to increase reverse-thrust efficiency is to use variable-pitch propellers actuated by servomotors (as have been implemented in some quadrotors for example [77]) to change the direction and magnitude of the thrust.

When on-board rotors do not suffice an additional mechanism must be implemented. One example consists of a beam attached to the platform that pushes against the ground and is powered by an additional actuator such as a DC motor. This beam can be driven directly or can be attached to the platform using a torsion spring which itself is loaded using a DC motor.

Modelling and Morphological Optimization

Once a self-recovery mechanism is selected the next step is to modify the platforms morphology to facilitate self-recovery. For most flying systems the position of the COG must be set according to flight stability requirements [28], and thus cannot be moved for uprighting. The morphology of the protective cage however can be modified in relation to the COG to change the platform's contact points a and b. When the platform is on its side, for example, increasing the diameter of the top of the platform and decreasing that of the bottom increases the angle θ_{ga}, reducing the required uprighting force F_{uamin}. In some cases modifying the morphology can even lead to a negative θ_{ga} and gravity-based self-recovery, removing the need for any additional uprighting force.

As the platform rotates around point a, the direction of the uprighting force may change, as does the force due to the weight of the platform. A model should thus be created based on equations 3.1 and 3.4 to gain insight into the magnitude, position and direction of the force required to perform this action. The model can then be used to evaluate the required force during the entire uprighting action to dimension the force generation method to provide enough uprighting force. As the force output of an actuator is generally proportional to its weight and power requirements, minimizing the uprighting force is essential for a flying system.
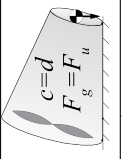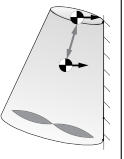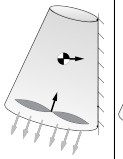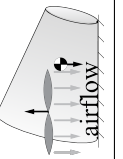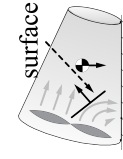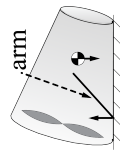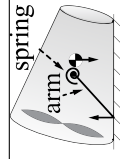
Method	Schematic	Description	Weight, Complexity	Ideal Morphology	Disadvantages
Gravity-based self-recovery					
Gravity-based	$c=d$ $F_g=F_u$	θ_{ga} is negative, gravity acting on the COG used for uprighting	Low	Platforms with very low COG	Sensitive to ground angle and presence of obstacles
COG Displacement		The COG is displaced within the platform to enable gravity-based self-recovery	High	Platforms with low COG	Can affect platform aerodynamics
Self-recovery with flight motors					
Reverse Thrust		One/several flight motors are reversed to provide thrust in the opposite direction	Low	Short and wide, multi-propeller platforms (e.g. quadrotors)	Propellers are less efficient, force may not be in the right direction
Propeller Rotation	airflow	One/several motors are rotated/displaced to provide thrust in a different direction	High	Single- or coaxial-motor platforms	Space is required around the propeller to prevent damage, motor mount can be fragile
Thrust Vectoring	surface	Airflow from one/several propellers is deviated using control surfaces	Low (existing surfaces) or High (additional surfaces)	Platforms with control surfaces (e.g. tailsitters, ducted fans)	Thrust deflected by control surfaces can be limited and may not be pointing in the right direction
Self-recovery with additional mechanisms					
Leg - Direct Actuation	arm	A mechanical appendage actuated using a DC or servomotor pushes against the ground	Medium	Any	Actuator with enough force is heavy, and can be damaged if appendage comes into contact with an object
Leg - Spring Actuation	spring arm	A mechanical appendage driven by a spring pushes against the ground	Medium	Any	Spring can be heavy, and must be wound using an additional mechanism.

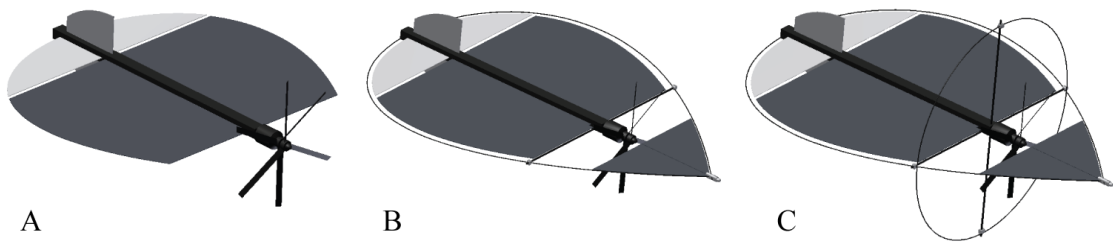Table 3.1: Methods of Uprighting Force Generation

Figure 3.2: A simple schematic of (A) a winged flying platform, (B) modified with a teardrop-shaped spring for collision energy absorption and (C) a ring to protect the propellers and enable gravity-based self-recovery.

3.3 Gravity-Based Self-Recovery and Forward Flight

This section is partially based on the semester project work of Grégoire Boutinard-Rouelle.

The self-recovery mechanism design methodology is first applied to a small wing-based flying platform optimized for forward flight. The advantage of winged platforms is that they can take off and fly horizontally and do not need to be in a vertical position to take off again. *Self-recovery* in this case is the process of returning the platform to a position lying on its side.

The platform is once again based on a basic design of a central frame with wings for lift generation, coaxial motors and propellers for thrust and control surfaces behind the wing for pitch and yaw control (Fig. 3.2A). Its weight is limited to 30 g in order limit the wing loading to allow efficient forward flight in the order of 1-2 m/s.

3.3.1 Self-Recovery Mechanism Design

Uprighting Force Generation

In the case of a winged platform a gravity-based self-recovery mechanism by means of the morphology of the platform and positioning of the COG is the simplest option to implement. Following the method and conclusions of Sec. 2.3, the platform is surrounded by a teardrop-shaped spring to provide protection from head-on collisions (Fig. 3.2B) as well as a first contact point with the ground at the front of the platform. Similarly, a ring around the propellers (Fig. 3.2C) both protects the propellers from contacting objects and provides a second contact point with the ground.

When the platform lands on its front (Fig. 3.3A) the tip of the teardrop spring and the protection ring provide the two contact points *a* and *b* with the ground. Placing the COG far enough towards the back of the platform will then cause the platform to rotate around the ring into a stable position on its side (Fig. 3.3B), ready to take off.
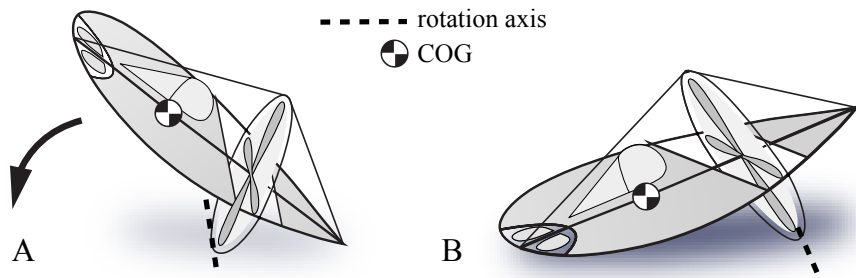
Figure 3.3: Gravity-based self-recovery based on platform morphology. When the platform falls on its front (A) gravity will act on its COG and subsequently upright it onto its side (B), ready for takeoff.
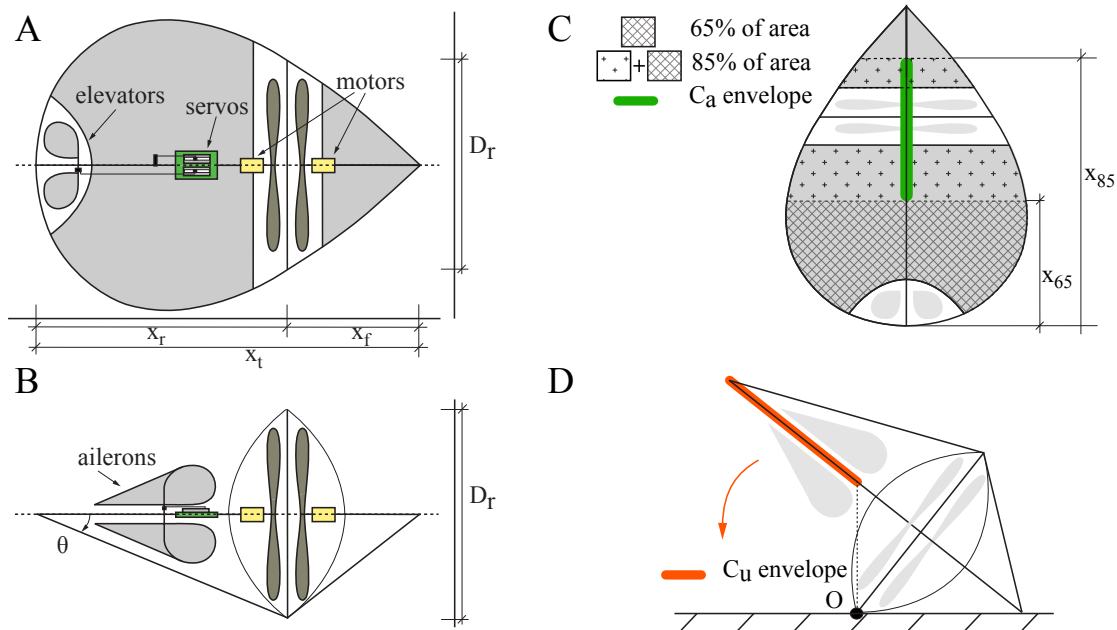
Figure 3.4: Left, Top (A) and side (B) views of the conceptual design of the platform. The teardrop shape of the wing and the takeoff angle θ are defined by the diameter D_r and position x_r of the ring protecting the propellers, and the total length x_t of the platform. Right, (C) aerodynamic constraints (top view of platform) require the COG to be placed between 65% and 85% of the wing surface area; this defines the C_a envelope. (D) Self-recovery (side view of platform) requires the COG to be placed behind the point perpendicular to the pivot point O; this defines the C_u envelope. The COG must be within both the C_a and the C_u envelopes to ensure flight and self-recovery.

Modelling and Optimization

The selected design has to be dimensioned carefully to fulfill the requirements of aerodynamic stability, efficiency and self-recovery capabilities. Maximizing the surface area A of the wing increases its lift, which in turn decreases required flight speed for a given weight [27]. Increasing the diameter of the propellers increases their efficiency [10] as well as the available thrust for a given motor size, required when hovering. Aerodynamic stability in forward flight is defined by the correct placement of the COG with respect to the wing. Self-recovery also constrains the position of the COG to allow gravity-based recovery. In addition the takeoff angle θ should be maximized to facilitate takeoff.

All of these parameters except for the position of the COG are defined by the geometry of the platform, which in turn is defined by three geometric parameters: the diameter of the ring D_r, its position x_r along the main axis of the platform, and the total length x_t of the platform. Figure 3.4A and B presents a schematic view of the platform from above and the side, respectively. A length x_t of 40 cm was chosen to remain within the size constraints of indoor flight, thus there remain only two dimensions that can be optimized to find a suitable platform shape.

The COG of the platform is an important constraint, as it must be placed to allow both upturning when on the ground and aerodynamic stability while in flight (Fig. 3.4C-D). These two constraints must therefore be evaluated to ensure that a position exists in which they overlap. It is assumed that the COG can be placed in any position during construction by strategically displacing heavy components such as the battery or the electronics.

The first step is the dimensioning of the wing. Bending a thin carbon rod into a circle and then connecting the two ends at any desired angle results in a teardrop shape that can be closely approximated by the following parametric equation:

$$x = \cos(t) \tag{3.5}$$
$$y = \sin(t)\sin^m(\frac{1}{2}t)$$

which can be rearranged into the equation:

$$y = \sin(\arccos(x))\sin^m(\frac{\arccos(x)}{2}) \tag{3.6}$$

The parameter m defines the shape of the wing (Fig. 3.5), and can be calculated by solving Eq. 3.6 at the point $x = x_r$, $y = \frac{D_r}{2}$, defined by the position and size of the ring. Once the parameter m is known, the total surface area of the wing can be calculated by integrating Eq. 3.6 from
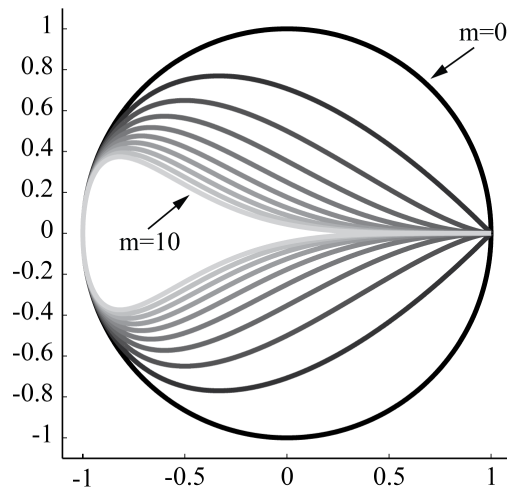
Figure 3.5: The Teardrop curves, the natural shape taken by a single carbon fibre rod with its ends attached, for m=0 (circle) to m=10.

$x = -1$ to $x = 1$, while taking into account the space required for the propellers.

The takeoff angle θ of the platform at rest (Fig. 3.4B) can be calculated geometrically using the formula:

$$\theta = \arctan(\frac{D_r}{2x_r}) \tag{3.7}$$

The position of the COG for self-recovery from a nose-down position, C_u, must be placed behind the pivot point O on the ring (Fig. 3.4D). The force of gravity acting on the COG then creates a moment that rotates the platform into takeoff position. It can be calculated as follows:

$$C_u < x_u, \qquad\qquad x_u = x_t - (\frac{D_r^2}{4x_f} + x_f) \tag{3.8}$$

where C_u is the COG required for self-recovery and x_u is the minimum distance of C_u from the front of the platform.

The COG position allowing aerodynamically-stable flight C_a is more difficult to calculate. It must be far enough forward to prevent stalling yet far enough back to prevent diving. Formulas exist for many standard shapes of wing and airfoil. For example, a straight wing in a classical plane with a tail should have its COG at 1/4 the chord distance from the leading edge [28]. However, the dual wings, flat yet flexible wing material and teardrop shape of the proposed
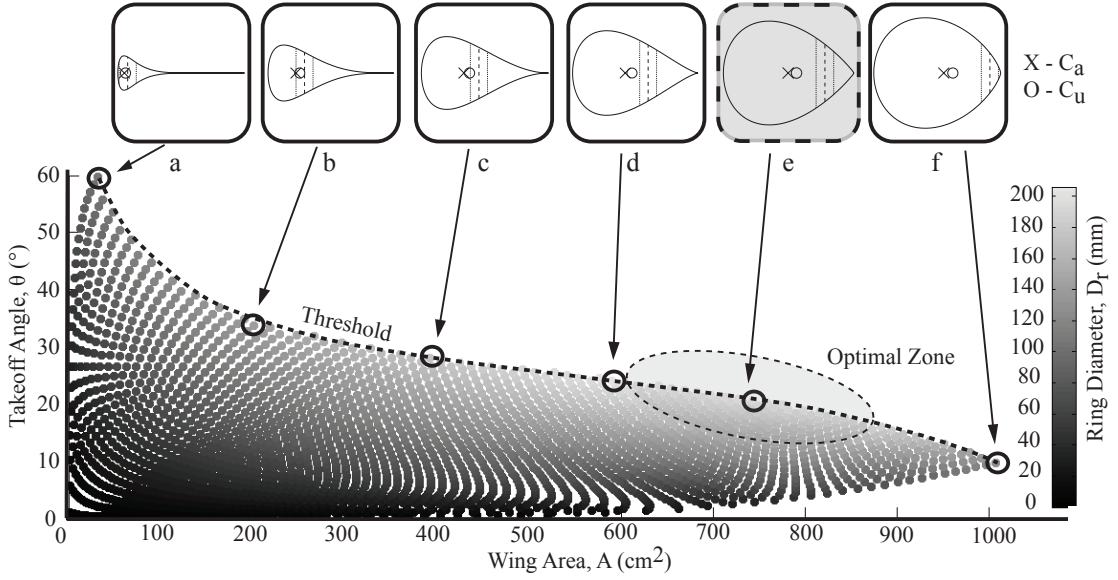
54

Figure 3.6: To maximize takeoff angle, wing surface area and ring diameter various configurations of these parameters for a platform length x_t of 40 cm are presented. All points below the threshold line represent configurations at which the COG requirements of flight and self-recovery are fulfilled. An optimal zone exists where both the wing area and ring diameter are maximized without greatly affecting the takeoff angle. Above the graph are six sample configurations that aid to visualize the parameters corresponding to the threshold line, with C_a represented by an X and C_u represented by a circle. Although all these configurations meet the COG requirements in theory, some are impractical to implement in a physical platform (such as the examples a and b due to their small wing area and f due to its small ring size). Configuration e is the one that was selected for the prototype flying platform.

design are all unconventional. Experiments were thus conducted using a mockup wing with a 10 g weight placed in varying positions along the wing's main axis to simulate the weight of the platform. The performance of the wing was evaluated through repeated trials to determine the COG positions that yield aerodynamically stable flight. Based on flight tests with the mockup, the value of C_a can be conservatively estimated using the equation:

$$x_{65} > C_a > x_{85} \tag{3.9}$$

where x_{65} and x_{85} are the points behind which 65% and 85% of the total surface area of both the front and the back parts of the wing reside, respectively (Fig. 3.4C).

The takeoff angle θ, wing surface area A and COG envelopes C_a and C_u were calculated for a series of ring positions x_r and diameters D_r ranging from 1 to 40 cm and with a fixed platform length x_t of 40 cm. C_a and C_u were computed for each configuration, and only those that fulfilled both requirements were considered valid. The main parameters to maximize are the

wing area, takeoff angle and the size of the ring, which defines the diameter of the propellers.

Fig. 3.6 presents the range of possible configurations that satisfy the requirements of COG positioning. Though configurations exist with takeoff angles of up to 60°, they do not have sufficient wing area for flight. Considering a minimum wing area of 200 cm^2, practical solutions begin with a takeoff angle of less than 30°. This angle diminishes by only 10° for wing areas ranging from 300 to over 800 cm^2, and thus the area can be maximized without greatly affecting the takeoff angle. The ring size also increases with the wing area, though it reaches a maximum at a wing area of around 750 cm^2.

There is no single architecture that maximizes all required parameters, though there is a certain optimal zone in which wing area and ring diameter can be maximized without greatly affecting the takeoff angle. A design within this optimal zone was chosen, with the maximum ring size of 206 mm, a wing area of 759 cm^2 and takeoff angle of 20.1°, which corresponds to a ring position of 281 mm from the back of the platform. This configuration has C_a and C_u positions of 186.5 mm and 191.85 mm, respectively, thus there exists a margin of 5 mm to position the COG to allow both aerodynamic stability and upturning.

3.3.2 Prototype Realization

A prototype flying platform is built using the above-mentioned optimized values (Fig. 3.7). Thrust is generated by two 6 mm DC motors with 14 mm contra-rotating propellers placed within the ring, providing a total of 30 g of static thrust. Energy is stored in a 110 mAh lithium-polymer battery. The total weight of the platform is of 20.5 g. The platform is controlled through two miniature servo-motors actuating a rudder and an elevator, which regulate altitude and yaw in forward flight. In addition to forward flight, the two coaxial motors provide enough thrust for hovering flight, and the control surfaces can be used to regulate roll and pitch in this flight mode. Off-the-shelf electronics enable individual remote control of the two servo motors and synchronous control of the two coaxial DC motors[1].

3.3.3 Characterization and Validation

The prototype is put through remote-controlled flight tests in a 6x7 m experimentation room and proves an agile flyer both in forward flight and in hover. Transition between hover and forward flight, and vice versa, is smooth and easily controllable, partly due to the backward placement of the COG. The platform can fly for approximately 10 min with a fully-charged 110 mAh battery, while spending some time in hover and some time in forward flight. A video presenting the flight characteristics of the platform in both forward and hover mode can be viewed at http://lis.epfl.ch/airburr.

---

[1] No control of yaw was implemented for hover mode due to limitations of the off-the-shelf electronics, though this could be implemented through individual control of the propellers or the use of an additional servo and differential actuation of the two elevators.
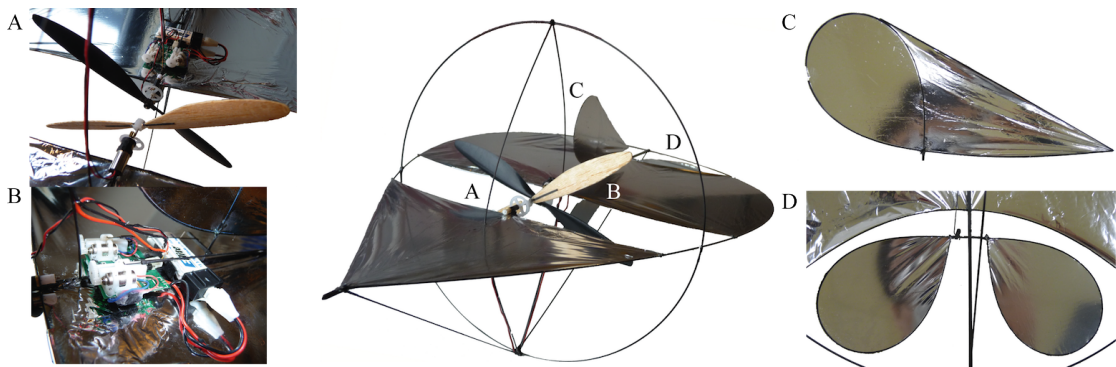
Figure 3.7: The prototype flying platform with details of various subsystems. (A) Two 6 mm DC motors power counter-rotating propellers for thrust. (B) A miniature off-the-shelf flight package includes two linear servo-motors to displace the rudders and elevators, a radio receiver and a single transistor to control both DC motors simultaneously. The wing, (C) dual rudders, (D) and dual elevator are all made of carbon rod frames over which an ultra thin mylar layer is stretched and glued.

During flight tests the prototype had numerous collisions with objects or surfaces such as walls or the ceiling. These collisions provide several insights into the self-recovery capabilities of the platform:

- Light contact with walls does not always cause the platform to fall to the ground. It can in fact fly along the wall, its front tip grazing the surface. This behaviour resembles insects flying against a window pane looking for an exit.

- After collisions with an object that cause a fall to the flat ground, the prototype's self-recovery mechanism is always successful in uprighting the platform onto its side, and in most cases can take off again without human intervention.

- Though always finishing on its side, if the platform does not have enough flat ground ahead of it it gets stuck against a wall or object and cannot take off again.

To further test the platform's resilience to collisions and ability to self-recover the platform is dropped from a height of 1 m from a variety of different starting positions. High-speed video is used to analyze the deformation of the structure during a collision. Similarly to the prototype designed in Sec. 2.3, as the platform hits the ground collision energy is absorbed through the deformation of the teardrop-shaped wing. Fig. 3.8 shows frames from a typical collision and subsequent righting of the platform after a head-on collision with the ground.

3.3.4 Discussion

A gravity-based self-recovery system greatly constrains the position of the COG, making it difficult to fulfill the aerodynamic constraints required for flight and limiting the possible
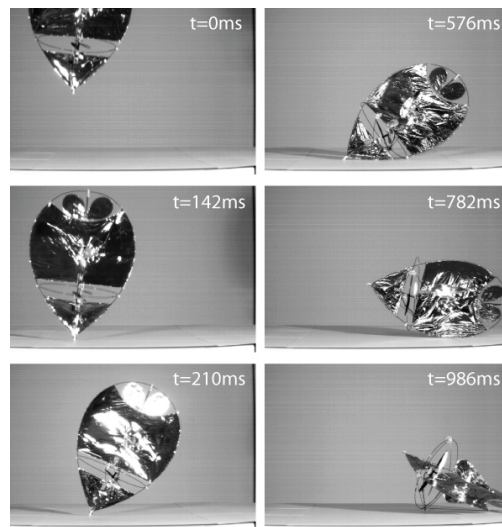
Figure 3.8: Time-sequence of a typical head-on collision with the ground and subsequent self-recovery, taken with a high-speed camera. The platform rolls onto its side before rolling into takeoff position.

platform geometries. Though able to self-recover autonomously in many situations, there are still many real-life scenarios that remain a challenge to the platform, such as landing against walls or objects, in rough and uneven terrain or underneath tables or chairs. The simple passive mechanism is thus not yet sufficient for autonomous self-recovery in all cases. Indeed, this work seems to have reached the limits of gravity-based recovery, and thus the development of an active self-recovery mechanism will be presented in the next section.

3.4 Leg-Based Self-Recovery and Hovering Flight

In this section a new platform is designed to overcome some of the limitations of gravity-based self-recovery. Once again the design is based on two coaxial motors with control surfaces, as shown in Fig. 3.9A, but with several design changes to previous platforms:

- To avoid the need for a runaway to take off, the platform must be able to take off vertically. A circular pedestal is added underneath the control surfaces to provide a stable position for takeoff.

- The platform will be designed to be autonomous instead of remote controlled as the platform from the previous section and thus will feature an on-board IMU.

- The two coaxial motors are mounted on either side of a stiff carbon-fibre cage to protect the propellers.

- The platform will be heavier (similar in weight to the platform presented in Sec. 2.3.1 and thus will spend most of its time flying in hover mode.)
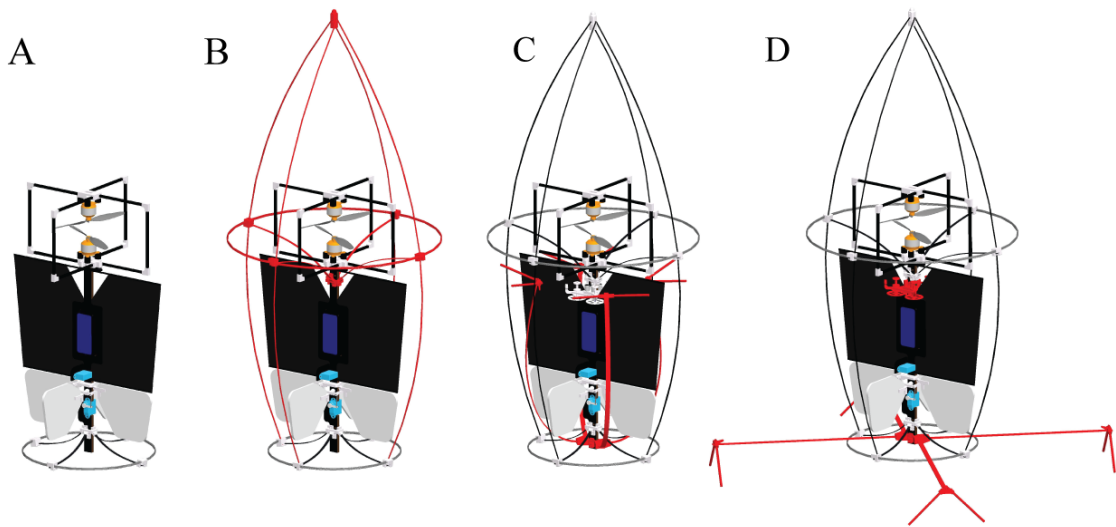
Figure 3.9: (A) A simplified schematic of the tailsitter platform in the upright position with a round pedestal providing a stable position. (B) A protective cage (in red), who's morphology has been adapted for gravity-based self-recover, is added to the robot. Four legs (in red), shown in their (C) retracted and (D) extended positions, are used to upright the platform when it is lying on its side.

In the case of this platform *self-recovery* will be the process of returning the platform to a vertical position, ready for takeoff.

3.4.1 Self-Recovery Mechanism Design

Uprighting Force Generation

This platform design how has three positions it can lie in: upside-down, on its side or upright. The gravity-based self-recovery mechanism in the previous section was very successful in returning the previous platform onto its side and is thus reused in the current design. Teardrop-shaped springs, attachment springs and a ring are once again added around the platform (Fig. 3.9B) for both collision energy absorption and self-recovery. The teardrop springs are modified to attach to the landing gear ring at the base of the platform. The COG is placed within the C_u envelope to enable self-recovery, though this time its position is not optimized for forward flight as the platform is primarily meant to hover. If the landing surface is slanted, reverse thrust from the main rotors can easily provide the extra force required.

Uprighting the platform when it is on its side requires an additional self-recovery mechanism. The platform morphology could potentially be further modified to allow gravity-based self-recovery into the upright position but the sensitivity to ground angle and obstacles would remain. Using thrust from the on-board propellers cannot provide force in the correct direction to upright the platform, as they are almost inline with the bottom ring and thus provide little uprighting torque. Thrust vectoring with the control surfaces has a similar issue.
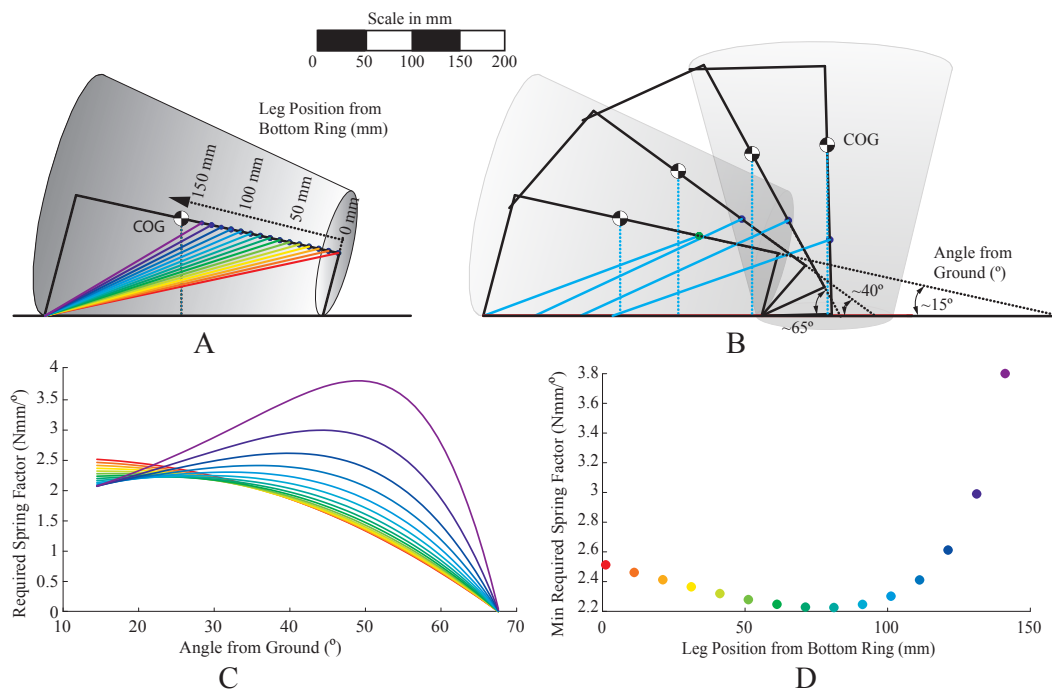
Figure 3.10: Optimization of leg attachment position on the fuselage. (A) shows the different attachment positions modelled, each with a respective colour. The leg is made as long as possible while still remaining within the protective cage when retracted. All of these attachment positions will result in a rotation around the bottom ring and not the top ring (Eq. (3.4)). (B) shows four example positions during the uprighting process. (C) plots the required spring factor at each angle during uprighting. (D) plots the minimum spring factor that must be dimensioned for uprighting to be successful.

An additional mechanism using extending 'legs' attached to the fuselage through a spring is thus chosen, as it can be built lightweight and can be integrated without greatly affecting aerodynamic performance. During flight the spring is fully loaded and the leg is held within the protective cage of the platform (Fig. 3.9C). When the platform is lying on its side the leg is extended providing the necessary uprighting force (Fig. 3.9D). Using spring-based legs decouples the driving motors from the legs in case of shock that can occur during flight, and thus is better adapted to cluttered environments.

Modelling and Morphological Optimization

A model based on Eq. 3.1 and 3.4 is used to evaluate the force required from the legs at various attachment points (Fig. 3.10A) to optimize the size of the spring and the attachment point of the legs during the entire uprighting process (Fig. 3.10B). A fuselage length of 270 mm, top ring radius of 135 mm, bottom ring radius of 70 mm and a mass of 250 g are used to correspond to the desired dimensions of our platform. The length of the leg is always maximized to provide the highest possible uprighting moment about the bottom ring while still fitting within the
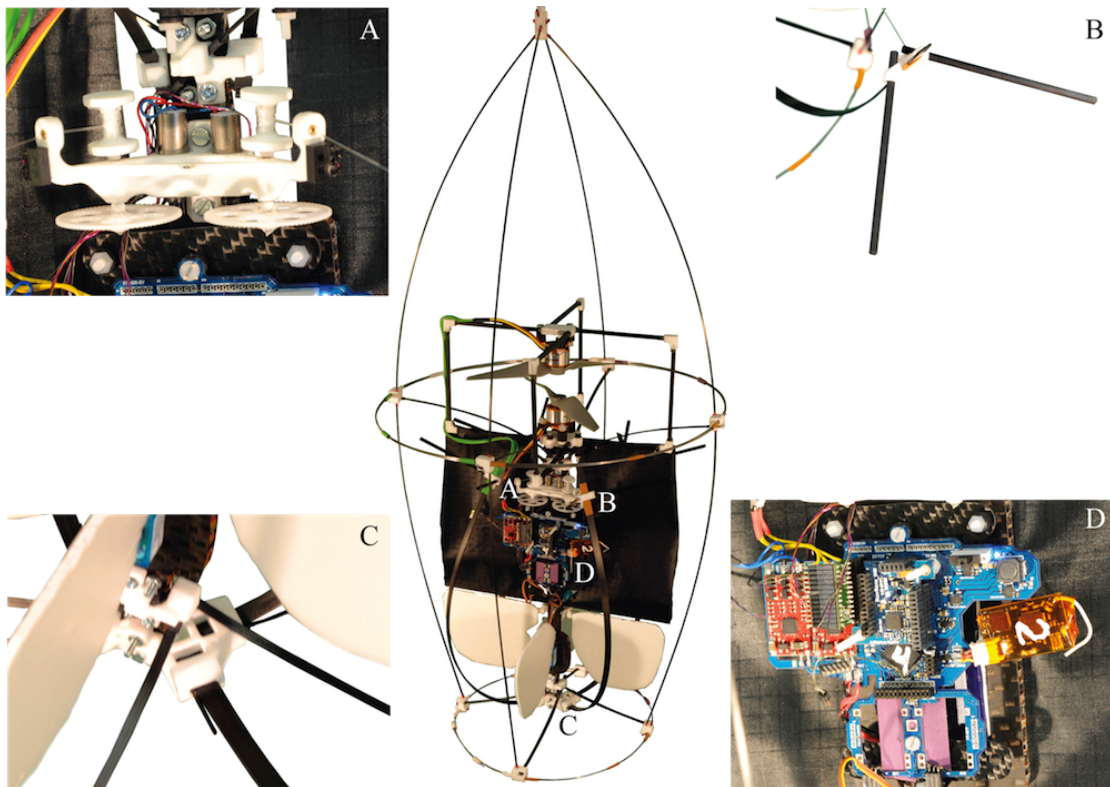
Figure 3.11: The AirBurr prototype with integrated active uprighting mechanism. (A) shows one half of the rollup mechanism used to close the legs for flight, made of 6 mm DC motors that wind nylon string. (B) shows the end of the 'leg' with attached 'feet' for stability. (C) The attachment point of the legs to the platform frame made of 3D-printed plastic. (D) The control electronics and on-board sensors.

top ring of the platform. Figure 3.10C shows the varying spring factor profiles based on the spring's attachment point to the fuselage. As the attachment point moves from the bottom of the platform to the top, the initial spring factor decreases since the length of the leg decreases. However, the angle between the leg and the ground increases and thus a smaller component of the force at the tip of the leg is used to upright the platform. There is thus an optimal attachment position of 80 mm (Fig. 3.10D) from the back of the platform at which the spring constant k, and thus the size of the spring, is minimized. It should be noted, however, that any attachment point of less than 110 mm from the bottom ring will provide a spring factor within 15% of the minimum possible value.

3.4.2 Prototype Realization

The modified cage and optimized leg-based self-recovery mechanism is integrated into a flying platform, as seen in Fig. 3.11. The platform requires 4 legs, one for each quadrant, to be able to upright from any possible position on its side. Instead of using a stiff (and thus heavy) leg attached to a high-torque (also heavy) spring, we use flexible carbon-fibre beams that

integrate the spring within the leg itself. The legs are dimensioned to provide the spring factor required by the model and are anchored near the optimal attachment point using 3D-printed plastic. Two carbon-tube 'feet' at the end of each beam (Fig. 3.11B) provide a more stable anchor point on uneven ground. The legs are retracted using nylon string attached to their tips which are rolled up using 4 individual 6 mm DC motors with a 225:1 gear ratio (Fig. 3.11A). All four legs, including feet and attachment pieces, weigh a total of 21.2 g whereas the rollup mechanism with associated electronics weighs 18.2 g, for a total self-recovery mechanism weight of 39.4 g.

The platform is equipped with the BurrMove v4.1 and BurrSens v4.2 electronics package (as the platform in Sec. 2.3.1). In addition to these two boards (which are required for flight) two more daughter boards were designed: one to control all 4 DC motors individually and a second that can interface up to 9 infrared (IR) proximity sensors. As the DC motors are small and have no encoders, 4 IR proximity sensors on the tips of the rollup mechanism are used to detect when the legs are fully retracted. A simple autonomous uprighting controller is implemented on top of the regular flight controller. The controller uses the accelerometer (also used for flight control) to detect the orientation of the platform. If the controller detects that the platform is on its side it will unravel all four legs to return the platform to a vertical position. Once the platform is vertical and standing on its bottom ring, all legs are retracted into their closed position, ready for takeoff.

3.4.3 Characterization and Validation

The platform is put through a series of tests to evaluate its performance based on the design requirements: repeatability, adaptability to the environment, and integration. A successful uprighting is one that can return the platform to an upright position ready for takeoff, that is with an angle between the ground and the fuselage of more than 70°.

Repeatability

The first round of tests is aimed at measuring repeatability of the uprighting motion on flat, smooth ground to show that the uprighting motion is independent of the starting position. The platform is placed upright, manually knocked over 20 times in random directions and subsequently uprighted using the autonomous controller. Figure 3.12A shows the angle along the axis of the fuselage facing the ground during uprighting, calculated using the on-board IMU. As the legs extend, the platform rotates until two of the four legs are touching the ground, which occurs in the first 5-10 s of the uprighting maneuver. These two legs and the back ring form three points of contact and thus a stable orientation for the rest of the uprighting maneuver. As there are four legs symmetrically spaced around the platform, there are four stable positions during uprighting, as can be seen in the figure. A typical uprighting sequence is shown in Fig. 3.13.
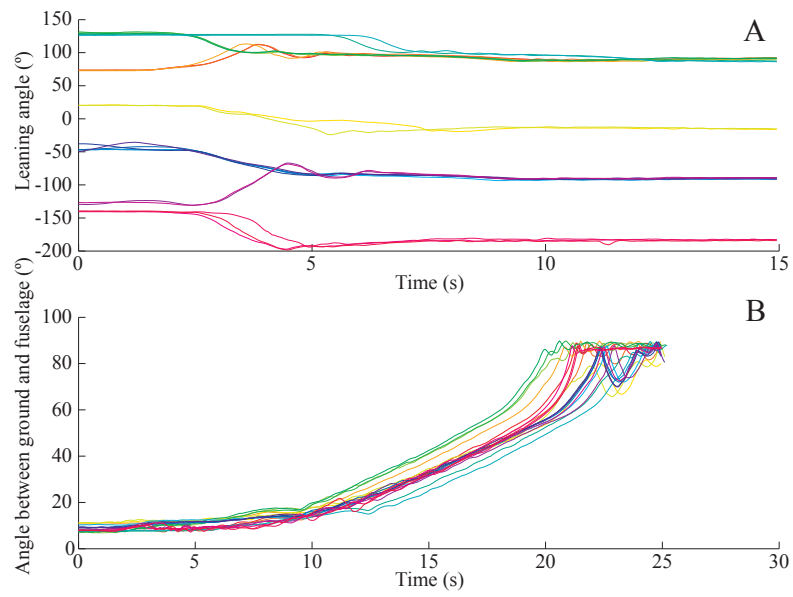
Figure 3.12: Platform orientation sequences during 20 uprighting maneuvers, each denoted by a different shade. (A) plots the robot's leaning angle. (B) plots the angle between the fuselage and the ground during uprighting.
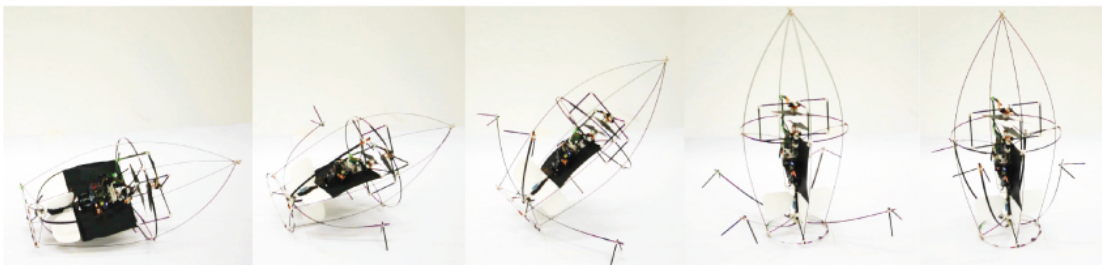

Figure 3.13: From left to right, a typical uprighting sequence using the autonomous controller.
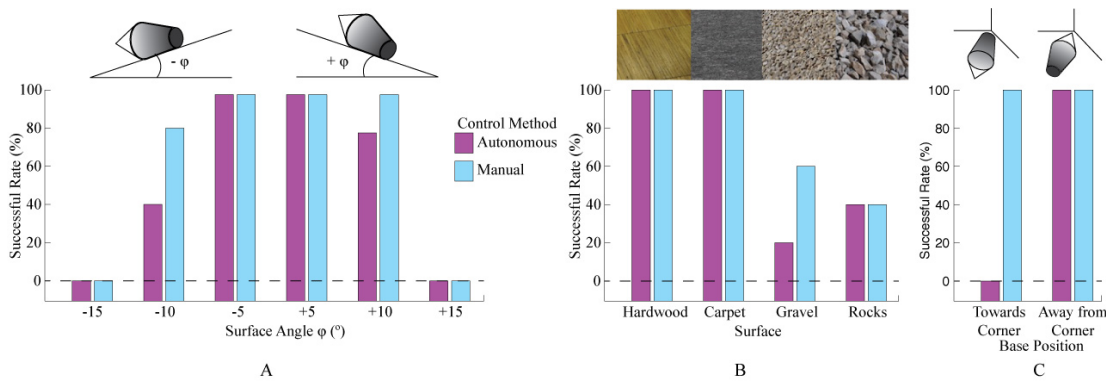
63

Figure 3.14: Uprighting success rate for various environments based on 5 trials using the autonomous controller (purple) and 5 trials by a human operator (blue). (A) plots uprighting on ground angles between +/- 15°. (B) plots uprighting in various surface textures, whereas (C) plots uprighting in corners.

Figure 3.12B plots the angle between the fuselage and the ground (uprighting angle) for each uprighting trial. Irrespective of the starting position, the platform consistently uprights at the same speed, between 20 and 25 s. The speed is limited by the motor and gear ratio selected for the rollup mechanism, which are optimized for weight rather than speed. This test successfully demonstrates the ability of the robot to consistently upright irrespective of its starting position on the ground.

Adaptability to the Environment

The next set of experiments tests the mechanism's adaptability to differences in surrounding obstacles, ground angles and surface textures. In each case the experiment is run 5 times using the autonomous controller and 5 times using individual, manual control of the four legs by a human operator. The success rate of the various experiments is shown in Fig. 3.14.

The first set of experiments varies the angle of the ground between -15° and +15° to simulate the often uneven ground found in unstructured environments. A second set of experiments varies the ground texture between hardwood, carpet (found in typical indoor office environments), gravel (found in outdoor environments) and small rocks (to simulate a cave environment). A third experiment evaluates the performance of the mechanism in right-angle corners, a common and difficult landing position for flying robots after a collision. The prototype is placed on its side in a right-angle corner on hardwood, with its base pointing first towards and then away from the corner.

As demonstrated, the mechanism works successfully in many common situations. In the cases that uprighting does not succeed there are several ways of increasing the success rate:

- When the ground angle is below -15° (Fig. 3.14A) the force from the legs is only able to

partially upright the platform. In most of these cases the platform is vertical enough to still be able to take off, stabilize and close its legs. Manual control can increase success by extending one leg more than the other, slightly changing the angle and direction of the resulting uprighting force.

- When the ground angle is above +15° the platform topples over itself and falls down the slope. In these cases, once again the platform can take off before being fully upright, or close its legs and upright a second time. Manual control increases success by slowing down the final stage of uprighting thus preventing the platform from toppling over.

- High surface roughness can cause the carbon 'feet' to occasionally get stuck (Fig. 3.14B). Retracting and then re-extending the legs in manual mode can help the feet get unstuck.

- Extending all four legs at once is not well suited for difficult situations such as corners (Fig. 3.14C), where the legs simultaneously push agains walls or other obstacles and get stuck. In such situations simply extending some legs and not others in manual mode will lead to successful uprighting.

Most of the failure modes are due to the simplicity of the on-board automatic controller, which only opens or closes the four legs all at once.

Integration into flight systems

The final experiment demonstrates that the mechanism can be integrated into a flying robot and not impede on its primary activity of flying. The total weight of the mechanism, including legs, rollup mechanism, sensors and electronics is 39.8 g, which represents 16 % of the total weight of the platform (250 g). The symmetry of the mechanism about the fuselage does not significantly alter the COG or the flight aerodynamics of the entire platform. The extra weight does however reduce flight time from an average of 4:21 min to 2:11 min (based on three flights in each configuration with a full battery).

A series of 5 test flights are performed during which the robot is kept flying for approximately 30 s, then purposely flown into a wall causing the platform to drop to the flat, obstacle-free ground. In all cases the robot is able to upright itself autonomously and return to flight within 30 s of the collision. A video with a sample of these flights can be seen at http://lis.epfl.ch/airburr.

3.4.4 Discussion

The platform described in this section is the first demonstration of a flying robot that is built specifically to survive collisions with its environment and that is capable of returning to a takeoff position autonomously irrespective of its falling position. Its active self-recovery mechanism has been shown to work in a variety of environments that can be encountered in

realistic applications. In particular, it is successful on slanted ground and around obstacles, environments that are difficult for gravity-based self-recovery.

The current controller is a simple one that only uses the signals from on-board accelerometers. A more advanced controller could be written if there was information available about the position of the legs and the force they are providing. Initial investigations show that strain gauges mounted directly on the leg near its connection point to the frame can accurately measure the shape of the leg, and thus the force that it provides at its tip. Further strain gauges at the interface between the rollup string and the leg can be used to measure the tension in the string. Combining information about the leg position and string tension would allow the controller to detect whether the legs are touching an object in its environment. As an example, when the platform has its base pointed into a corner (Fig. 3.14C) the lack of tension in the strings of all the legs can indicate that the platform is stuck. A smarter controller can then use this information to retract the legs pushing against the walls, allowing the platform to continue uprighting.

3.5 Conclusions

This chapter introduced the basic theory of uprighting of a rotorcraft platform after a collision as well as a method to design self-recovery mechanisms that can be applied to many types of flying robots. The method was then then implemented on two separate platforms resulting in robots capable of autonomously returning to the air without the need for help from a human operator.

Uprighting is only useful if a platform has enough space above it to take off vertically. In environments where this is not the case (i.e. under a table or chair, or in a room with a low ceiling) it would be beneficial if the platform could displace itself on the ground to reach a more open area to take off. Indeed, all flying animals also have legs to move on the ground when flight is not possible. Actuators already present on the robot can provide some of this functionality. For example, the main thrusters can drag the robot forward on the ground, or even backward if both motors are reversed. If only one of the motors are reversed, the resulting torque on the platform makes it roll on its top and bottom rings, displacing itself sideways.

Similarly, the legs mechanism may also have uses beyond uprighting when on the ground. For example, the legs can be used as a contact point on a vertical surface while in flight, allowing the robot to position itself and subsequently perch on a wall. Integrated strain gauges can also provide information on the surface quality of a wall before a perching behaviour.

4 Exploiting Crash-Proof Flying Robots

The goal of this chapter is to integrate the methods developed in the previous two chapters into a single robotic platform that can absorb collision energy, upright itself and return to flight repeatedly and consistently. A controller is implemented in the robot's on-board processor enabling it to take off, stabilize its orientation and altitude, fly in the direction of a light source, detect collisions and self-recover, all fully autonomously. The platform's unique capabilities are successfully demonstrated using two tasks that have traditionally been difficult for flying robots: flight in a completely dark environment and phototaxis in a narrow corridor.

This chapter is based partly on the publication *Flying, crashing and recovering: random search and phototaxis with minimal sensing* [78].
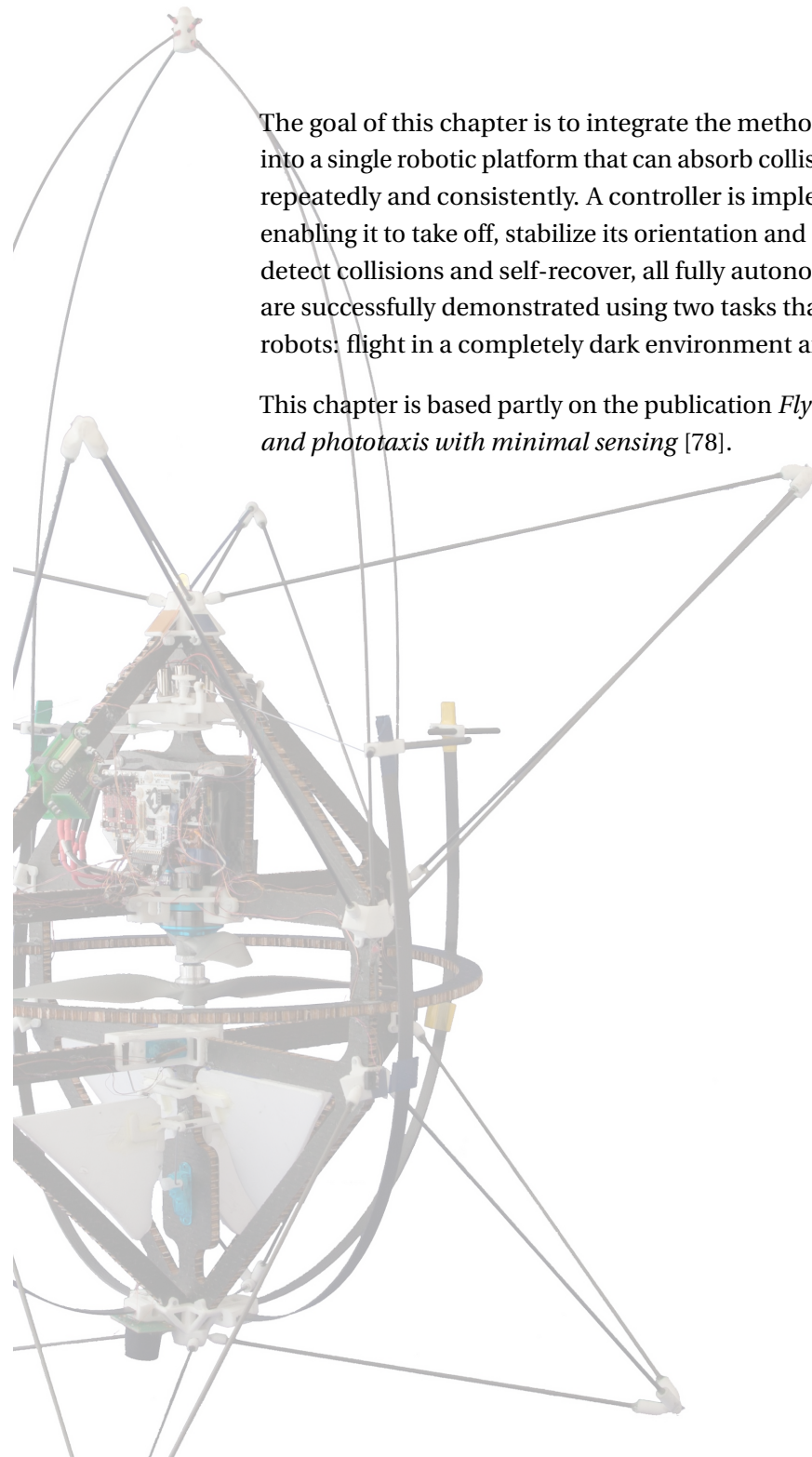
4.1   Motivation

The previous two chapters presented methods for designing collision energy absorption and self-recovery mechanisms and validated their individual functioning through detailed experiments. A robot cannot self-recover if it doesn't survive a collision, however, and conversely cannot complete a task if its in one piece but upside-down on the ground. To be truly useful, energy absorption and self-recovery must be integrated into a single platform.

The ability to resist and recover from contact frees a flying platform from the constraints of obstacle avoidance and thus simplifies many navigation tasks. As was presented in Sec. 1.2.1, any platform that depends on obstacle detection and avoidance to navigate cluttered environments is sensitive to the quality of the information it receives from its sensors, and thus vulnerable to the sensors' shortcomings. Navigating a dark room filled with smoke such as a burning building, for example, is not possible for platforms depending on visual [35] or laser-based [25, 34, 24] SLAM. The ability to bump against walls removes the need to detect all obstacles and can thus enable simple gradient-based navigation techniques. Platform payload being used for heavy laser scanners or computers can instead be used to increase the flight time of the platform or to mount remote cameras or chemical sensors more useful to the platform's human operators.

4.2   Platform Design

This section details the design of an autonomous flying platform that integrates collision energy absorption, self-recovery and the sensing required for autonomous navigation. As the platform requires a variety of sensors and should navigate in a highly constrained environment, a hovering design similar to the one presented in Sec. 2.4 represents the core of the platform (Fig. 4.1A). Once again, two coaxial motors are used for thrust and yaw control and two control surfaces for pitch and roll control.

Collision Energy Absorption

The platform core is first outfitted with Euler-spring protective mechanisms for absorbing collision energy (Fig. 4.1B). As the core is the same shape as the one presented in Sec. 2.4, the same dimensioned carbon fibre rods (20 cm length, 1 mm radius) are used for the four tetrahedrals protecting the bottom of the platform. The top tetrahedrals are made slightly longer to prevent the platform from staying against the wall when in flight, though still using the same radius (25 cm length, 1 mm radius). Their slightly decreased energy absorption ability due to their increased length[1] is justified by the fact that the hovering platform is much more likely to fall onto its bottom tetrahedrals when flight motors are cut due to a collision.

---

[1]The critical buckling force of a column is inversely proportional to the square of its length, and thus longer columns can absorb less energy. The longer length also translates to less loading in the axial direction. For a more detailed analysis see Sec. 2.4.
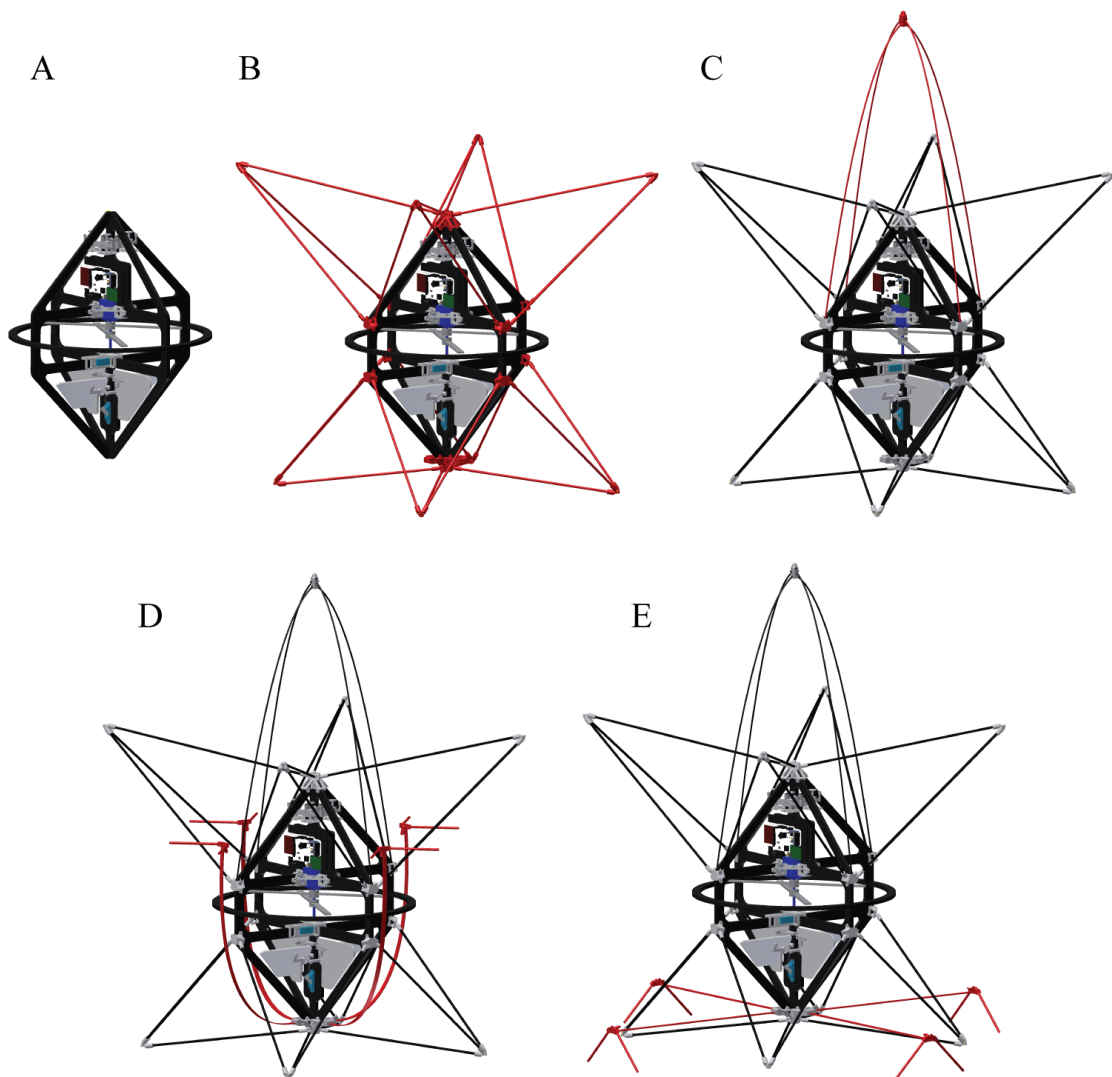
Figure 4.1: A schematic of the integrated platform as it's adapted for collision energy absorption and self-recovery. Each additional mechanism is outlined in red. (A) The core of the platform with all the actuators and electronics required for flight. (B) Euler-spring tetrahedral protective structures are added for collision energy absorption. (C) An additional contact point with the ground is created to enable gravity-based self-recovery when the platform is upside-down. (D) A spring-leg-based self-recovery mechanism with its legs retracted and (E) extended.

Self-Recovery

The configuration of the eight tetrahedral protective structures results in a platform that can land upright, on its side or upside-down. To upright when upside-down a gravity-based self-recovery mechanism is selected. The platform's contact points with the ground are set by the dimensions of the platform and its tetrahedrals. An additional contact point is created at the top of the platform using four carbon fibre rods (Fig. 4.1C) whose length is defined using equations (3.1) and (3.4). Detailed modelling of this mechanism as presented in Sec. 3.3 is not required, as the platform does not have a wing and does not have to be optimized for forward takeoff and flight. Though not explicitly designed for collision energy absorption, the four rods bend on contact and thus do provide some additional protection.

A spring-leg-based active self-recovery mechanism is implemented to upright the platform when it is on its side. As shown in Sec. 3.4, as long as the legs are positioned near the bottom of the platform their spring factor remains close to the minimum required value. The legs are thus mounted at the bottom of the platform's frame (Fig. 4.1D in their retracted state, Fig. 4.1E in their extended state), their exact position defined by the mechanical constraints of the rest of the platform rather than through precise modelling.

4.3 Prototype Realization

A new flying platform named Nighthawk (Fig. 4.2) is built based on the same core platform as presented in Sec. 2.4. The flexible, 3-blade propellers used in the previous platform (GWS HD-8040x3 and HD-8040x3R) are replaced by stiffer 2-blade propellers (APC 7x5 and 7x5P) to prevent them from flexing and contacting the frame during a collision. The high-G accelerometers are moved onto a support bar to free up space for the rollup mechanism which uses the same design as previously but with slightly more powerful DC motors (Fig. 4.2B). The platform retains the same BurrMove v5 and BurrSens v5 electronics package which is mounted just below the rollup mechanism. A dual-colour red and green Light-Emitting Diode (LED) is mounted at the top of the frame to indicate the robot's status (Fig. 4.2A). A Maxbotix LV-MaxSonar-EZ1 ultrasonic (US) range sensor is mounted on the bottom of the frame to measure the platform's altitude when in flight (Fig. 4.2C). The sensor has a detection range of 15-645 cm. The self-recovery legs are made using four carbon fibre beams (dimensions: 7x1x330 mm).

4.4 Autonomous Controller and State Machine

An autonomous controller is implemented in the embedded microcontroller to demonstrate the platform's ability to navigate in cluttered environments using minimal sensing and computation. Flight parameters can be monitored and modified through a radio connection to a base station, but all sensing, processing and control is implemented on-board. The controller is designed to navigate either in a random direction or towards a source of light (phototaxis) but
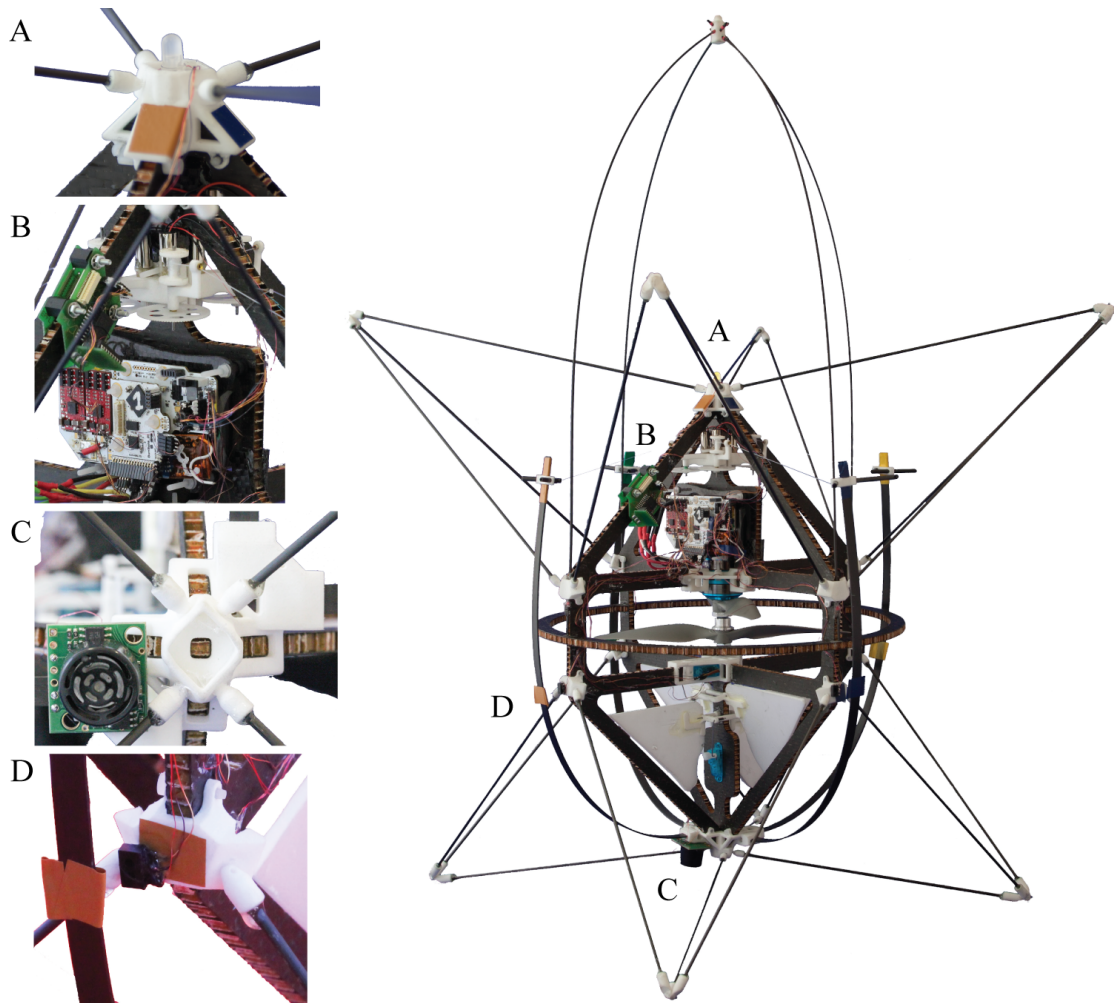
Figure 4.2: The Nighthawk flying robot with integrated Euler-spring collision energy absorption and leg-based self-recovery mechanisms. (A) A status LED is used to indicate the robot's state when flying in the dark. (B) On-board electronics including high-G accelerometers are used to control the robot's flight, and 4 DC motors wind the legs when in flight. (C) An ultrasonic distance sensor is used to control altitude. (D) IR proximity sensors are used to detect the retraction status of the legs as well as the ambient light.

with one major difference compared to traditional navigation algorithms: instead of avoiding obstacles the controller detects collisions and recovers from them (Fig. 4.3A). The controller uses a state machine that cycles through 5 possible states depending on the platform's condition: Idle, Takeoff, Directed Flight, Contact Detected and Self-Recovery (Fig. 4.3B). The bi-color status LED is green in the Takeoff and Directed Flight states and red in the Contact Detected and Self-Recovery states.

Takeoff, flight stabilization and collision detection algorithms were implemented by Adrien Briod.

State 0: Idle

The *Idle* mode is the default mode at startup. The platform waits for a connection with the remote control with flight motors turned off as a failsafe measure before beginning the behaviour. The controller can be returned to this state at any time using a command from the remote control.

State 1: Takeoff

This state occurs when the platform detects that it is on the ground and upright, ready for takeoff. The altitude controller is enabled which sets a high thrust to give the platform a strong push into the air. Once the target height is reached or a predefined time has passed the controller switches to Directed Flight.

State 2: Directed Flight

Once in the air the platform is stabilized in a vertical hover using the on-board IMU. Sensor information from a 3-axis rate gyroscope, a 3-axis accelerometer and a US distance sensor is fused using a Kalman filter [79] to estimate the platform's orientation in the roll, pitch and yaw axes (Fig. 4.4A) and its distance from the ground. The control flaps are then used to stabilize the roll and pitch angles, whereas the coaxial motors stabilize the yaw angle and altitude. Figure 4.4B presents the estimated angle and stabilization outputs for the three orientation axes of the platform during a typical flight. The orientation estimation filter and stabilization controller was implement by Adrien Briod, and more information can be found in [80].

During stabilized flight the platform is given one of two possible direction commands, set by a switch on the remote control: random or phototaxis. The random direction θ_r is reset to a new value after every takeoff, and can be used to perform a random search exploration of an environment. The phototaxis direction θ_{ph} is calculated using the 4 IR proximity sensors[2] that are also used by the self-recovery mechanism to detect the retraction status of the legs (Fig. 4.2D). The sensors are equally spaced at 90°angles around the perimeter of the platform

_____

[2]Vishay Semiconductors TCRT1000

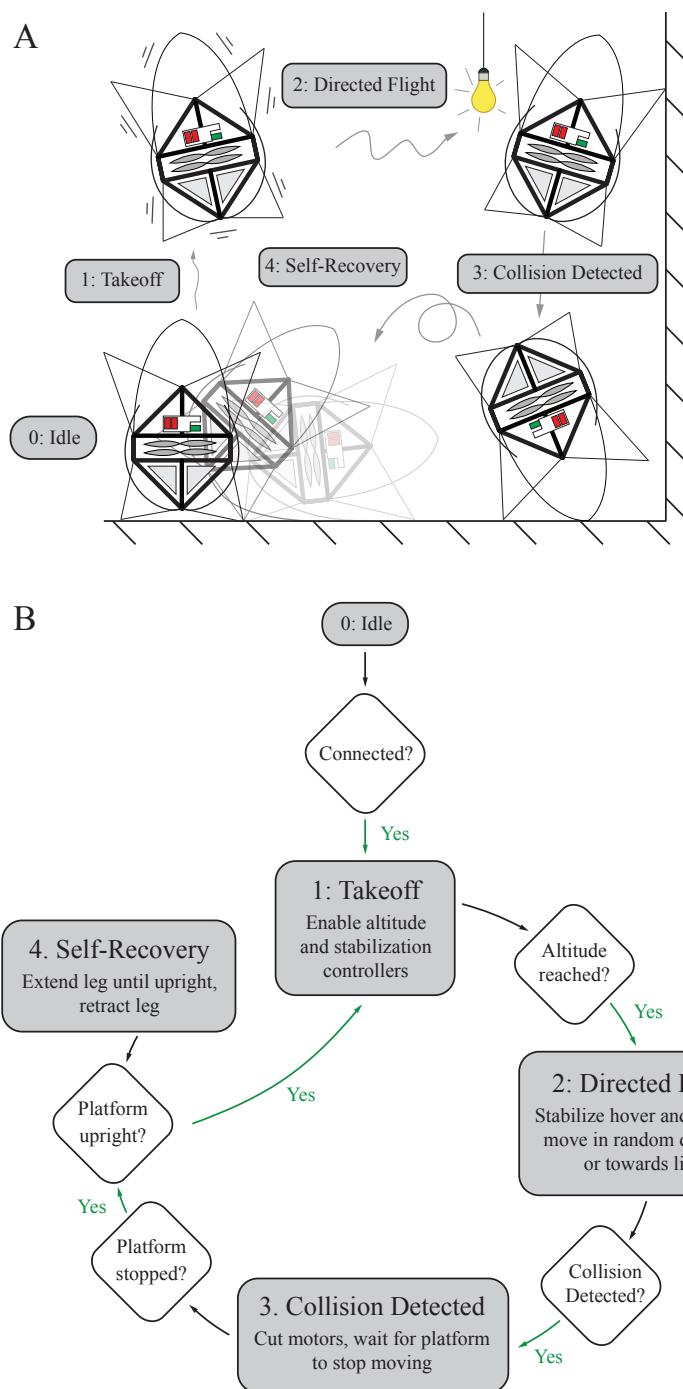Figure 4.3: The autonomous controller implemented on the flying platform. (A) A schematic of the robot's behaviour shows the 5 possible states that it can be in: (0) Idle, (1) Takeoff, (2) Directed Flight, (3) Collision Detect and (4) Self-Recovery. (B) A detailed state machine diagram presents the states as grey squares, state change conditions as diamonds and the flow between states as arrows.
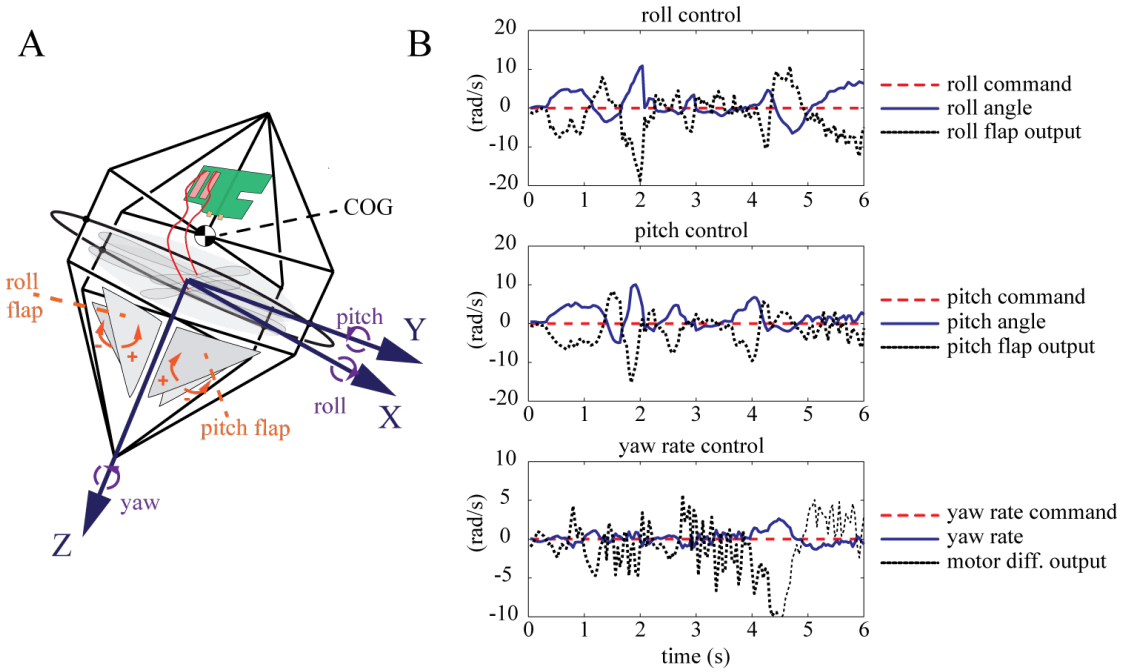
Figure 4.4: Stabilization of the three orientation axes during hovering flight. (A) A schematic representation of the platform with a definition of the controlled axes. Only the core of the platform is shown for simplicity. (B) Command, platform angle and actuator output for roll, pitch and yaw angles during a typical flight.

and have an integrated photodiode that can be used to detect ambient light. The bearing to the strongest light source around the platform is calculated using the signal of the sensor with the highest ambient light s_0 and the two sensors to either side of it s_{-1} and s_{+1} using the formula:

$$\theta_{ph} = \theta_{s0} + \pi\left(\frac{s_{-1} - s_{+1}}{s_{-1} + s_0 + s_{+1}}\right) \tag{4.1}$$

where θ_{s0} is the pointing direction of s_0. Though a more accurate bearing could be calculated using a greater number of sensors and more complex algorithms [81], using only 4 sensors which are already present on the platform better demonstrates the robustness of the platform and behaviour to low signal quality.

State 3: Collision Detected

A simple collision detection algorithm that constantly samples the on-board accelerometers is implemented, inspired by similar algorithms used in the automotive industry to trigger airbags [82, 83, 84]. If an acceleration of more than 2 G (19.6 m/s^2) is detected (after com-

pensating for gravity) while in Takeoff or Directed Flight states the controller switches to the Collision Detected state and the flight motors are cut. Using a threshold of 2 G, selected based on initial flight tests, allows the platform to stay in flight after small impacts or when flying against a wall but protects its from high-energy collisions that destabilize the platform and are difficult to recover from. Once the platform stops moving for 1 s after a fall to the ground the controller switches to the Self-Recovery state. The on-board accelerometers have enough range to detect collisions, and thus the high-G accelerometers are currently only used for experimental characterization.

State 4: Self-Recovery

The self-recovery behaviour is a slightly improved version of the one presented in Sec. 3.4. As opposed to the previous platform which would lie on its side on two circular rings, the current platform contacts the ground with four tetrahedrals and thus has four stable positions on its side. The leg closest to the ground can thus be extended alone without causing the platform to roll on its side. Extending a single leg avoids the problem of getting stuck when in a corner or against a wall. Once the platform is uprighted the leg is retracted until it is fully enclosed within the tetrahedrals, as detected using the IR proximity sensor, and the controller returns to Takeoff state.

4.5 Contact-Based Behaviours

4.5.1 Random Exploration

In this first experiment the platform performs a random search behaviour to explore a small (3.5x6 m) enclosed experimentation room. In the Directed Flight state the platform uses the random direction command and continues flying until it comes into contact with a wall. Similar simple algorithms are commonly used by vacuum cleaning robots such as the Roomba and are designed to maximally cover floor area even in the presence of clutter [85].

Figure 4.5 presents a bird's-eye view of an example flight. Beginning in the centre of the room, the platform takes off and flies in a random direction, contacts a wall and subsequently uprights in preparation for takeoff. This process is repeated 7 times and lasts 140 s, during which time the platform explores a large portion of the experimentation room.

Figure 4.6 presents the measured altitude, pitch angle and maximum force acting on the platform[3] through time for the same example flight. Takeoff and Directed Flight states are best seen on the altitude graph[4] whereas the Collision Detected state coincides with high values of maximum force. In some cases the state changes from Collision Detected directly to Takeoff; this happens when the platform lands upright (represented as a triangle in Fig. 4.5). Four of

---

[3]Maximum force is measured using the high-G accelerometers.
[4]Spikes in altitude are due to the low-quality signal of the US altitude sensor.
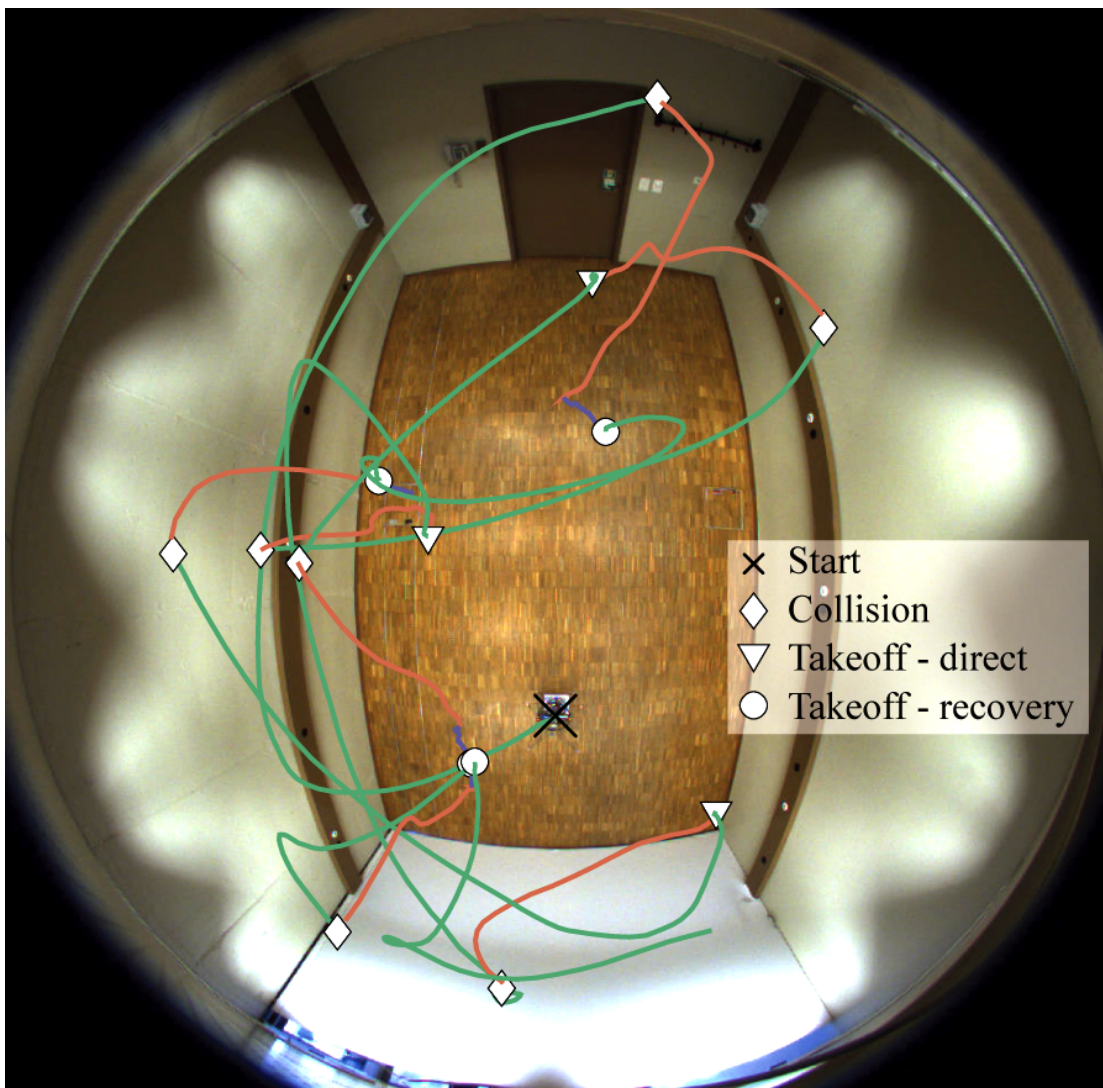
Figure 4.5: Autonomous flight trajectory of the collision-robust and self-recovering platform in a small (3.5x6 m) experimentation room as recorded from above using a 180° fish-eye lens. The platform takes off, flies in a random direction until it collides with an obstacle, uprights itself and takes off again, all autonomously. Takeoff and Directed Flight states are outlined in green, the Collision Detection state in red and the Self-Recovery state in blue. Starting position is marked with a black X, collisions by diamonds, takeoffs that require uprighting with a circle and takeoffs with no uprighting with a triangle.

Figure 4.6: Altitude, pitch angle, and force amplitude measured over time during a test flight in the experimentation room. The state of the robot is overlaid on the graphs. Takeoff and Directed Flight states can be seen in the altitude graph, force amplitude indicates Collision Detected state whereas Self-Recovery can be seen in the pitch angle graph.
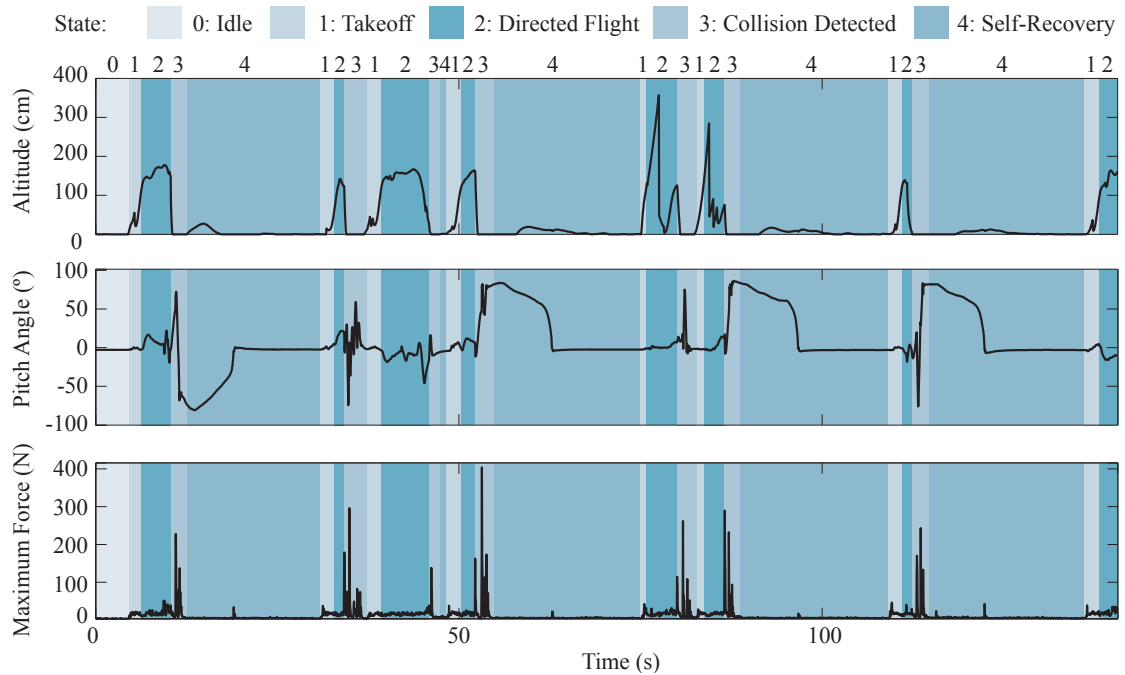
the seven collisions result in a landing on its side (represented as a circle in Fig. 4.5) and the subsequent Self-Recovery state is best reflected in the platform's pitch angle.

A main advantage of contact-based random exploration is its ability to navigate environments where obstacle detection is difficult, such as dark or smoke-filled rooms. To demonstrate this capability the same experiments is performed but this time in complete darkness. The position of the platform during a 3-minute flight is tracked by recording its status LED in a long-exposure photograph taken using a camera with a rectilinear wide angle lens placed in a corner of the room. Figure 4.7 shows three trials of the experiment.

Contact-based random exploration is successfully demonstrated in a completely dark environment and provides a good basis for subsequent experiments in goal-directed exploration.

4.5.2 Phototaxis with Minimal Sensing

This experiment expands the ability of contact-based exploration by replacing the random direction command during the Directed Flight state with a phototaxis command. The platform is placed at one end of a 13x2.2 m corridor at the other end of which is a bright light (Fig. 4.8B) that can be differentiated from ambient light using IR proximity sensors. The platform then navigates autonomously towards the light using the same controller and state machine as in

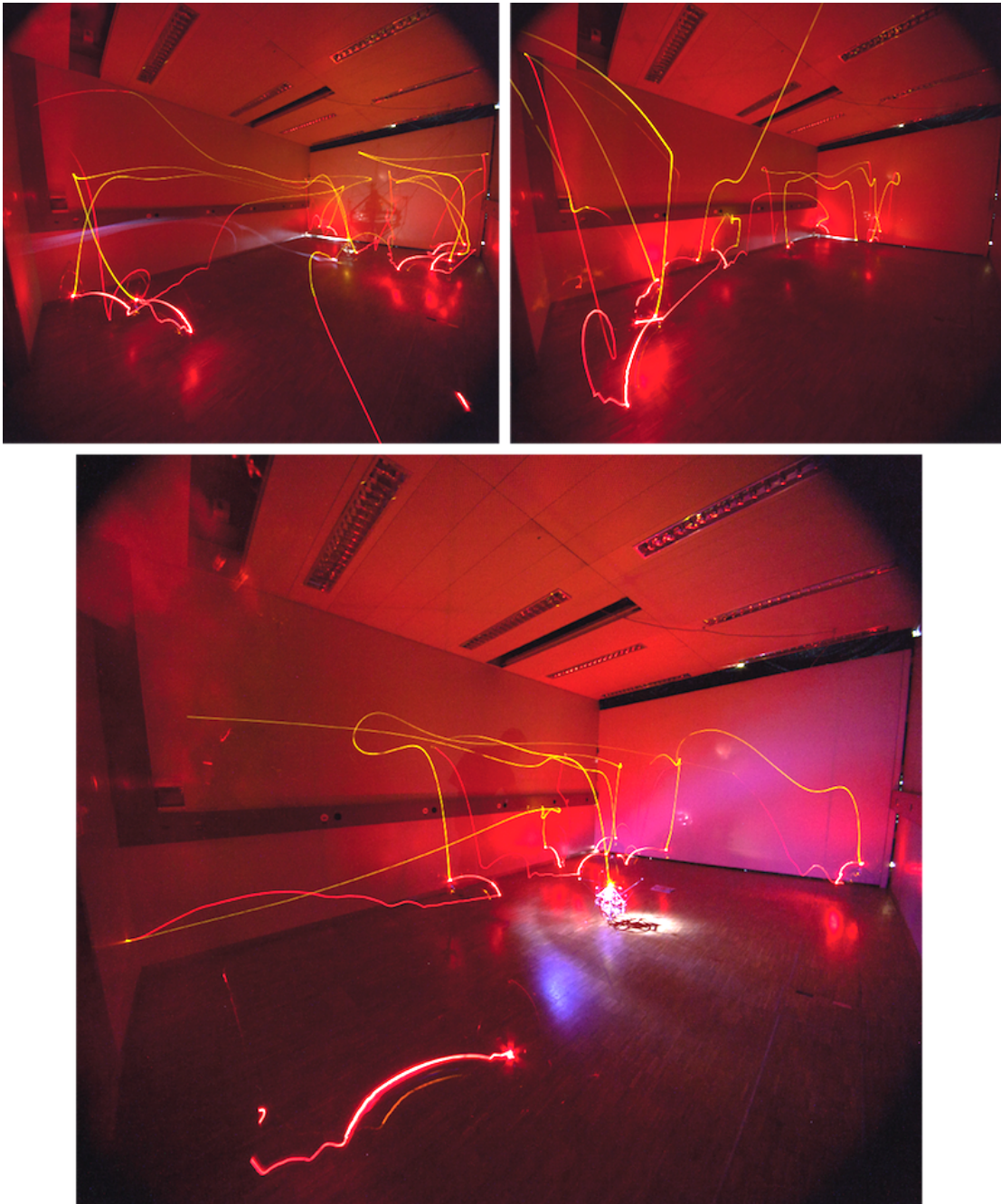Figure 4.7: Long-exposure images of three flights in complete darkness using a contact-based random exploration behaviour, in the same experimentation room as in Fig. 4.6. The trajectories are created using the on-board Status LED, which is green during Takeoff and Directed Flight states and red during Collision Detected and Self-Recovery states. The images are recorded using a 3-minute-long exposure.

the previous experiment. Figure 4.8A shows the trajectories of 10 trials in which the platform succeeded in traversing the corridor and passing through the 2x1.2 m doorway (Fig. 4.8C).

Looking at the trajectories individually (Fig. 4.9) shows that the most difficult parts of the navigation task were at either end of the corridor. At the start of the experiment the Nighthawk is quite far from the light source. Plotting the total detected ambient light throughout each trial (Fig. 4.10) shows that the detected signal begins at <1 % of full scale. This creates a large error in the estimated light source direction causing the platform to fly towards the corridor walls. Nevertheless, its ability to self-recover allows it to slowly advance down the corridor until the signal strength increases.

As the platform navigates the corridor it often comes into contact with the walls. After low-energy collisions, however, the platform often stays in contact with the wall and follows it in the direction of the light (the green flight trajectory of Trial 7 in Fig. 4.9 is a perfect example of this behaviour). High-energy collisions can also be beneficial; if the platform is already moving towards the doorway contacting a wall can cause it to rebound even farther down the corridor without using energy (this can typically be seen in trials 3, 6 and 9 in Fig. 4.9).

The second difficulty occurs when trying to cross the doorway as the platform is not always able to pass through without its tetrahedral protective mechanisms coming into contact with the doorway. Once again its ability to self-recover allows the platform to try again repeatedly until it successfully reaches the other side.

Table 4.1 presents some statistics on the 10 trials which reveal several interesting insights on the phototaxis behaviour:

- There is a large variability in the time taken to traverse the corridor. If there are few collisions and the light signal is detected immediately the robot can traverse the space in less than 6 s. Every collision takes time to recover from, especially if uprighting is required, and can thus increase traversal time by an order of magnitude.

- On average 71% of collisions result in the platform landing on its side and requiring uprighting. This goes a long way to increasing the required traversal time but also demonstrates the necessity of the mechanism.

- Though the average traversal time is 68.6 s, the platform only spends 26% of that time with its flight motors on (Fig. 4.11). This navigation strategy can thus compete with other strategies based on careful traversing at slow hovering speed to avoid contact with obstacles.

- The platform spends half of its time recovering from collisions. Though this has little cost in terms of energy consumption (as the main flight motors are shut off), it may be a problem for time-sensitive applications. The speed of the leg-based self-recovery mechanism could be improved by re-dimensioning the DC motors used for rollup, though at a higher weight cost.
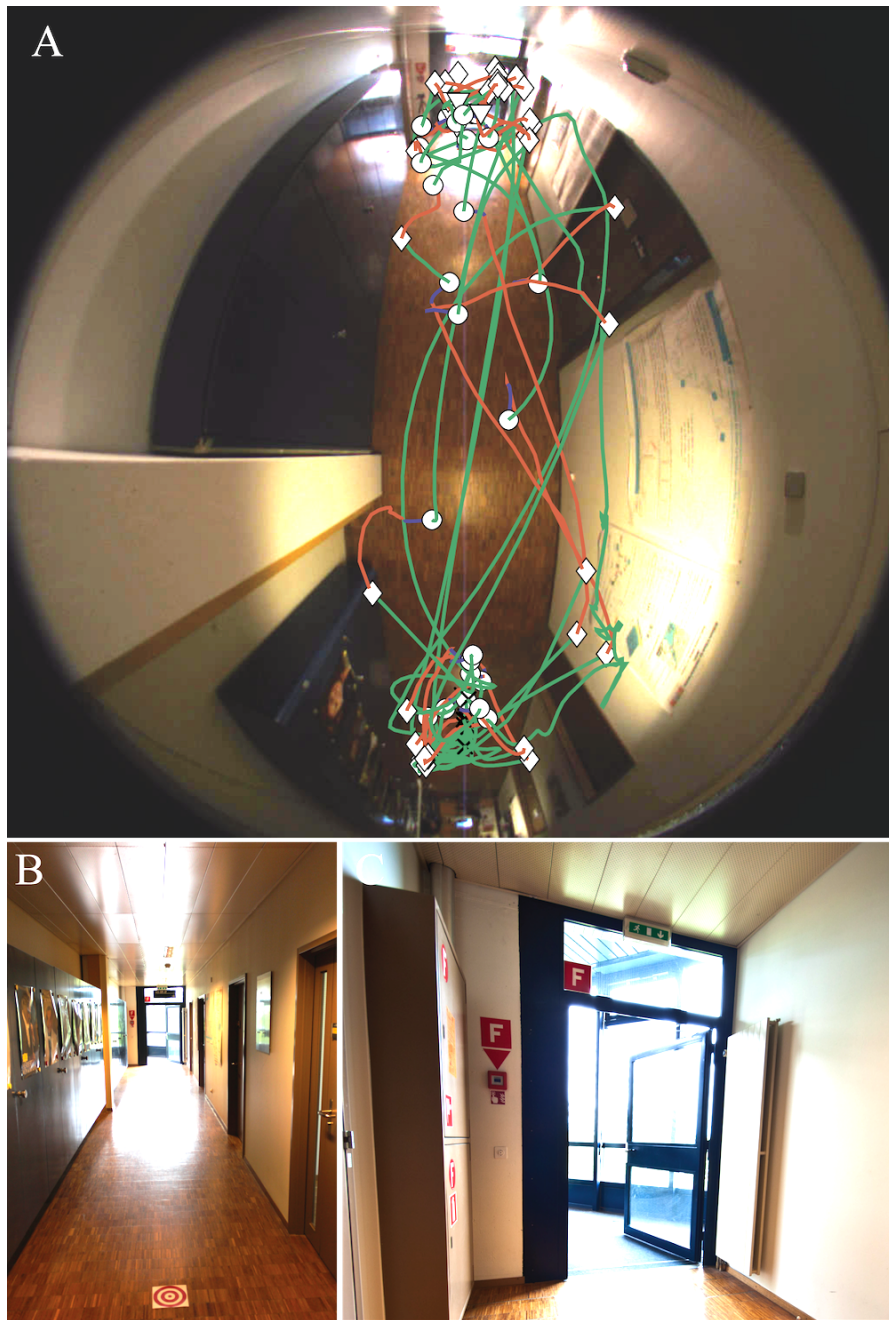
Figure 4.8: Environment and results for phototaxis experiments. (A) Flight trajectories of 10 flights recorded using a fish-eye lens hanging from the ceiling. The platform begins at one end of the 13x2.2 m corridor (bottom of image) and flies towards the doorway at the other end of the corridor (top of image). Takeoff and Directed Flight states are outlined in green, the Collision Detection state in red and the Self-Recovery state in blue. Starting position is marked with a black X, collisions by diamonds, takeoffs that require uprighting with a circle and takeoffs with no uprighting with a triangle. (B) An undistorted view of the corridor and doorway with a target marking the takeoff position. (C) The 2x1.2 m doorway at the end of the corridor. Every trial was considered completed when the platform passed through this doorway.

Figure 4.9: Individual trajectories for the same 10 trials of the phototaxis experiment presented in Fig. 4.8 with trajectory colours and marker shapes having the same meaning.

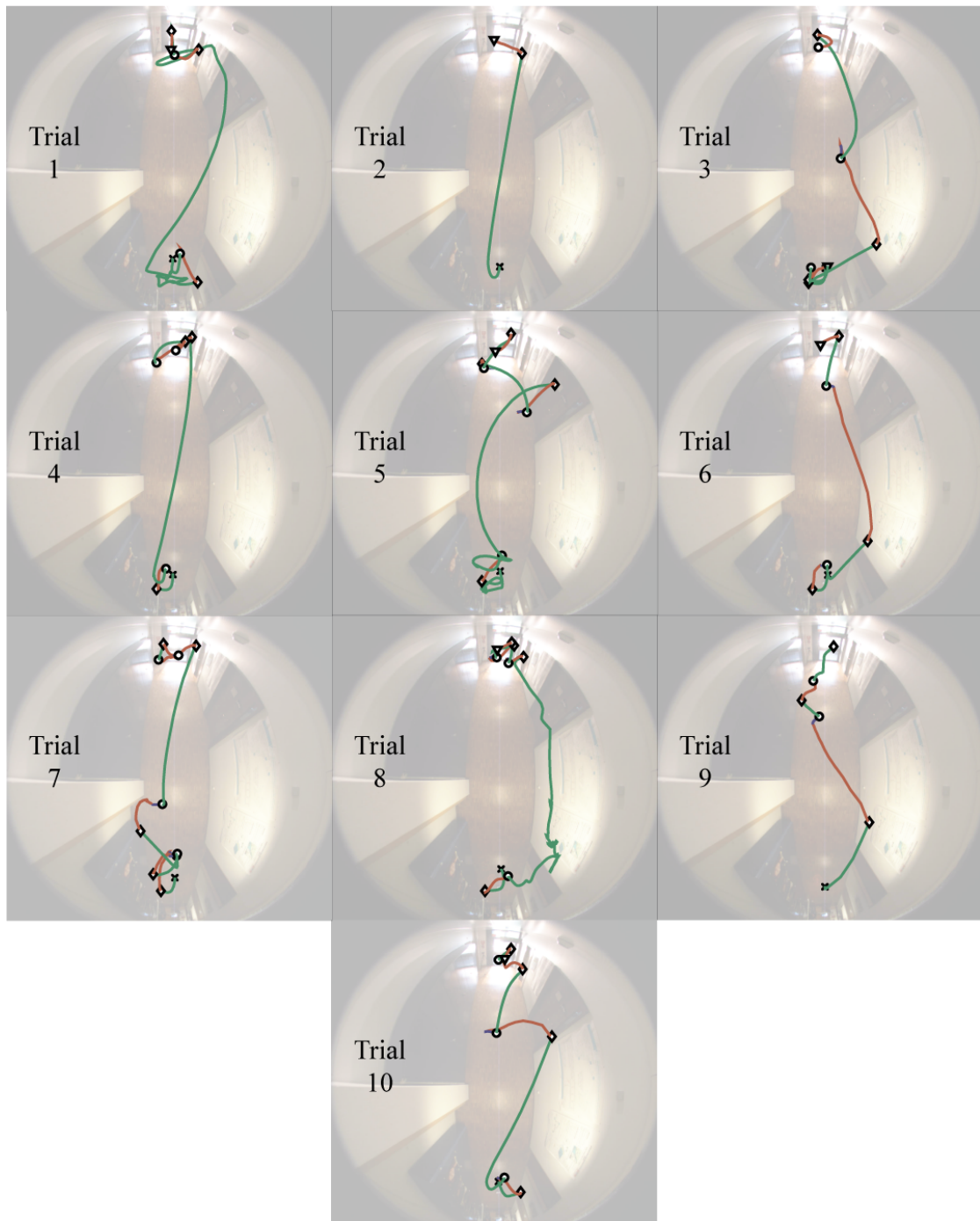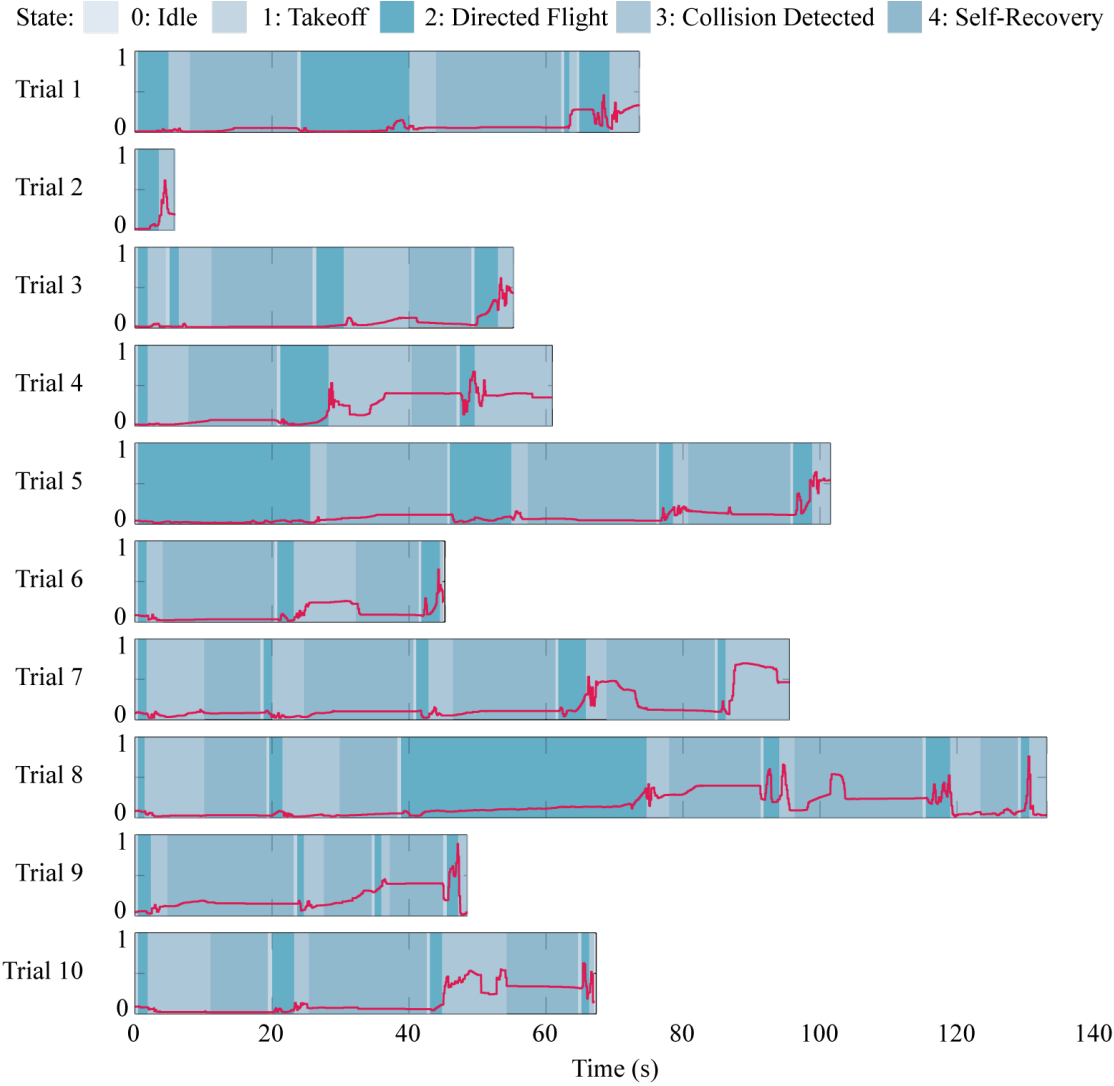Figure 4.10: Total ambient light detected by all four photodiodes over time for the same 10 trials of the phototaxis experiment presented in Fig. 4.8, normalized for maximum detectable signal. The state of the robot is overlaid on the graphs.
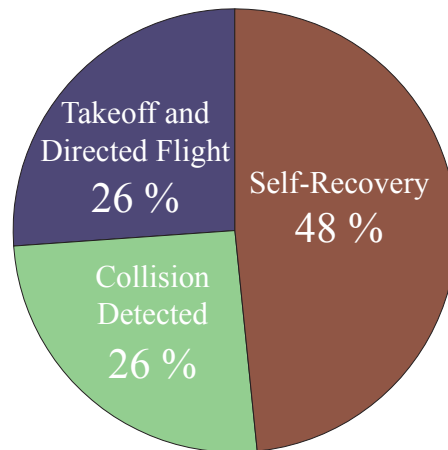
Figure 4.11: Average distribution of time in the various states during phototaxis in corridor experiment for a total average trial time of 68.6 s.

Parameter	Minimum	Maximum	Mean	Standard Deviation
Number of Collisions	1	6	3.8	1.32
Number of Uprightings	0	5	2.7	1.34
Flight Time [s]	5.9	133.1	68.6	35.2
Time in Takeoff or Directed Flight [s]	3.5	48.4	17.9	15.4
Time in Collision Detected [s]	2.5	30.1	17.5	9.9
Time in Self-Recovery [s]	0	54.7	33.2	17.3

Table 4.1: Phototaxis in Corridor Statistics

4.6 Conclusion

Indoor navigation remains a difficult problem for flying robots. At this moment the only platforms capable of navigating confined spaces such as narrow corridors do so by mapping their environment with high-density laser scanners and computation-intensive SLAM algorithms, hovering slowly to avoid any chance of collisions [25, 34, 24] or by deploying a fleet of ceiling-attaching-capable robots that help each other thanks to relative positioning sensors [81].

This chapter presents the first example of a robot capable of flying, colliding with obstacles without damage, uprighting itself on unstructured terrain and taking off again without human assistance. The importance of these abilities is demonstrated when the platform repeatedly traverses a corridor without any contact detection, localization or mapping, but simply based on a faint signal from four simple photodiodes.

5 Concluding Remarks

This final chapter summarizes the main contributions of the thesis in enabling flying robots to safely access cluttered environments. Some possible applications of the methods, platforms and algorithms developed in this thesis are then presented. Collision survival and self-recovery can enable many other interactions between flying robots and their environment, and thus the chapter concludes with some avenues for further research.

5.1   Main Accomplishments

The objective of this thesis was to investigate and design mechanisms that enable flying robots to venture beyond wide-open spaces and into the confined, cluttered environments of their human creators. This thesis has contributed to bring this vision closer to reality by enabling robots to survive, recover from and even physical exploit contact with their environment.

A method for designing protective structures particularly adapted to small flying systems presents a new angle on absorbing collision energy and the first contribution of this thesis. A teardrop-shaped protective cage is proposed and implemented on two winged platforms with an order of magnitude difference in weight, successfully absorbing energy from head-on collisions. A second mechanism using Euler springs in a tetrahedral configuration is proposed as a way of protecting hovering platforms by minimizing the force transmitted to a robot's frame while optimizing its weight. When implemented on a hovering platform the mechanism is able to absorb the energy of hundreds of collisions that would damage or destroy most other flying robots.

The second major contribution of this thesis is a method of designing self-recovery mechanisms and its application to both winged and hovering platforms. The limits of gravity-based self-recovery are demonstrated and complemented with the design of an active self-recovery mechanism using carbon fibre legs optimized to provide the required uprighting force at a minimum weight. The mechanism is validated on two flying platforms that use their legs to consistently upright themselves in corners, on rough and on sloped surfaces, ready to return to the air.

Finally, a platform named the Nighthawk is presented that demonstrates how both collision absorption and self-recovery mechanisms can be integrated into a single robot without greatly affecting its aerodynamics and ability to fly. The ability to crash, recover and take off again, implemented for the first time in a flying robot, enables the use of new navigation algorithms inspired by flying insects such as contact-based random search and phototaxis in the dark [86]. The final and most important contribution of this work is the successful navigation of a 13 m corridor with no contact detection or localization but simply the ambient light detected using four photodiodes. This result demonstrates the importance of self-recovery to flying robots in enabling navigation when sensor quality is limited or nonexistent.

5.2   Potential Applications

The results on collision energy absorption shown in this thesis can be applied to any robotic platform that risks coming into unforeseen (or even planned) contact with objects in its environment. It is adapted to platforms where weight is a critical factor, such as jumping, gliding and flying robots but can also be applied to ground platforms optimized for maximum endurance. Jumping robots in particular can benefit from this work, as their mode of locomotion involves constant collisions and saving weight on collision protection can increase the robots'

jump efficiency. Elastic energy absorption is best adapted to low-speed impacts (<5 m/s and free-falls from heights of less than 2 m[1].

The self-recovery design method can also be immediately applied to other robotic platforms provided that they are also equipped to survive collisions. The most likely to benefit are other flying platforms such as the quadrotors most commonly used for indoor exploration. Even the most advanced platforms using laser-based SLAM to navigate can benefit from self-recovery when their laser scanners fail to detect a window or other indiscernible object. Jumping robots can also implement active self-recovery mechanisms, as they are usually unable to control their landing position after a jump.

The most obvious application of the resilient flying robots and exploration algorithms developed in Chapter. 4 is the exploration of confined spaces that are dangerous or inaccessible to humans. Typical examples include search and rescue in damaged buildings [87] and mines [7], inspection of nuclear plants and other industrial buildings or even the exploration of other planets.

A flying robot that can take off and land repeatedly in unstructured environments can also be useful as a mobile sensor platform. A payload 20 g is already sufficient for equipping a variety of sensors such as visible and infrared cameras, thermopiles, gas and temperature sensors or microphones [88]. Deploying such platforms equipped with gas sensors in larger groups, for example, can be used to track the plume of a chemical gas spill inside an industrial plant. As the plume changes shape due to wind individual platforms can be redeployed to follow suit. If equipped with wireless data transmitters a group of robots can create a continuously-expanding wireless mesh network [89]. Such a network could be used, for example, to relay a video feed from the end of a mine to the command post at its entrance.

5.3   Future Directions

Advanced Self-Recovery

The active self-recovery mechanism developed in this thesis features four individually-controlled legs, allowing the robot to upright in a variety of different terrains and in the presence of obstacles. There are many situations, however, when simply extending all four legs or the closest leg to the ground is not the best strategy to upright, as demonstrated by the higher success rates of human-controlled uprighting compared to the autonomous controller.

In its current state the platform is only aware of its orientation and whether its legs are retracted or not. Strain gauges are a promising technology for increased sensing in a flying platform due to their low power, weight and cost. Embedding strain gauges into the self-recovery legs can provide information on the deflection of a leg, and thus its extension position compared to the

---

[1]Alternately, free-falls from higher heights can be absorbed if speed can be limited through the use of parachutes or retro-rockets.
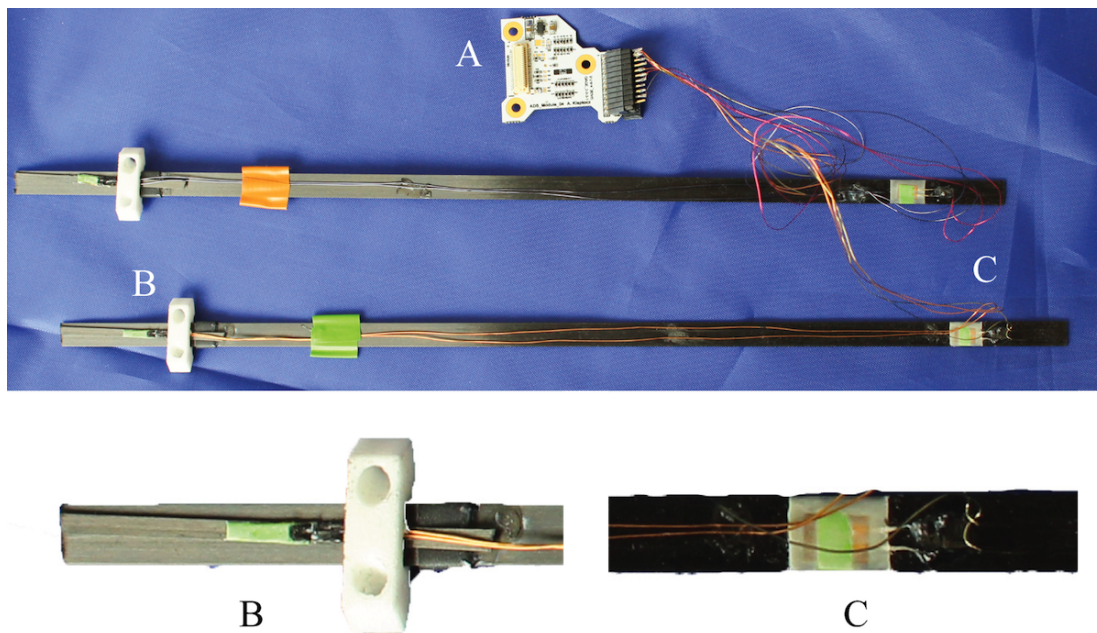
Figure 5.1: Strain gauges attached to the platform's legs can increase the sensing capability of the robot at a minimal weight cost. (A) A single miniature circuit board contains all the electronics required to interface 8 strain gauges at a weight of 4.5 g. (B) A first strain gauge mounted on the leg can detect the leg's deformation and perhaps even the quality of surface it is in contact with. (C) A second strain gauge mounted on a small bar between the leg and the retraction string can sense the tension in the string.

platform's frame, whereas a second strain gauge on the retraction string can detect the string's tension. In an initial implementation eight strain gauges, two in each leg, were embedded within the self-recovery mechanism with total weight cost of 4.5 g (Fig. 5.1) including all required electronics. Once characterized, the deflection and string tension information can be used to design more advanced uprighting controllers that can autonomously recover from even more difficult situations.

Contact Detection and Surface Identification

Using on-board accelerometers, as presented in Sec. 4.4, is an efficient way of detecting the force and duration of a collision using already-existing sensors, but cannot detect whether the platform remains in contact with the impacting surface. Information on continued contact with a wall after a low-energy collision could be very useful for more advanced contact-based navigation strategies. Just as humans resort to using their hands to follow walls and navigate in the dark, flying robots could use contact detection and wall following to traverse corridors when other sensory information is unavailable.

There is a well-established body of research in contact sensing for robotic manipulators,

including several reviews of existing contact sensors and technologies [90, 91]. In general contact can be sensed either at the interface (i.e. the point of contact between the object and the robot) or indirectly in the robots structure. Interface sensors typically take the form of tactile arrays, similar to laptop touch-pads, single-point pressure sensors or IR proximity sensors [92]. Though quite suitable for the fingertips of robotic manipulators, covering the entire surface of a flying robot with such an array of sensors would likely be too heavy and power-consuming to be practical.

Intrinsic sensors usually take the form of strain gauges or force sensors embedded within the robots structure that measure deformation due to contact with the environment. Initial experiments using the same strain gauges as in Fig. 5.1 placed throughout the platform's frame show some promise in detecting the position and force of contact and present an interesting avenue of future research. Their main disadvantages is that they cannot differentiate between single-point and multi-point contact.

Surface identification is an extension to collision detection that measures not only the force, direction and duration of contact with an obstacle, but also the surface characteristic such as texture and detail. Such information could be used, for example, to identify surfaces that are easier or harder to follow based on their roughness.

Though not yet shown in flying robots, there are several examples of surface identification in ground robots. [93] presents the Whiskerbot, a 'blind' ground robot inspired by the rat that has no camera, but uses a mobile 'head' covered in plastic whiskers to navigate by touch. The whiskers on the head move actively in a back-and-forth motion, similarly to the whiskers of a rat, and their motion is detected using embedded strain gauges. Subsequent work on the SCRATCHBot [94] improved the motion detection of the whiskers using 3-axis magnetometers to detect a miniature magnet embedded in the whisker. A more classical approach was presented in [95], where a Roomba floor-cleaning robot is fitted with an aluminum bar with an accelerometer at its tip used to detect vibration in the bar. The resulting vibration signal is used to distinguish between different surfaces as the robot passes over them.

Prescott et al. [96] provides a nice overview of technologies that can be used for contact surface detection. If applied to flying robots, surface identification could be used in contact-based navigation tasks such as wall following or for finding surfaces on which the robot can safely perch. An interesting first implementation could be to use the strain gauges embedded within the self-recovery mechanism (Fig. 5.1) to rub up against a surface while in flight.

Perching

The ability to self-recover allows a flying platform to return to the air when it is on the ground, but also implies that it may stay on the ground and perform other tasks, such as surveillance or environmental monitoring, without expending energy required for flight. Certain situations require a higher point of view than on the ground, and thus the ability to perch on non-

horizontal surfaces and return to the air is an interesting extension of self-recovery. Perching of flying robots has been demonstrated on vertical walls using grippers [97, 51], on metallic ceilings [98], on power lines [99, 100] and more recently on a human hand [101]. In the field of climbing robots there has been much interest in gecko-inspired dry adhesives, such as those used on the Waalbot II [102] or the Stickybot III [103]. Using dry adhesives on a flying robot can give it the ability to perch on smoother surfaces such as windows common in urban environments.

Hybrid Air-Ground Locomotion

Adding ground locomotion capabilities to a flying robot can be beneficial in certain very confined spaces such as underneath tables or in caves with low ceilings. The simplest solution for a flying robot is to drag itself on the ground by displacing air to the side. Adding a set of passive wheels [29] can increase locomotion efficiency, though only on flat, obstacle-free ground. Using active wheels powered by the same motors as used for flight has been considered [55], but the difference in rotation speed and required torque between wheels and propellers makes using the same drive motor difficult. Perhaps the solution most adapted to unstructured environments is the one found in insects and birds: adding separately-actuated legs. Recent demonstrations, including flying robots adapted with legs [50, 104] and legged robots adapted with wings [104] are a promising start to building flying machines that are equally comfortable in the air as on the ground.

5.4 Outlook

The automation of flying systems is moving at a lighting pace and flying robots are increasing filling our skies. Modern commercial airliners feature autopilots whose abilities rival those of their human counterparts. Flying robots capable of completely autonomous takeoff, waypoint navigation and landing can now be purchased and operated without any knowledge of how they actually work[2]. In a few years autonomous flying systems will be prevalent in the skies above us, monitoring our crops, mapping our cities, transporting our goods and even helping to protect our lives.

Perhaps the faith we put in our algorithms is a bit too optimistic, however; mobile robotics is a developing technology, and has yet to reach the reliability rates of human-piloted systems[3]. Even the most sophisticated platforms and algorithms can fail, and the possibility of this failure must be taken into account when designing flying systems. Much like anti-lock brakes and airbags have become standard in modern cars, there must be a paradigm shift in the design of flying robots from collision avoidance to collision resistance. Protecting UAVs from contact with obstacles also protects humans from contact with UAVs and thus facilitates social acceptance of their operation in our vicinity.

---

[2]http://www.sensefly.com, accessed 21.05.2012
[3]http://goo.gl/uRDAc, accessed 21.05.2012

Ultimately, resilience and adaptability still separate current flying platforms from the impressive capabilities of the insects and birds we see in nature. There is a lot of work left to be done before we can create flying machines that can survive constant collisions like a fly on a window, navigate in the dark like a bat or stand up on its feet like a bird, but perhaps this thesis has brought that dream a little bit closer.
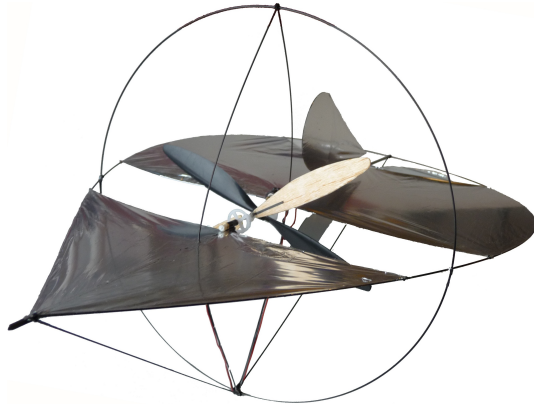
A A Brief History of the AirBurr Project

The flying platforms presented in this thesis are but some of the 11 platforms that were built, tested and sometimes destroyed as part of the AirBurr project. The goals of this two-person project are twofold: to develop robust flying platforms that can survive collisions with their environment and to develop novel strategies for speed limitation and contact sensing. This thesis tackled the former of the two goals.

This chapter presents the platforms in chronological order to highlight the iterative design process that yielded the final Nighthawk flying robot. Though sometimes globally referred to as "AirBurrs", each platform has a unique name based on its particular abilities. The robots are presented with their most important characteristics as well as their major innovations compared to previous platforms. It is hoped that this chapter can convey to the reader the source of some of the ideas presented throughout the thesis and the challenges of integrating multiple mechanisms into a single platform that is still capable of flight.

AirBurr 1: Hovermouse

Weight: 20.5 g
Drivetrain: 2x 6 mm DC pager motor, hand-made balsa propeller
Electronics: Spektrum AR6400
Innovations: Gravity-based self-recovery, teardrop spring
Battery: 1-cell LiPo, 110 mAh

The first prototype platform was not completely new, as it was based on some of the ideas developed in a previous thesis on optic-flow based navigation for ultralight winged platforms [21]. As described in Sec. 3.3, the goal of the HoverMouse is to design an ultralight platform capable of gravity-based self-recovery while protecting its propellers from contact with the environment. The platform is built using traditional construction techniques; all carbon fibre rods and mylar surfaces are glued together, making repair difficult. The HoverMouse inaugurated the teardrop-shaped spring, is remote-controlled and has no on-board sensing.

AirBurr 2: ICRA2010

Weight: 25 g
Drivetrain: 2x 6 mm DC pager motor, hand-made balsa propeller
Electronics: Spektrum AR6400
Innovations: 3D-printed connection joints
Battery: 1-cell LiPo, 110 mAh

ICRA2010, as its namesake may suggest, is a modified version of the HoverMouse built for publication at the IEEE International Conference on Robotics and Automation. The main improvements include the use of 3D-printed connection points between the carbon fibre rods to increase repairability. The extrusion process used to produce the parts was of low quality and the resulting parts were not very resistant, but the experience gained with the 3D-printing machines was used in all subsequent platforms.

AirBurr 3: Flying Stick
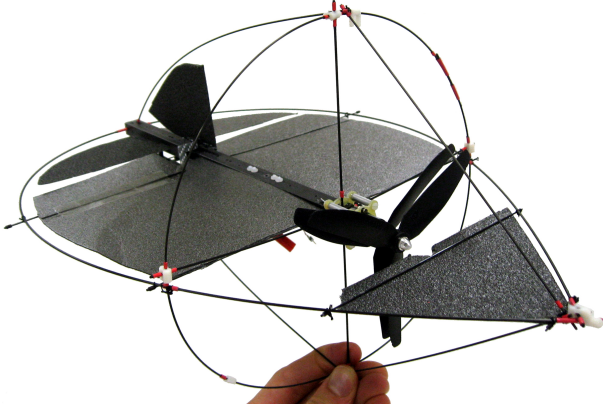
Weight: 110 g
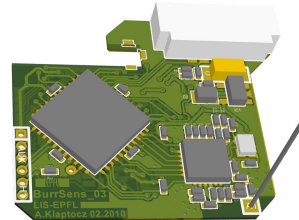**Drivetrain:** HK-13DZ 2000kv Counter Rotating Micro BL System, GWS 3-blade 6-inch propellers
Electronics: BurrSens v3

Innovations: IMU and stabilized hovering
Battery: 2-cell LiPo, 480 mAh

The Flying Stick represented a major change in design. The weight of the platform was increased by a factor of four to accommodate the 20 g payload required by the project. The platform's fuselage is built using an 8x10 mm rectangular carbon fibre tube, much more robust than the 1.4x1.4 mm bar used in the previous platforms. This new overhead allowed the first use of embedded sensors in the form of the BurrSens v3 sensor board, which contained 3-axis accelerometers and gyroscopes for stabilization, an on-board microcontroller and a miniature radio for data transfer, all in a 3 g package. This platform was also the first to use the HK-13DZ coaxial brushless DC (BLDC) motor, the lightest one available on the market, weighing a mere 13 g (18 g with two three-blade propellers). BLDC controllers and a satellite receiver are connected to the BurrSens board through wires.

AirBurr 4: Crashy

Weight: 124 g
Drivetrain: HK-13DZ 2000kv Counter Rotating Micro BL System, GWS 3-blade 6-inch propellers
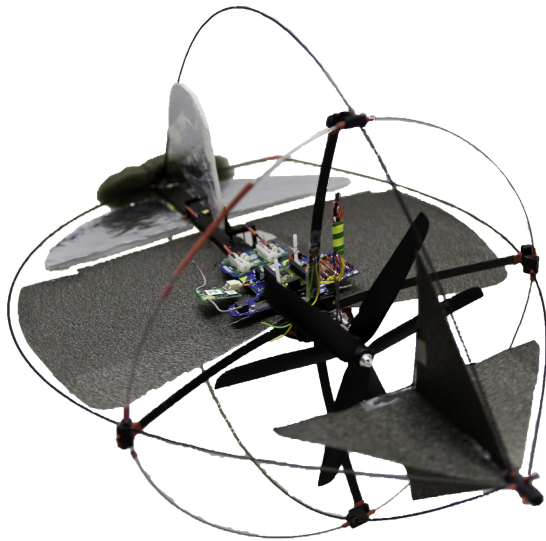**Electronics:** BurrMove v4 and BurrSens v4
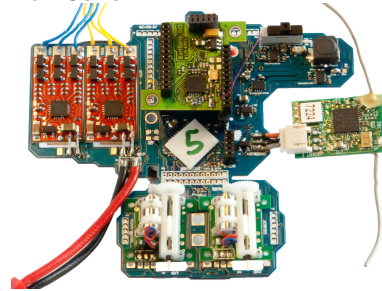
Innovations: Head-on collision energy absorption
Battery: 2-cell LiPo, 480 mAh

Crashy was developed to improve the collision energy absorption capabilities of the previous platform and is presented in detail in Sec. 2.3. It is the first platform to use carbon fibre and aramid honeycomb sandwich as a fuselage material, a material used for all subsequent platforms. It is also the first platform to feature the BurrMove v4 integrated actuator board which is meant to replace the loose speed controllers, servos and receivers of the previous platform by integrating them all into a motherboard. The BurrMove has power management circuits for stepping down the 7.4 V power from the battery to the various voltages required by the platform's actuators and sensors, as well as protecting sensitive components from current surges. It has its own microcontroller which is used to control all on-board actuators and a dock for the BurrSens v4 which is now dedicated to sensing and higher-level algorithms.

AirBurr 5: Bumpy

Weight: 130 g
Drivetrain: HK-13DZ 2000kv Counter Rotating Micro BL System, GWS 3-blade 6-inch propellers
Electronics: BurrMove v4 and BurrSens v4
Innovations: Strain-gauge-based contact detection
Battery: 2-cell LiPo, 480 mAh

Bumpy was developed as part of a student project on contact detection. Taking some inspiration from previous designs, Bumpy is the first platform designed with only hovering flight in mind and to feature a second ring at the base of the platform to be used as landing gear. Its main innovation, however, are the four strain gauges integrated into its attachment springs between the frame and the propeller protection ring. The signals from these four sensors is analyzed using an embedded algorithm and can detect the position and amplitude of a force on its outer ring to an accuracy of around 0.5 N and 10°.

AirBurr 6: Sticky
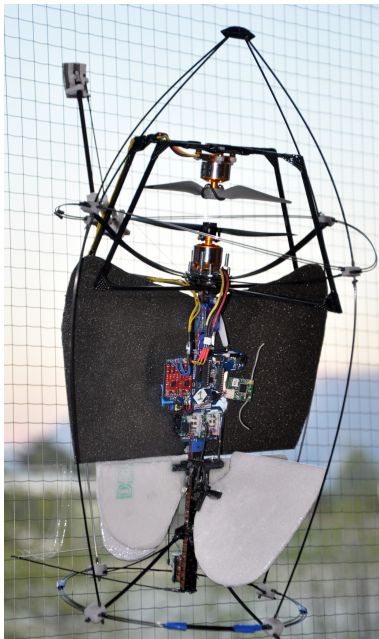
Weight: 200 g
Drivetrain: 2x CR2028 BLDC motors, APC 6- and 7-inch propellers
Electronics: BurrMove v4 and BurrSens v4
Innovations: Attachment mechanism, stiff propeller protection
Battery: 3-cell LiPo, 730 mAh

Sticky was developed as part of another student project with the goal of implementing an attachment mechanism for flying robots using gecko-inspired dry adhesives. The mechanism is connected between the attachment spring and the protection ring of the platform and can be used to perch on glass and other smooth vertical surfaces. A similar mechanism is currently being developed and integrated into the Nighthawk. Sticky was also used as a test platform for new drivetrains when it was decided to further increase the weight of the platform to accommodate more sensors. Several configurations were tested, including the use of a single motor for thrust and a third servo-motor for yaw stabilization, before a final configuration using two BLDC motors facing each other was selected. The second motor is mounted upside-down on a stiff propeller cage which is also used for protection. Sticky also marked the move to 3-cell LiPo batteries.

AirBurr 7: Multitasky
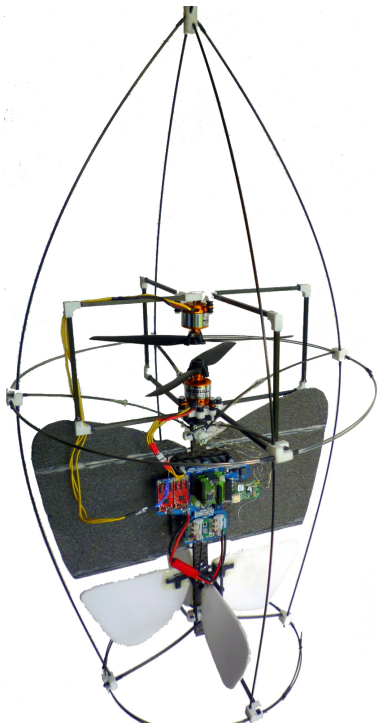
Weight: 210 g
Drivetrain: 2x CR2028 BLDC motors, APC 7-inch propellers
Electronics: BurrMove v4 and BurrSens v4
Innovations: Altitude stabilization and autonomous takeoff
Battery: 3-cell LiPo, 730 mAh

Multitasky got its name as it was originally supposed to integrate attachment and leg-based uprighting mechanisms, but in the end was used more for flight experiments. Its design applied the drivetrain lessons of the previous platform and uses two separate BLDC motors instead of an integrated contra-rotating system. A US distance sensor is mounted pointed downward to provide altitude stabilization and autonomous takeoff capability.

AirBurr 8: Samurai
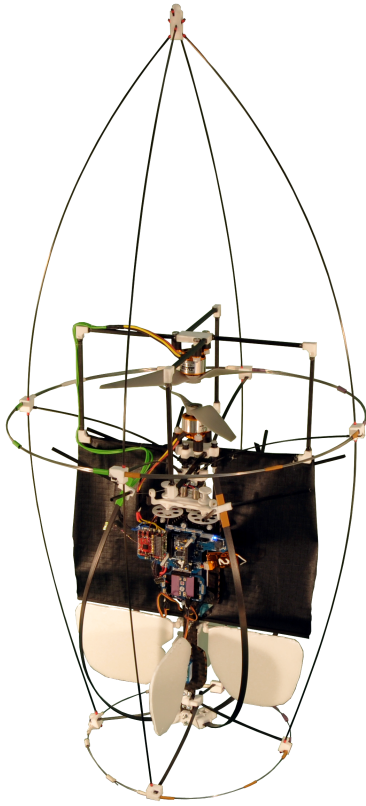
Weight: 250 g
Drivetrain: 2x CR2028 BLDC motors, APC 7-inch propellers
Electronics: BurrMove v4 and BurrSens v4
Innovations: Active self-recovery
Battery: 3-cell LiPo, 730 mAh

Samurai is based on the same platform design as Multitasky but with the addition of the leg-based active self-recovery mechanism explained in greater detail in Sec. 3.4

AirBurr 9: Beefy

Weight: 280 g
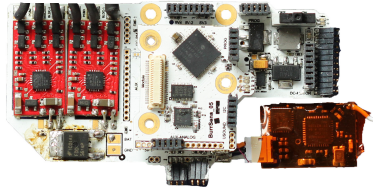**Drivetrain:** HobbyKing contra-rotating BLDC motors, APC 7-inch propellers
Electronics: BurrMove v5 and BurrSens v5

Innovations: triangular beam Euler springs
Battery: 3-cell LiPo, 730 mAh

Beefy is an interim platform used to study some new design ideas in collision energy absorption and propeller protection. The teardrop springs used in previous platforms are expanded to triangular springs using carbon fibre beams, a precursor to the tetrahedral configuration. The beams absorb energy through buckling when loaded correctly, but their inability to flex in all directions (as opposed to rods) causes damage to connection points in certain loading conditions, thus leading to the idea of tetrahedrals.

Despite the flexible protection around previous platforms there are still some situations in which the propellers can come into contact with parts of the platform and get damaged. Beefy was built with a stiff protection ring made of moulded carbon fibre surrounding a new coaxial motor that was more powerful than the previous two-motor system. This protection system proved to be heavy, however, and shattered after a high-energy contact, providing further arguments against stiff protection for propellers that are outside the platform's frame.

Before it suffered permanent damage Beefy was a nimble flyer and served as a testbed for the newest version of the BurrMove and BurrSens electronics which have upgraded power management to interface more sensors and actuators for future platforms. Beefy also featured a leg-based active self-recovery mechanism.

AirBurr 10: Blackstar
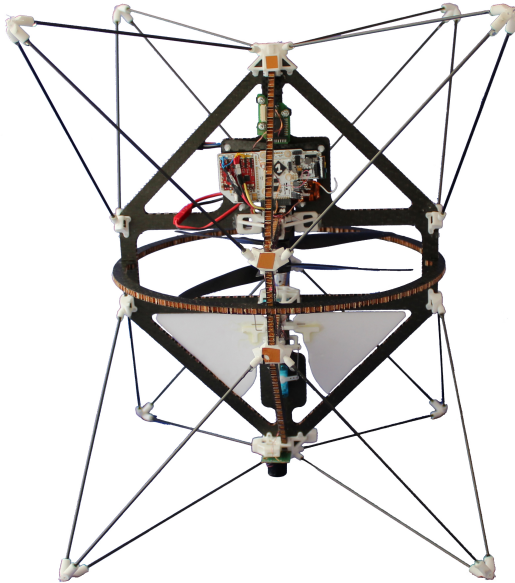
Weight: 282 g
Drivetrain: HobbyKing contra-rotating BLDC motors, GWS 3-blade 8-inch propellers
Electronics: BurrMove v5 and BurrSens v5
Innovations: Tetrahedral Euler-spring protective structures, high-G accelerometers
Battery: 3-cell LiPo, 730 mAh

Visually, Blackstar presents the biggest departure from previous designs, but at its core it remains a coaxial platform with flaps for controlling roll and pitch. The lessons learned with Beefy are evident in this new design: propellers are now housed within the platform's frame and the motors are mounted rigidly to its centre. The triangular protective mechanisms have been replaced by the tetrahedral structures explained in detail in Sec. 2.4. Blackstar also has integrated high-G accelerometers for measuring collision force amplitude on its frame.

AirBurr 11: Nighthawk

Weight: 350 g
Drivetrain: Himax CR2805 contra-rotating BLDC motors, APC 7-inch propellers
Electronics: BurrMove v5 and BurrSens v5
Innovations: Fully-integrated collision energy absorption and self-recovery. Status LED for night flights.
Battery: 3-cell LiPo, 730 mAh

Nighthawk is the final platform developed during this thesis, and also the first to fully integrate tetrahedral springs, gravity-based self-recover and leg-based self-recover into a single platform. Based around the same core as Blackstar, Nighthawk has an upgraded coaxial motor and uses stiff propellers to prevent flexion during collisions. Its features and autonomous navigation abilities are best explained in Ch. 4.

Bibliography

[1] K. Nonami, F. Kendoul, S. Suzuki, W. Wang, and D. Nakazawa, *Autonomous Flying Robots*. Springer, 2010.

[2] T. Mueller, *Fixed and Flapping Wing Aerodynamics for Micro Air Vehicle Applications (Progress in Astronautics and Aeronautics)*. AIAA, 2001.

[3] O. Küng, C. Strecha, A. Beyeler, J.-C. Zufferey, D. Floreano, P. Fua, and F. Gervaix, "The Accuracy of Automatic Photogrammetric Techniques on Ultra-Light UAV Imagery," in *UAV-g 2011 - Unmanned Aerial Vehicle in Geomatics*, 2011.

[4] L. Merino, F. Caballero, J. Martinez-de Dios, J. Ferruz, and A. Ollero, "A cooperative perception system for multiple UAVs: Application to automatic detection of forest fires," *Journal of Field Robotics*, vol. 23, no. 3-4, pp. 165–184, 2006.

[5] B. Mendelow, P. Muir, B. Boshielo, and J. Robertson, "Development of e-Juba, a preliminary proof of concept unmanned aerial vehicle designed to facilitate the transportation of microbiological test samples from remote rural clinics to National Health Laboratory Service laboratories," *South African Medical Journal*, vol. 92, no. 3, pp. 1215–1218, 2010.

[6] P.-J. Bristeau, F. Callou, D. Vissière, and N. Petit, "The Navigation and Control technology inside the AR.Drone micro UAV," in *Internation Federation of Automatic Control (IFAC) World Congress*, 2011.

[7] R. R. Murphy, J. Kravitz, S. L. Stover, and R. Shoureshi, "Mobile Robots in Mine Rescue and Recovery," *IEEE Robotics & Automation Magazine*, no. June, pp. 91–103, 2009.

[8] L. Frantsevich, "Righting kinematics in beetles (Insecta: Coleoptera)." *Arthropod structure & development*, vol. 33, no. 3, pp. 221–35, Jul. 2004.

[9] A. A. Faisal and T. Matheson, "Coordinated righting behaviour in locusts." *The Journal of experimental biology*, vol. 204, pp. 637–648, Feb. 2001.

[10] A. Klaptocz and J. Nicoud, "Technology and Fabrication of Ultralight Micro-Aerial Vehicles," in *Flying Insects and Robots*. Springer, 2009, pp. 299–316.

[11] M. Kovač, M. Schlegel, J.-C. Zufferey, and D. Floreano, "Steerable miniature jumping robot," *Autonomous Robots*, vol. 28, no. 3, pp. 295–306, Dec. 2010.

[12] E. W. Beyer, "Design, Testing and Performance of a Hybrid Micro Vehicle - The Hopping Rotochute," Ph.D. dissertation, Georgia Institute of Technology, 2009.

[13] R. J. Wood, S. Avadhanula, E. Steltz, M. Seeman, J. Entwistle, A. Bachrac, G. Barrows, S. Sanders, and R. S. Fearing, "An Autonomous Palm-Sized Gliding Micro Air Vehicle," *IEEE Robotics & Automation Magazine*, no. June 2007, pp. 82–91, 2007.

[14] M. Kovač, A. Guignard, J.-D. Nicoud, J.-C. Zufferey, and D. Floreano, "A 1.5g SMA-actuated Microglider looking for the Light," in *IEEE International Conference on Robotics and Automation*, Apr. 2007, pp. 367–372.

[15] J.-C. Zufferey, A. Guanella, A. Beyeler, and D. Floreano, "Flying over the reality gap: From simulated to real indoor airships," *Autonomous Robots*, vol. 21, no. 3, pp. 243–254, 2006.

[16] S. Bermúdez i Badia, P. Pyk, and P. F. M. J. Verschure, "A Biologically Based Flight Control System for a Blimp-based UAV," in *IEEE International Conference on Robotics and Automation*, 2005.

[17] D. Lentink, S. Jongerius, and N. Bradshaw, "The Scalable Design of Flapping Micro-Air Vehicles Inspired by Insect Flight," *Flying Insects and Robots*, pp. 185–205, 2009.

[18] S. S. Baek, F. L. G. Bermudez, and R. S. Fearing, "Flight Control for Target Seeking by 13 gram Ornithopter," in *2011 IEEE/RSJ International Conference on Intelligent Robots and Systems (IROS2011)*, 2011, pp. 2674–2681.

[19] C. P. Ellington and J. R. Usherwood, "Lift and Drag Characteristics of Rotary and Flapping Wings," in *Fixed and Flapping Wing Aerodynamics for Micro Air Vehicle Applications*, T. Mueller, Ed. AIAA, 2001, ch. 12, pp. 231–248.

[20] G. R. Spedding and P. B. S. Lissaman, "Technical aspects of microscale flight systems," *Journal of Avian Biology*, vol. 4, no. 29, pp. 458–468, 1998.

[21] J.-C. Zufferey, A. Klaptocz, A. Beyeler, J.-D. Nicoud, and D. Floreano, "A 10-gram vision-based flying robot," *Advanced Robotics*, vol. 21, no. 14, pp. 1671–1684, Oct. 2007.

[22] G. K. A. Krishnan, M. Griffis, D. Addai-Gyansa, H. Bagheri, and R. Krashanitsa, "Design of Fixed-Wing Micro Air Vehicles for Indoor and Outdoor Missions," in *3rd US-European Competition and Workshop on Micro Air Vehicle Systems (MAV07) & European Micro Air Vehicle Conference and Flight Competition (EMAV2007)*, 2007.

[23] J. P. How, J. Teo, and B. Michini, "Adaptive Flight Control Experiments using RAVEN," in *14th Yale Workshop on Adaptive and Learning Systems*, 2008.

[24] S. Shen, N. Michael, and V. Kumar, "Autonomous Multi-Floor Indoor Navigation with a Computationally Constrained MAV," in *Proceedings 2011 IEEE International Conference on Robotics and Automation*, 2011.

[25] S. Grzonka, G. Grisetti, and W. Burgard, "Towards a Navigation System for Autonomous Indoor Flying," in *IEEE International Conference on Robotics and Automation*, 2009.

[26] D. Schafroth, S. Bouabdallah, C. Bermes, and R. Siegwart, "From the Test Benches to the First Prototype of the muFly Micro Helicopter," *Journal of Intelligent and Robotic Systems*, vol. 54, no. 1-3, pp. 245–260, Jul. 2008.

[27] H. Tennekes, *The Simple Science of Flight: From Insects to Jumbo Jets.* MIT Press, 2009.

[28] M. Simons, *Model Aircraft Aerodynamics*, 2nd ed. London: Argus Books, 1987.

[29] M. Itasse and J.-M. Moschetta, "Equilibrium Transition Study for a Hybrid MAV," *International Journal of Micro Air Vehicles*, vol. 3, no. 4, pp. 229–245, 2011.

[30] J. F. Roberts, T. S. Striling, J.-C. Zufferey, and D. Floreano, "Quadrotor Using Minimal Sensing For Autonomous Indoor Flight," in *EMAV2007*, 2007.

[31] W. A. Lewinger, M. S. Watson, and R. D. Quinn, "Obstacle Avoidance Behavior for a Biologically-inspired Mobile Robot Using Binaural Ultrasonic Sensors," in *IEEE/RSJ International Conference on Intelligent Robots and Systems*, 2006.

[32] J.-C. Zufferey and D. Floreano, "Fly-inspired visual steering of an ultralight indoor aircraft," *IEEE Transactions on Robotics*, vol. 22, no. 1, pp. 137–146, 2006.

[33] S. Scherer, S. Singh, L. Chamberlain, and M. Elgersma, "Flying Fast and Low Among Obstacles: Methodology and Experiments," *The International Journal of Robotics Research*, vol. 27, no. 5, pp. 549–574, May 2008.

[34] W. Morris, I. Dryanovski, J. Xiao, and S. Member, "CityFlyer : Progress Toward Autonomous MAV Navigation and 3D Mapping," in *IEEE International Conference on Robotics and Automation*, 2011.

[35] M. Achtelik, M. Achtelik, S. Weiss, and R. Siegwart, "Onboard IMU and Monocular Vision Based Control for MAVs in Unknown In- and Outdoor Environments," in *IEEE International Conference on Robotics and Automation*, 2011, pp. 3056–3063.

[36] C. Brunner, T. Peynot, and T. Vidal-calleja, "Combining Multiple Sensor Modalities for a Localisation Robust to Smoke," in *IEEE/RSJ International Conference on Intelligent Robots and Systems*, 2011.

[37] T. Peynot, J. Underwood, and S. Scheding, "Towards Reliable Perception for Unmanned Ground Vehicles in Challenging Conditions," in *IEEE/RSJ International Conference on Intelligent Robots and Systems*, Oct. 2009, pp. 1170–1176.

[38] A. Natraj, C. Demonceaux, P. Vasseur, and P. Sturm, "Vision Based Attitude And Altitude Estimation For UAVs In Dark Environments," in *IEEE/RSJ International Conference on Intelligent Robots and Systems*, 2011, pp. 4006–4011.

[39] G. Wang, H. Sheng, T. Lu, D. Wang, and F. Hu, "Development of an Autonomous Flight Control System for Small Size Unmanned Helicopter *," in *IEEE International Conference on Robotics and Biomimetics*, 2007, pp. 1804–1809.

[40] R. Oung, F. Bourgault, M. Donovan, and R. D'Andrea, "The Distributed Flight Array," in *IEEE International Conference on Robotics and Automation*, 2010, pp. 601–607.

[41] E. Beyer and M. Costello, "Performance of a hopping rotochute," *International Journal of Micro Air Vehicles*, vol. 1, no. 2, pp. 121–137, 2009.

[42] J. W. Flower, "On the Origin of Flight in Insects," *Journal of Insect Physiology*, vol. 10, no. 1963, pp. 81–88, 1964.

[43] A. Hoover, E. Steltz, and R. Fearing, "RoACH: An autonomous 2.4 g crawling hexapod robot," in *IEEE/RSJ International Conference on Intelligent Robots and Systems*. IEEE, 2008, pp. 26–33.

[44] N. O. Pérez-Arancibia, K. Y. Ma, K. C. Galloway, J. D. Greenberg, and R. J. Wood, "First controlled vertical flight of a biologically inspired microrobot." *Bioinspiration & biomimetics*, vol. 6, no. 3, p. 036009, Sep. 2011.

[45] G. Caprari, T. Estier, and R. Siegwart, "Fascination of Down Scaling – Alice the Sugar Cube Robot," *Journal of Micromechatronics*, vol. 1, no. 3, pp. 177–189, 2001.

[46] J. D. Currey, "The failure of exoskeletons and endoskeletons," *Journal of Morphology*, vol. 123, no. 1, pp. 1–16, 1967.

[47] N. Mills, "Protective Capability of Bicyle Helmets," *British journal of sports medicine*, vol. 24, no. 1, 1990.

[48] R. Armour, "A Biologically Inspired Jumping and Rolling Robot," Ph.D. dissertation, University of Bath, 2010.

[49] M. Kovač, M. Schlegel, J.-C. Zufferey, and D. Floreano, "A miniature jumping robot with self-recovery capabilities," in *IEEE/RSJ International Conference on Intelligent Robots and Systems*, Oct. 2009, pp. 583–588.

[50] R. J. Bachmann, F. J. Boria, R. Vaidyanathan, P. G. Ifju, and R. D. Quinn, "A biologically inspired micro-vehicle capable of aerial and terrestrial locomotion," *Mechanism and Machine Theory*, vol. 44, no. 3, pp. 513–526, Mar. 2009.

[51] M. Kovač, J. Germann, C. Hürzeler, R. Y. Siegwart, and D. Floreano, "A perching mechanism for micro aerial vehicles," *Journal of Micro-Nano Mechatronics*, vol. 5, no. 3-4, pp. 77–91, May 2010.

[52] A. Desbiens, A. Asbeck, and M. Cutkosky, "Scansorial Landing and Perching," in *Robotics Research*. Springer, 2011, pp. 169–184.

[53] R. Armour, K. Paskins, A. Bowyer, J. Vincent, W. Megill, and R. Bomphrey, "Jumping robots: a biomimetic solution to locomotion across rough terrain." *Bioinspiration & biomimetics*, vol. 2, no. 3, pp. S65–82, Sep. 2007.

[54] P. Fiorini and J. Burdick, "The development of hopping capabilities for small robots," *Autonomous Robots*, vol. 14, no. 2, pp. 239–254, 2003.

[55] A. Kossett and N. Papanikolopoulos, "A Robust Miniature Robot Design for Land / Air Hybrid Locomotion," in *IEEE International Conference on Robotics and Automation*, 2011, pp. 4595–4600.

[56] D. Cabecinhas, R. Naldi, L. Marconi, C. Silvestre, and R. Cunha, "Robust take-off and landing for a quadrotor vehicle," in *IEEE International Conference on Robotics and Automation*, 2010, pp. 1630–1635.

[57] S. Saripalli, J. Montgomery, and G. Sukhatme, "Vision-based autonomous landing of an unmanned aerial vehicle," in *IEEE International Conference on Robotics and Automation*, 2002, pp. 2799–2804.

[58] S. Bayrakar and E. Feron, "Experiments with small helicopter automated landings at unusual attitudes," *CoRR*, pp. 1–20, 2008.

[59] A. Kossett, R. D'Sa, J. Purvey, and N. Papanikolopoulos, "Design of an Improved Land / Air Miniature Robot," in *IEEE International Conference on Robotics and Automation*, 2010, pp. 632–637.

[60] J. Grasmeyer and M. Keennon, "Development of the black widow micro air vehicle." *Progress in Astronautics and Aeronautics*, vol. 195, pp. 519–535, 2001.

[61] A. Noth and R. Siegwart, "Solar Powered MAVs , The Scaling Down Problems of Solar," in *Flying Insects and Robots*, 2009, pp. 285–298.

[62] W. Green, "A MAV that flies like an airplane and hovers like a helicopter," *Advanced Intelligent Mechatronics.*, 2005.

[63] K. Kotwani, S. Sane, H. Arya, and K. Sudhakar, "Experimental characterization of propulsion system for mini aerial vehicle," in *31st National Conference on FMFP*, 2004.

[64] R. Albertani, B. Stanford, J. P. Hubner, and P. G. Ifju, "Aerodynamic Coefficients and Deformation Measurements on Flexible Micro Air Vehicle Wings," *Experimental Mechanics*, vol. 47, no. 5, pp. 625–635, Feb. 2007.

[65] A. Klaptocz, A. Briod, L. Daler, J.-C. Zufferey, and D. Floreano, "Elastic Collision Protection for Flying Robots Using Euler Springs," *IEEE Transactions on Mechatronics*, p. In review, 2012.

[66] A. Christoforou, "Impact dynamics and damage in composite structures," *Composite structures*, vol. 52, 2001.

Bibliography

[67] G. Davies and X. Zhang, "Impact damage prediction in carbon composite structures," *International Journal of Impact Engineering*, vol. 16, no. 1, pp. 149–170, 1995.

[68] W. Cantwell, P. Curtis, and J. Morton, "Impact and subsequent fatigue damage growth in carbon fibre laminates," *International journal of fatigue*, vol. 6, no. 2, pp. 113–118, 1984.

[69] T. D'Arcy, *On Growth and Form.* Campbridge: Cambridge University Press, 1961.

[70] R. J. Templin, "The spectrum of animal flight : insects to pterosaurs," *Progress in Aerospace Sciences*, vol. 36, pp. 393–436, 2000.

[71] C. Creighton and T. Clyne, "The compressive strength of highly-aligned carbon-fibre/epoxy composites produced by pultrusion," *Composites Science and Technology*, vol. 60, no. 4, pp. 525–533, Mar. 2000.

[72] R. Frisch-Fay, *Flexible Bars.* London: Butterworths, 1962.

[73] B. Brown and G. Zeglin, "The bow leg hopping robot," in *IEEE International Conference on Robotics and Automation*, 1998, pp. 781–786.

[74] W. C. Young and R. G. Budynas, *Roark's Formulas for Stress and Strain.* McGraw-Hill, 2002.

[75] A. Klaptocz, G. Boutinard-Rouelle, A. Briod, J.-C. Zufferey, and D. Floreano, "An Indoor Flying Platform with Collision Robustness and Self-Recovery," in *IEEE International Conference on Robotics and Automation*, 2010, pp. 3349–3354.

[76] A. Klaptocz, L. Daler, A. Briod, J.-C. Zufferey, and D. Floreano, "An Active Uprighting Mechanism for Flying Robots," *IEEE Transactions on Robotics*, p. To appear, 2012.

[77] B. Michini, J. Redding, N. K. Ure, M. Cutler, and J. P. How, "Design and Flight Testing of an Autonomous Variable-Pitch Quadrotor," in *IEEE International Conference on Robotics and Automation*, 2011, pp. 2978–2979.

[78] A. Klaptocz, A. Briod, J.-C. Zufferey, and D. Floreano, "Flying, crashing and recovering: random search and phototaxis with minimal sensing," *IEEE Robotics & Automation Magazine*, p. In review, 2012.

[79] G. Welch and G. Bishop, "An Introduction to the Kalman Filter," *SIGGRAPH 2001 Course 8*, 2001.

[80] A. Briod, A. Klaptocz, and J. Zufferey, "The AirBurr: A Flying Robot That Can Exploit Collisions," in *International Conference on Complex Medial Engineering*, 2012.

[81] J. F. Roberts, T. Stirling, J.-C. Zufferey, and D. Floreano, "3-D relative positioning sensor for indoor flying robots," *Autonomous Robots*, Feb. 2012.

[82] C. K. Chan, H. Peng, G. Liu, K. McIlwrath, X. F. Zhang, R. a. Huggins, and Y. Cui, "High-performance lithium battery anodes using silicon nanowires." *Nature nanotechnology*, vol. 3, no. 1, pp. 31–5, Jan. 2008.

[83] L. Spangler and C. J. Kemp, "ISAAC : integrated silicon automotive accelerometer," *Sensors and Actuators A*, pp. 523–529, 1996.

[84] Y.-j. Mon, "Intelligent airbag deployment algorithm design and implemented by DSP," in *Fourth Annual ACIS International Conference on Computer and Information Science*, 2005, pp. 3–8.

[85] J. L. Jones, "Robots at the Tipping Point," *IEEE Robotics & Automation Magazine*, no. March, pp. 76–78, 2006.

[86] H. S. Hsiao, "Flight paths of night-flying moths to light." *Journal of insect physiology*, vol. 19, no. 10, pp. 1971–6, Oct. 1973.

[87] S. Tadokoro, *Rescue Robotics: DDT Project on Robots and Systems for Urban Search and Rescue*. Springer Verlag, 2009.

[88] A. Briod, "Review of Light-weight Payloads for MAVs and Experiments with Thermopiles," EPFL, Tech. Rep., 2010.

[89] S. Hauert, J.-C. Zufferey, and D. Floreano, "Evolved swarming without positioning information: an application in aerial communication relay," *Autonomous Robots*, vol. 26, no. 1, pp. 21–32, Oct. 2008.

[90] J. Tegin and J. Wikander, "Tactile Sensing in Intelligent Robotic Manipulation – A Review," *Industrial Robot: An International Journal*, vol. 32, no. 1, pp. 64–70, 2005.

[91] M. H. Lee and H. R. Nicholls, "Tactile Sensing for Mechatronics - A State of the Art Survey," *Mechatronics*, vol. 9, no. 1, pp. 1–31, Feb. 1999.

[92] D. Balek, "Using Gripper Mounted Infrared Proximity Sensors for Robot Feedback Control," in *IEEE International Conference on Robotics and Automation*, 1985, pp. 282–287.

[93] M. J. Pearson, a. G. Pipe, C. Melhuish, B. Mitchinson, and T. J. Prescott, "Whiskerbot: A Robotic Active Touch System Modeled on the Rat Whisker Sensory System," *Adaptive Behavior*, vol. 15, no. 3, pp. 223–240, Sep. 2007.

[94] M. J. Pearson, B. Mitchinson, J. Welsby, T. Pipe, and T. J. Prescott, "SCRATCHbot : Active Tactile Sensing in a Whiskered Mobile Robot," in *From Animals to Animats 11*. Springer Berlin / Heidelberg, 2010, pp. 93–103.

[95] P. Giguere and G. Dudek, "Surface Identification Using Simple Contact Dynamics for Mobile Robots," in *IEEE International Conference on Robotics and Automation*, 2009, pp. 3301–3306.

Bibliography

[96] T. J. Prescott, M. J. Pearson, B. Mitchinson, J. C. W. Sullivan, and A. G. Pipe, "Whisking with robots," *IEEE Robotics & Automation Magazine*, no. September, pp. 42–50, 2009.

[97] A. Lussier Desbiens, A. T. Asbeck, and M. R. Cutkosky, "Landing, perching and taking off from vertical surfaces," *The International Journal of Robotics Research*, vol. 30, no. 3, pp. 355–370, Jan. 2011.

[98] J. Roberts, J.-C. Zufferey, and D. Floreano, "Energy management for indoor hovering robots," in *IEEE/RSJ International Conference on Intelligent Robots and Systems*, 2008, pp. 1242–1247.

[99] J. Moore and R. Tedrake, "Magnetic Localization for Perching UAVs on Powerlines," in *IEEE/RSJ International Conference on Intelligent Robots and Systems*, 2011, pp. 2700–2707.

[100] R. Cory and R. Tedrake, "Experiments in Fixed-Wing UAV Perching," in *AIAA Guidance, Navigation, and Control Conference*, 2008.

[101] A. A. Paranjape, J. Kim, and S.-J. Chung, "Closed-Loop Perching of Aerial Robots with Articulated Flapping Wings," *IEEE Transactions on Robotics*, pp. 1–12. In Review., 2012.

[102] M. P. Murphy, C. Kute, Y. Menguc, and M. Sitti, "Waalbot II: Adhesion Recovery and Improved Performance of a Climbing Robot using Fibrillar Adhesives," *The International Journal of Robotics Research*, Oct. 2010.

[103] E. W. Hawkes, J. Ulmen, N. Esparza, and M. R. Cutkosky, "Scaling Walls : Applying Dry Adhesives to the Real World," in *IEEE/RSJ International Conference on Intelligent Robots and Systems*, 2011, pp. 5100–5106.

[104] K. Peterson, P. Birkmeyer, R. Dudley, and R. S. Fearing, "A wing-assisted running robot and implications for avian flight evolution," *Bioinspiration & Biomimetics*, vol. 6, no. 4, p. 046008, Dec. 2011.

Curriculum Vitae

Born in Baghdad, Iraq to polish parents on February 5, 1983, I spent two great years in the sun before moving to Toronto, Canada for my next 20 in the snow. I completed a Bachelor's degree in Electrical Engineering at the University of Waterloo (UW), one of the country's top engineering schools, in 2006. As a part of the co-operative program at UW I had the chance to complete 5 four-month work placements in industry. My placements spanned several industries, ranging from a small 12-person waste management company (EWI) to a medium-sized federal-affiliated energy company specializing in nuclear power plants (AECL) all the way to the research labs of Xerox.

It was during my final work placement at the Laboratory of Intelligent Systems at the Swiss Federal Polytechnic in Lausanne (EPFL) that I began work in mobile robotics, being involved in the design of the e-Puck educational robot. I then completed a Master's degree in Microengineering, specializing in robotics, in 2008 and immediately began as a research assistant working towards a Ph.D under the co-supervision of Prof. Dario Floreano and Dr. Jean-Christophe Zufferey.

My main professional interests include aerial robotics, sensing, automation, computer hardware, and robot design as well as project management and product development. In May 2008 I became one of the founders and main interviewers for Robots, a podcast that features interviews with top professionals in robotics, remaining on the team for the first 50 bi-weekly episodes.

Beyond robotics I am an avid practitioner of mountain sports, including ski touring, rock climbing, mountaineering and mountain biking. I enjoy participating in long-endurance competitions such as the Patrouille des Glaciers ski touring race (2008 and 2010).

Publications

Peer-Reviewed Journal Papers

A. Klaptocz, A. Briod, J.-C. Zufferey, and D. Floreano, "Flying, crashing and recovering: random search and phototaxis with minimal sensing," in *IEEE Robotics and Automation Magazine.* In review.

A. Klaptocz, A. Briod, L. Daler, J.-C. Zufferey, and D. Floreano, "Elastic Collision Protection for Flying Robots Using Euler Springs," in *IEEE Transactions on Mechatronics.* In review.

A. Klaptocz, L. Daler, A. Briod, J.-C. Zufferey, and D. Floreano, "An Active Uprighting Mechanism for Flying Robots," in *IEEE Transactions on Robotics*, 2012. To appear.

J.-C. Zufferey, A. Klaptocz, A. Beyeler, J.-D. Nicoud and D. Floreano. "A 10-gram Vision-based Flying Robot," in *Advanced Robotics*, vol. 21, num. 14, p. 1671-1684, 2007.

Peer-Reviewed Conference Proceedings

L. Daler, M. Sitti, A. Klaptocz, A. Briod, D. Floreano. "A Fiber Adhesives Based Perching Mechanism for Flying Robots," in *IEEE International Conference on Robotics and Automation.* 2013. To be submitted.

A. Briod, A. Klaptocz, J.-C. Zufferey and D. Floreano. "The AirBurr: A Flying Robot That Can Exploit Collisions," in *International Conference on Complex Medial Engineering.* Kobe, Japan, July 1-4, 2012.

D. Floreano, J.-C. Zufferey, A. Klaptocz, J. M. Germann and M. Kovac. "Aerial Locomotion in Cluttered Environments," in *15th International Symposium on Robotics Research.* Flagstaff, Arizona, USA, August 28-September 1, 2011.

A. Klaptocz, G. Boutinard-Rouelle, A. Briod, J.-C. Zufferey, and D. Floreano, "An Indoor Flying Platform with Collision Robustness and Self-Recovery," in *IEEE International Conference on Robotics and Automation.* Anchorage, USA, May 3-7, 2010.

Publications

F. Mondada, M. Bonani, X. Raemy, J. Pugh, C. Cianci, A. Klaptocz, S. Magnenat, J.-C. Zufferey, D. Floreano and A. Martinoli. "The e-puck, a Robot Designed for Education in Engineering," in *9th Conference on Autonomous Robot Systems and Competitions.* Castelo Branco, Portugal, May 7, 2009.

J.-C. Zufferey, A. Klaptocz, A. Beyeler, J.-D. Nicoud and D. Floreano. "A 10-gram Microflyer for Vision-based Indoor Navigation," in *IEEE/RSJ International Conference on Intelligent Robots and Systems.* Beijing, China, October 9-15, 2006.

Book Chapters

A. Klaptocz and J. Nicoud, "Technology and Fabrication of Ultralight Micro-Aerial Vehicles," in *Flying Insects and Robots.* Springer, 2009, pp. 299-316.

114